

Temperature Influence on Rock Mechanical Properties

High-Porosity, Low-Cemented Chalk



Katrine Alling Andreassen

PhD Thesis

**Department of Civil Engineering
2011**

DTU Civil Engineering Report R-236 (UK)
May 2011

Temperature Influence on Rock Mechanical Properties

High-Porosity, Low-Cemented Chalk

*Temperature Influence on Rock Mechanical Properties.
High-Porosity, Low-Cemented Chalk*

Ph.D. dissertation
Copyright © 2010 Katrine Alling Andreassen

DTU Byg, Technical University of Denmark
Brovej – Building 118
2800 Kgs. Lyngby

Byg report R-236
ISBN: 9788778773166

Typeset in L^AT_EX
Frontpage SEM-picture: Liège chalk
Courtesy of M.L. Hjuler

To Nikoline, Pauline & Filippa

Preface

Often a research plan needs to be changed as unexpected new subjects require considerations and this was the case for my thesis work. Originally, my research plan focused only on temperature effects but along the way (halfway in the study, when we broadened the survey) the pore fluid effect interestingly turned out to reveal a temperature related correlation. The situation where pieces of a jig saw suddenly fit together to show an almost clear picture (albeit not the whole) is a good experience and was definitely worth the many hours put in the project.

This thesis is submitted as a partial fulfilment of the requirements for the Danish Ph.D. degree. The work was performed at DTU Byg, the Department of Civil Engineering at the Technical University of Denmark. The main supervisor is Director of Research Niels Foged, together with Associate Professor Ole Hededal and Associate Professor Anette Krogsbøll. All three affiliated with DTU Byg. Additionally, there has been an extensive collaboration with Associate Professor Ida Lykke Fabricius, DTU Environment, Department of Environmental Engineering at the Technical University of Denmark, now DTU Byg. It was Ida's idea to investigate the whole set of published results in the literature in order to look for physical parameters that might govern the yield or strength properties of chalk.

6th of May 2011

Katrine Alling Andreassen

Included manuscripts:

Andreassen, K.A., and Fabricius, I.L. (2010). Biot Critical Frequency Applied to Description of Failure and Yield of Highly Porous Chalk with Different Pore Fluids. *Geophysics*, 75(6):E205–213.

Andreassen, K.A., Fabricius, I.L., and Foged, N.N. (accepted). Biot Critical Frequency Applied as Common Friction Factor for Pore Collapse and Failure of Chalk with Different Pore Fluids and Temperatures. *SPE Journal*, SPE-130447-PA.

Included conference papers or abstracts:

Andreassen, K.A., and Fabricius, I.L. (2010). Biot Critical Frequency Applied as Common Friction Factor for Chalk with Different Pore Fluids and Temperatures. Paper ARMA 10-453 presented at the 44th US Rock Mechanics Symposium and 5th U.S.-Canada Rock Mechanics Symposium, Salt Lake City, Utah, June 27–30. Awarded “Best student floor presentation, Monday”.

Andreassen, K.A., and Fabricius, I.L. (2010). Water Weakening of Chalk Explained from a Fluid-Solid Friction Factor. Paper presented at Rock Mechanics in the Nordic Countries Conference, 9–12 June, Kongsberg, Norway.

Andreassen, K.A., Fabricius, I.L., and Foged, N.N. (2010). Biot Critical Frequency Applied as Common Friction Factor for Pore Collapse and Failure of Chalk with Different Pore Fluids and Temperatures. SPE Paper MS-130447 presented at the SPE EUROPEC/EAGE Annual Conference and Exhibition, Barcelona, Spain, 14–17 June.

Andreassen, K.A., Fabricius, I.L., and Foged, N.N. (2010). Creep of Highly Porous Chalk and Biot Critical Frequency. Student abstract SP-44 presented at the 72nd EAGE Conference & Exhibition, Barcelona, Spain, 14–17 June.

Abstract

In petroleum engineering, the concepts of water-weakening and temperature-weakening are important phenomena for achieving increased production of hydrocarbons. Consequently, there is a need to understand the physical behaviour behind these phenomena. This thesis reviews previously published results of mechanical tests on dry chalk and chalk with different pore fluids: fresh water, synthetic seawater with varying chemical composition, methanol, formamide, glycol, and oil of varying viscosity as well as at different temperatures.

The thesis covers an analysis of which physical properties correlate with the failure and pore collapse strengths. It is proposed that the strength of chalk is correlated with the Biot critical frequency which is a function of the fluid properties viscosity and density, and the material properties porosity and permeability. The critical frequency is interpreted as a measure of the solid-fluid friction and as such suggested as a measure of the energy dissipated before the critical state of failure or pore collapse is reached. The time-dependence is included and this leads to an expression for the material dependent parameter, the b-factor.

The solute ions affected by the charge on the calcite surface represents an electrical skin depth. The layer reduces the porosity available for fluid flow. It is observed that the Biot critical frequency based on pore scale data can be used to explain effects on the macro scale.

The results show good correlation with critical frequency including rate dependence independently of fluid or gas in the pore space and with temperature effects inherently nested in the model.

Resumé

I olie-gas industrien er vandsvækkelses- og temperatursvækkelseskoncepterne vigtige mekanismer for at opnå øget produktion af kulbrinter. Dermed er der et behov for at forstå den bagvedliggende, fysiske situation. Denne afhandling gennemgår tidligere publicerede bjergartsmekaniske forsøgsresultater på tør kalk og kalk med forskellig porevæske: Ferskvand, syntetisk havvand med varierende kemisk sammensætning, methanol, formamid, glykol og olie med varierende viskositet ved forskellig temperatur.

Afhandlingen giver en analyse af hvilke fysiske egenskaber, der korrelerer med brud og pore kollaps styrker. Det er foreslået, at kalks styrke er korreleret med Biots kritiske frekvens, der indeholder væske egenskaberne: Viskositet og densitet, og materiale egenskaberne: Porøsitet og permeabilitet. Den kritiske frekvens er tolket til et mål for faststof-væske friktionen og er foreslået som mål for fordelt energi, før brud eller pore kollaps indtræffer. Tidsafhængigheden er inkluderet, og dette fører til et udtryk for den materiale-afhængige parameter, b-faktoren.

Opløste ioner i væsken påvirkes af ladningen på calcitens overflade og repræsenterer et elektrisk dobbelt lag. Laget reducerer porøsiteten tilgængelig for væskens gennemstrømning. Det er observeret, at Biots kritiske frekvens baseret på pore skala data kan bruges til at forklare effekter på makroskala.

Resultaterne viser god korrelation med kritisk frekvens med indbygget rate afhængighed upåvirket af hvilken væske eller gas, der er i porerummet og med temperatureffekter iboende i modellen.

Acknowledgements

In the course of the project several people have been an invaluable help and assisted me and these I would like to thank:

- *Niels Foged* for his patience, extensive knowledge, and skills in the laboratory. His impact with the laboratory work has been invaluable.
- *Ida L. Fabricius* for excellent guidance into the world of rock physics and inspire new thoughts when things do not seem to succeed.
- *Ole Hededal* for always provide answers and relevant references to difficult questions.
- *Bertold Plischke* for welcomed help in the start-up phase of my project.
- *Anette Krogsbøll* for taking the time as a co-supervisor.
- *Helle F. Christensen* for kindly provide access to the Pasachalk data.
- *Jonathan Zober Schwartz* for help and understanding with hydraulic matters.
- *Vita Larsen* for kind help and answers to many small problems in the laboratory.
- *Chris Humpheson* and *Rasmus T. Klinkvort* for proofreading and entertaining small talk in the office.
- *Kathrine Hedegaard* for interesting discussions on chalk.
- *Michael J. Andreassen* for patience and support.

I am also grateful to the anonymous reviewers from Geophysics, SPE Journal, ARMA, and SPE/EAGE for giving challenging comments and suggestions.

Contents

1	Introduction	1
1.1	Background	1
1.1.1	High-Porosity, Low-Cementation Chalk	2
1.1.2	Aspects	4
1.2	Purpose	5
1.3	Structure of the report	6
2	Literature Review	7
2.1	Laboratory Testing	7
2.2	Previously Proposed Mechanisms for the Effects	13
2.3	Evidence Opposing the Mechanisms	16
2.4	Time-Dependent Behaviour	16
2.5	Solid-Fluid Friction	19
3	Methods	21
3.1	Biot Critical Frequency	21
3.1.1	Electrical Skin Depth	22
3.2	Supplementary Experimental Test Series	25
3.3	Time-Dependent Behaviour	26
3.3.1	Incorporating Stress and Strain Rate	26
3.3.2	Previously Applied Stress and Strain Rate Functions	28
3.3.3	Creep	28
4	Results	31
4.1	Electrical Skin Depth	31
4.2	Biot Critical Frequency in Failure and Pore Collapse	32
4.3	Supplementary Experimental Test Series	35
4.4	Time-Dependent Behaviour and the b-Factor	37

5 Discussion	39
5.1 Causality	39
5.2 Electrical Skin Depth	40
5.3 Strain and Stress Rate Dependence	41
5.4 Supplementary Test Series	41
5.5 The Material Constant: The b-Factor	42
5.6 Temperature Effects	42
6 Conclusion	43
7 Recommendations for Future Work	45
Appendix	
Supplementary creep tests	59
Errata	61
Paper I	63
Paper II	73
Paper III	89
Paper IV	101
Paper V	113
Abstract I	123

List of Figures

1.1	Production curves from Ekofisk field	1
1.2	Scanning electron microscope images of chalk	3
1.3	Development from coccosphere to coccolith and to platelet	3
1.4	North Sea Basin with outcrop chalk localities	4
2.1	p' - q diagram without smooth transition	10
2.2	p' - q diagram with smooth transition	10
2.3	Reloading behaviour of oil-saturated Stevns chalk.	12
2.4	Oedometer test and reloading on oil-saturated Stevns chalk	17
2.5	Conceptual sketch of strain rate dependence in soft rock	18
2.6	CRS oedometer data set with dry, oil- and water saturated chalk.	19
2.7	The Biot critical frequency and quality factor for seismic wave propagation.	20
3.1	Overview of the ranges of f_c for an idealised fluid and rock	22
3.2	Sketch of viscous and electrical skin depths	23
3.3	Sketch of the equipment	25
3.4	The dimensionless critical frequency on oedometer data	27
3.5	Overview of the ranges of the different functions of f_c , $\dot{\epsilon}$ and $\dot{\sigma}$	28
3.6	Stress and fluid dependent creep index values	29
3.7	Stress and strain paths for Figure 3.6 with the Q-index.	29
4.1	Test of the skin depth hypothesis	31
4.2	Main result on p' - q plot covering all gathered data	32
4.3	Hydrostatic yield strength with specification of pore fluid and temperature	33
4.4	Location of water-glycol mixtures	33
4.5	Brazilian strength with specification of pore fluid and temperature	34

4.6 UCS strength with specification of pore fluid and temperature . . . 35

4.7 Sketches of failure planes for the supplementary test series 35

4.8 Similar to Figure 4.5 and 4.6 with marking of the supplementary
test results 36

4.9 Oedometer creep data results 37

4.10 Results from multiple calculation procedures for the b-factor . . . 38

List of Tables

2.1	Overview of test results included in this review	8
2.2	Physical properties of the pore fluids and air	9
3.1	Listing of Biot critical frequencies	23
3.2	Chemical composition of the water	24
3.3	Debye screening length	24
3.4	Supplementary experimental test series	26
4.1	The results for the supplementary experimental test series	36
A.1	Supplementary creep tests – classification data	60
A.2	Supplementary creep tests – the creep index	60

Nomenclature

Greek

δ_L	Viscous skin depth (m)
ϵ	Strain (% or fraction)
ϵ_0	Permittivity of vacuum ($8.854187817 \cdot 10^{-12}$ A·s/(V·m))
ϵ_r	Relative dielectric permittivity (-)
$\dot{\epsilon}$	Strain rate (s^{-1})
ϵ_s	Creep index (% or fraction pr log decade of time)
κ^{-1}	Debye screening length (m)
φ	Porosity (% or fraction)
φ_{reduced}	Porosity reduced by the electrical skin depth (% or fraction)
ϕ	Friction angle ($^\circ$)
ρ_{bulk}	Bulk density (g/cm^3)
ρ_{dry}	Dry density (g/cm^3)
ρ_s	Solid, grain density (g/m^3)
σ	Stress (MPa)
σ'_1	Effective major stress (MPa)
σ'_2	Effective intermediate stress (MPa)
σ'_3	Effective minor stress (MPa)

σ_c	Unconfined compression strength (MPa)
$\dot{\sigma}$	Stress rate (MPa/s)
σ_t	Tensile strength (MPa)
σ_{yield}	Yield strength (MPa)

Roman

c	Cohesion (MPa)
C_α	Secondary compression index (void ratio pr log decade of time)
C_c	Compression index (void ratio pr log decade of stress)
d	Diameter of the gas molecules (m)
e	Elementary charge ($1.602176487 \cdot 10^{-19}$ C)
f	Frequency (s^{-1})
f_c	Biot critical frequency (s^{-1})
\tilde{f}_c	Dimensionless Biot critical frequency (-)
k	Permeability (m^2 or mDarcy)
k_B	Boltzmann's constant ($1.3806504 \cdot 10^{-23}$ J K $^{-1}$)
N_A	Avogadro number ($6.02214179 \cdot 10^{23}$ mol $^{-1}$)
P	Absolute pressure (MPa)
p'	Effective mean stress (MPa)
Q	Compression index (% or fraction pr log decade of stress)
q	Generalised shear stress (MPa)
Q_{seismic}	Seismic quality factor (-)
R	Universal gas constant (8.314472 J K $^{-1}$ mol $^{-1}$)
S_a	Specific surface (m^2/g)
S_s	Specific surface (m^2/m^3)
T	Absolute temperature (K)
t	Time (s)
W	Water content (% or fraction)

Chapter 1

Introduction

In petroleum engineering, the concepts of water-weakening and temperature-weakening are important mechanisms for achieving increased production of hydrocarbons. Consequently, there is a need to understand the physical behaviour behind. This is the main subject of this study, but the work with the subject involves several different issues, which will be introduced here. Later, the issues will be elaborated to form the basis for the phenomenological understanding.

1.1 Background

Before the first water injection pilot was started there were questions about the usefulness, efficiency, and safety of the method (Norwegian Petroleum Directorate, 1997). However, as Figure 1.1 shows for the Ekofisk field in the North Sea the oil production increased due to the water injection, although preliminary laboratory tests did not show any effect of injected seawater (Johnson et al., 1989). It was also surprising that the water injection made the Ekofisk field subside in spite of no apparent pressure decrease, see e.g. Maury et al.

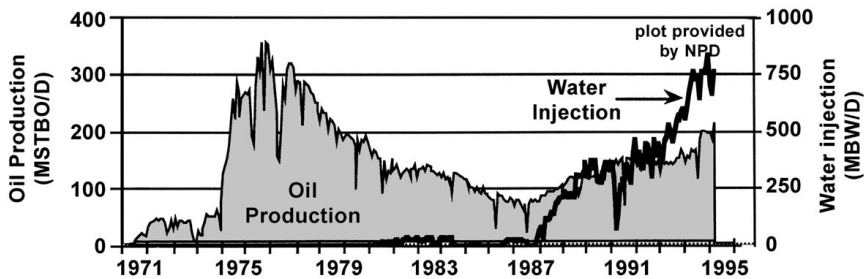


Figure 1.1: Production curves from the Ekofisk field, where the oil production stopped decreasing after the water injection (and other production changes) began.

From Andersen (1995, p. 88)

(1996) or Sylte et al. (1999). These observations sparked an extensive interest in the water weakening phenomenon. Today, water injection is considered as a relatively conventional method and is also used to maintain pressure in a reservoir.

The oil field behaviour is based on the mechanical response of the chalk at the actual reservoir conditions: 2.5–4 km depth, 85–130 °C, two fluid phases, reservoir brine and oil, besides a frequent gas phase in the pore space.

In the laboratory it is possible to design tests in order to isolate the impact from multiple changing variables, for instance the ones listed above. The aim when designing the tests is to extend the knowledge of the chalk behaviour. It is possible to vary the temperature, pore fluid, flow dynamics, stress path, confinement, time and specimen scale. Measured properties are porosity, bulk and dry density, cementation, specific surface area, yield strength, shear failure, tensile failure, elastic moduli, elastic response (Poisson's ratio), hardening/softening, acoustic velocities, poroelastic properties, time effects and draining/imbibition curves. It can be difficult to exclude the depositional characteristics as they can change on the very small scale, and vary from one specimen originating close to another. So the chalk is described based on a large range of properties and these significantly convey the mechanical properties.

Now, when dealing with the mechanical properties of chalk, defined by all the properties mentioned above, it is natural to pose the question:

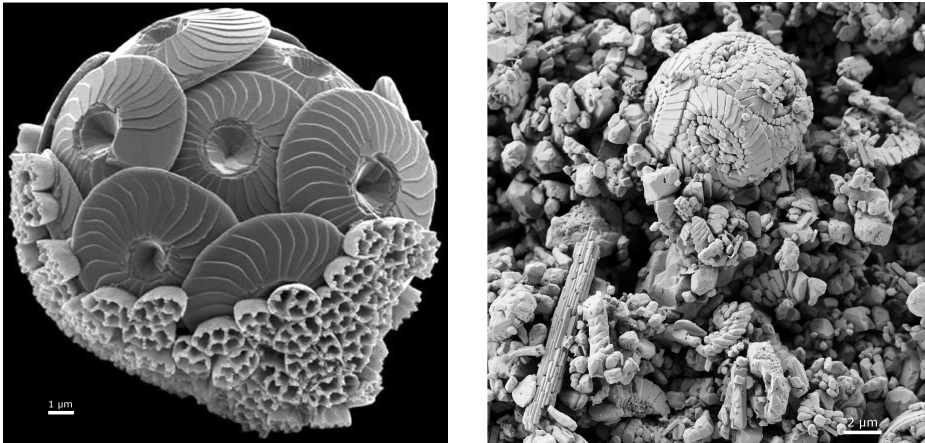
Which properties or characteristics of the chalk cross-correlate?

Before investigating this, it is necessary to state some basics on the characteristics of the chalk.

1.1.1 High-Porosity, Low-Cementation Chalk

Scanning electron microscope images, Figure 1.2, visualise the chalk – which all of the concepts relates to – and show the microscopic structure of it. The chalk is essentially made of skeletal carbonate, originally from the unicellular coccolithophorid algae, which is constructed of small platelets formed into assemblages of rings and rosettes called coccoliths (Viksund, 1998). The soft part of the algae is encircled by coccoliths to form a coccosphere as on Figure 1.3. The basic building block of chalk is therefore the platelet, and the chalk is formed as a micro-debris of platelets.

In order to narrow the focus, this investigation is limited to high-porosity, low-cementation outcrop chalk. The reason is the easy accessibility of the outcrop chalk and it has often been chosen in earlier research test programmes. The specific chalks are from three different localities (Figure 1.4): Liège or

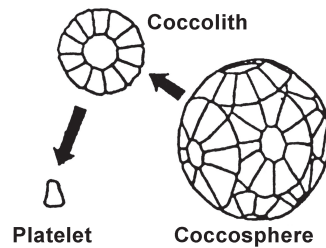


(a) Coccolithophore *Calcidiscus leptoporus*.
From [Natural History Museum \(2002\)](#).

(b) Liège chalk. Courtesy of M.L. Hjuler.

Figure 1.2: Scanning electron microscope images of chalk. At left a present-day whole coccosphere and at right a whole coccosphere in the outcrop chalk.

Figure 1.3:
Development from coccosphere to coccolith, and ultimately to platelet.
From [Sulak and Danielsen \(1989\)](#).



Lixhe chalk from a quarry in Belgium, Aalborg chalk from a quarry in western Denmark, and Stevns Chalk from a quarry in eastern Denmark. The physical properties vary among the outcrop chalks, with Liège being characterised by a porosity of generally 40% and a permeability of 1.5 mDarcy ($1.5 \cdot 10^{-15} \text{ m}^2$). Stevns chalk has a porosity of generally 45% and a permeability of 3.5 mDarcy ($3.5 \cdot 10^{-15} \text{ m}^2$), whereas Aalborg chalk generally has 45% porosity and a slightly higher general permeability of 4 mDarcy ($4 \cdot 10^{-15} \text{ m}^2$). These values are not exact and vary among the chalk blocks sampled for testing. Further characterisation of these chalk lithologies is found in [Hjuler \(2007\)](#) and [Hjuler and Fabricius \(2009\)](#). All the selected outcrop chalks have induration H2 (on induration scale according to [Larsen et al. \(1995\)](#)) and are weakly cemented.

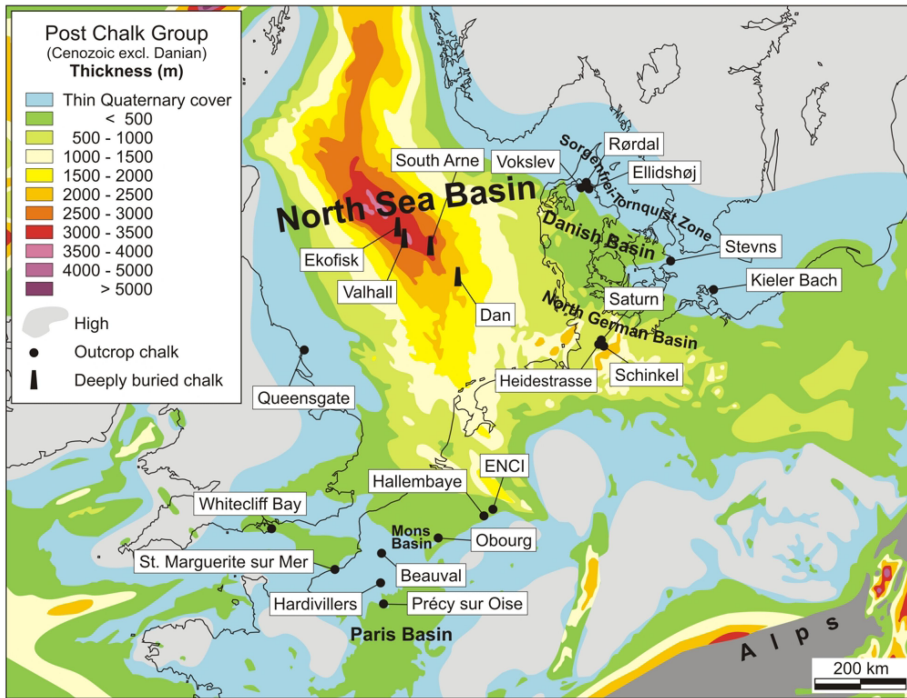


Figure 1.4: North Sea Basin with Aalborg (Rørdal), Stevns and Liège (Hallembaye) chalk localities and burial depths. From [Hjuler \(2007, p. 4\)](#).

1.1.2 Aspects

The scope of the study is broad and setting boundaries help the process. Originally, the aim was to investigate temperature effects and it was not intended to study the fluid effect. As it proved necessary to include the fluid effect aspect the time did not allow for covering numerical modelling even though this was planned.

The original hypothesis of this study was that the temperature influence for the time dependent properties follow an Arrhenius term with an activation energy quantifying the influence ([Ashby and Jones, 1996, p. 174](#)). Using this is common in temperature dependent creep tests where the material is allowed to deform under a constant stress ([Hellmann et al., 2002](#)). The assumption behind such a hypothesis require solid, frame (grain skeleton) and fluid to be treated as one and might create an ambiguity in the interpretation. Basically, it is chosen not to use the Arrhenius equation when dealing with failure/pore collapse properties as the Arrhenius term is interpreted as a diffusion process valid for single-phase materials. On the other hand, several authors have applied the concept for rock ([Carter and Kirby, 1978, Hellmann et al., 2002](#)).

In order to verify the interpretation and surpass the natural variation of

the chalk the number of tests should be high. This resulted in the choice of collecting previously published results from three different chalk types.

Chalk is by definition in the limit between a rock and a soil and belongs to a category of soft rock depending on the cementation. Here, I assume the cementation is low and within a narrow range for the three outcrop chalk types, with a Biot coefficient that is normally above 0.95. The mineralogy is not similar for the non-carbonate content in the three outcrop chalks as found by [Hjuler \(2007\)](#): Aalborg chalk has a non-carbonate content of 6% with a high opal-CT part, Liège chalk has a low non-carbonate fraction of approximately 1.5% and very low opal-CT content, and Stevns chalk is nearly 100% carbonate. I still assume similar mechanical response and so similar mechanical properties for the chalk. Other aspects influence the strength, e.g. [Schroeder \(2002, p. 100\)](#) show an influence of silica content on the strength of North Sea chalk. By choosing almost pure outcrop chalk for the analysis this aspect will not be further considered here. Also, the anisotropy of the chalk ([Talesnick and Shehadeh, 2007](#)) will not be dealt with here.

The fluid in the pore space needs considerations too. The survey is limited to full saturated pore spaces and no dissolved CO₂. The chalk has an average pore radius of 740 nm ([De Gennaro et al., 2004](#)) and calculating Poiseuille flow for a simple tube with this radius gives a Reynolds number of $1.25 \cdot 10^{-5}$ for water at 130 °C and with a strain rate of 18.5%/hour applied on a specimen of size 7.5 cm (a typical chalk specimen size and the max. strain rate seen in the later literature review). This value for the Reynolds number is very small and indicate no onset of turbulence even though the applied rate is high. Note that the irregularity of the pore space also will influence the flow but this is not taken into consideration. The onset of turbulence for the draining fluid is far from achieved and this back-of-the-envelope calculation suggest the draining fluid has laminar flow.

1.2 Purpose

Following the arguments above leads to the exact objectives with this study, which put concisely are

- ... to perform a literature survey collecting laboratory test results for high-porosity, low-cemented chalk.*
- ... to review previously proposed mechanisms for the fluid, time-dependent and temperature effects in chalk.*
- ... to investigate which physical parameters or their combinations correlate with the failure and pore collapse properties.*

- ... to subsequently propose a mechanism that combines the found physical properties and the failure and pore collapse of chalk.*
- ... to identify whether the proposed mechanism extends to the observed time dependence of chalk.*
- ... to include supplementary test series performed at DTU Byg to verify or refute the proposed mechanism.*

The overall expectation to this investigation is to add to the fundamental knowledge of the mechanical behaviour of chalk, and, accordingly, to give an answer to the above objectives.

1.3 Structure of the report

This report covers a state-of-the-art literature review on the mechanical properties of chalk in Chapter 2 presenting established theories and the extent of laboratory test series used in the further analysis. This chapter also covers previously proposed mechanisms to explain the water weakening and their supporting or opposing evidence. Applying a higher or lower stress or strain rate affects the mechanical properties of the chalk and this is dealt with in the time-dependent mechanisms section.

In the course of analysing the test results, different methods are applied and described in Chapter 3. I refer to the appended papers for specific details where possible in order to keep this summary as a presentation of the results and not as an extensive thesis covering every detail. The results follow in Chapter 4 with a short discussion on the individual results. A general discussion is covered in Chapter 5. Finally, a summary and conclusion in Chapter 6 with recommendations for future work in Chapter 7.

It is hoped that the results presented here might contribute to a better understanding of the processes or phenomena affecting the chalk and lead to increasing focus on the fluid effects in porous geomaterials.

As a start, I present some laboratory effects especially for chalk and review previous results for low-cemented, high-porosity chalk on the next pages.

Chapter 2

Literature Review

This review gathers published laboratory test results from a large number of laboratory test series. These are listed in the first section with a short comment on the different traditional laboratory tests and common ways to combine the results. The second section gives a detailed review of previously proposed mechanisms for the fluid and temperature effects observed in chalk. Although extensive, it does not cover every paper published on chalk and the few lines used here is not enough to cover the vast present knowledge. This is followed by description of the evidence supporting or opposing the mechanisms and on the time-dependencies. At the end of this chapter the concept of solid-fluid friction is dealt with.

2.1 Laboratory Testing

As many previously published laboratory test results on high-porosity, low-cemented chalk as possible are collected and listed in Table 2.1. Chapter 4 presents the actual results of the analysis of these.

The absolute viscosity and density pertaining to the pore fluids registered in Table 2.1 are listed in Table 2.2. Note that Soltrol 170 and kerosene sometimes are used interchangeable for the same oil type but according to references they have different properties (Dong and Chatzis, 1995, Liow et al., 2001).

In order to combine the failure or pore collapse information from the different mechanical test types in Table 2.1 it is common to use a p' - q plot, (Fjær et al., 2008), with

$$p' = \frac{1}{3} (\sigma'_1 + \sigma'_2 + \sigma'_3), \text{ and} \quad (2.1)$$

$$q = \frac{1}{\sqrt{2}} \sqrt{(\sigma'_1 - \sigma'_2)^2 + (\sigma'_2 - \sigma'_3)^2 + (\sigma'_1 - \sigma'_3)^2}. \quad (2.2)$$

Table 2.1: Overview of test results included in this review and their references. Ucs: Unconfined compression test. Glycol: Ethylene glycol. Liq. paraffin: Liquid paraffin of high viscosity. Eq. water: Water equilibrated with chalk. Ssw: for standard seawater, ssw-u: seawater without sulphate, ssw-u2: seawater without magnesium and sulphate, ssw-2: seawater with double the concentration of sulphate (Korsnes et al., 2006).

Test type	Fluid	T ($^{\circ}\text{C}$)	Applied rate	Chalk	Tests	Reference
Brazilian	Eq. water, seawater, oil	Room	5.4%/hour or 3 MPa/hour	Liège	8	Risnes et al. (1996)
Triax	Water	Room	18.5%/hour	Liège	13	Risnes and Kleppa (1996)
Hydrostatic, triax	Water, seawater, oil, liq. paraffin, dry	Room	0.4 MPa/hour	Liège	58	Schroeder and Shao (1996) [#]
Hydrostatic, ucs	Water	Room	300 MPa/hour	Liège	2	Fabre and Gustkiewicz (1997)
Hydrostatic	Methanol	Room	5.5 MPa/hour	Liège	1	Risnes et al. (1998)
Hydrostatic, ucs, triax	Seawater, methanol, decane, formamide, dry	130	12.4 MPa/hour	Liège	15	Rhett and Lord (2001)
Hydrostatic, triax	Water, oil	Room	3.6 MPa/hour	Liège	2	Collin et al. (2002)
Triax, ucs, Brazilian	Water, glycol	20, 130	0.5%/hour	Liège or Aalborg	194	Madland et al. (2002)
Triax, Brazilian	Eq. water, glycol, high salinity ssw	Room	2%/hour or 1%/hour	Liège or Aalborg	59	Risnes et al. (2003)
Hydrostatic, triax, Brazilian	Water, glycol, mixture hereof	Room	1%/hour or 0.35%/hour	Liège	191	Risnes et al. (2005)
Hydrostatic	Distilled water, ssw, ssw-2, ssw-u, ssw-u2	130	0.1%/hour	Stevns	10	Korsnes et al. (2006)
Hydrostatic	Tap water	20	2.6 MPa/hour	Aalborg	3 [¶]	Madland et al. (2006)
Hydrostatic	Distilled water, ssw, ssw-u	Room, 50, 70, 90	1%/hour or 0.1%/hour	Stevns	17	Korsnes et al. (2008a)
Hydrostatic, Brazilian	Tap water	Room	0.3%/hour	Liège or Stevns	63	Korsnes et al. (2008b)

[#]Similar dataset as in Delage et al. (1996).

[¶]Excluded CO₂ saturated samples.

Table 2.2: Physical properties of the pore fluids and air used in this review. The oil and liquid paraffin densities are either from the producent data-sheet or calculated based on the stated viscosity as described in Mavko et al. (2009, p. 342–343).

Fluid	T (°C)	Pressure [#] (MPa)	Density (g/cm ³)	Viscosity (mPa·s)	Ref.
Water	20	0.0	0.998207	1.001604	[1]
	20	0.2	0.998299	1.001519	[1]
	20	0.3	0.998345	1.001476	[1]
	130	0.3	0.934902	0.212930	[1]
	130	0.8	0.935162	0.213059	[1]
Brine	20	0.0	1.021064	1.070581	[2]
	50	0.7	1.011368	0.601857	[2]
	70	0.7	1.001315	0.444615	[2]
	90	0.7	0.989166	0.346164	[2]
	130	0.7	0.959477	0.234411	[2]
	130	0.8	0.959525	0.234440	[2]
Ssw: 50 g/l CaCl ₂ ·2H ₂ O	20	0.0	1.03	1.112404	[3]
Ssw: 500 g/l CaCl ₂ ·2H ₂ O	20	0.0	1.27	2.832159	[3]
Ssw: 700 g/l CaCl ₂ ·2H ₂ O	20	0.0	1.37	5.890002	[3]
Ssw: 100 g/l NaCl	20	0.0	1.07	1.199406	[3]
Ssw: 250 g/l NaCl	20	0.0	1.16	1.891164	[3]
80 mol% water, 20 mol% glycol	20	0.0	1.059507	3.145286	[4]
60 mol% water, 40 mol% glycol	20	0.0	1.086868	6.915085	[4]
40 mol% water, 60 mol% glycol	20	0.0	1.100052	11.05812	[4]
30 mol% water, 70 mol% glycol	20	0.0	1.104542	13.01528	[4]
20 mol% water, 80 mol% glycol	20	0.0	1.107905	14.85292	[4]
10 mol% water, 90 mol% glycol	20	0.0	1.109444	16.56379	[4]
5 mol% water, 95 mol% glycol	20	0.0	1.109114	17.37205	[4]
2 mol% water, 98 mol% glycol	20	0.0	1.108433	17.84227	[4]
Glycol	20	0.0	1.113401	21.81278	[5]
	130	0.0	1.031003	1.188431	[5]
Methanol	20	0.0	0.791765	0.576699	[5]
	130	0.0	0.674713	0.179010	[5]
Formamide	130	0.0	1.036	0.6095	[6]
Decane	130	0.0	0.6445	0.2866	[6]
Dodecane	20	0.0	0.7487	1.344	
Marcol 82	20	0.0	0.85	31.1	[7]
Isopar-L	25	0.0	0.763060	1.674325	
Soltrol 170	20	0.0	0.782551	3.0085	
Kerosene	20	0.0	0.796	1.94	[8]
Unnamed oil	20	0.0	0.7940417	6.9	[7]
Liquid paraffin	20	0.0	0.8835449	120	
Air [¶]	20	0.0	0.00119292	0.0182918	[9]
	25	0.0	0.00117173	0.0182918	[9]
	130	0.0	0.000863188	0.0232418	[9]

[#]Not including the atmospheric pressure. [¶]For tests on dry specimens.

- [1] NIST (2008), Mavko et al. (2009). [2] NIST (2008), Palliser and McKibbin (1998),
 [3] Risnes et al. (2003). [4] Knovel (1999), CRC (2008), Barr (2003, p. 22)
 [5] Knovel (1999). [6] NIST (2008). [7] Risnes et al. (1996).
 [8] Dong and Chatzis (1995). [9] CRC (2008).

The curve in the p' - q plot consists of a shear failure line and a pore collapse end cap. The shear failure indicates onset of ultimate strength for the material and the pore collapse indicates the onset of accelerated deformation. There are two slightly different representations of the p' - q curve in the literature, Figure 2.1 (Andreassen and Fabricius, 2010b, Paper I) and Figure 2.2 (Andreassen et al., 2011, Paper II), where the former is common in rock mechanics and the latter is common in soil mechanics and ensures a smooth transition phase from the shear failure line to the yield envelope (Krenk, 2000). There is not a clear trend from the actual recorded data points in this brittle-ductile region to decisively determine the shape for soft rock. Addis and Jones (1990), Schroeder and Shao (1996), Hickman et al. (2008), Baud et al. (2009), Omdal et al. (2010) use the former and Delage et al. (1996), Krenk (2000), Risnes (2001), Madland (2005) use the latter. Loe et al. (1992) present a third form, which do not cross the abscissa vertically. The authors also show strain isolines across the p' - q diagram.

Figure 2.1:
 p' - q diagram without smooth transition.

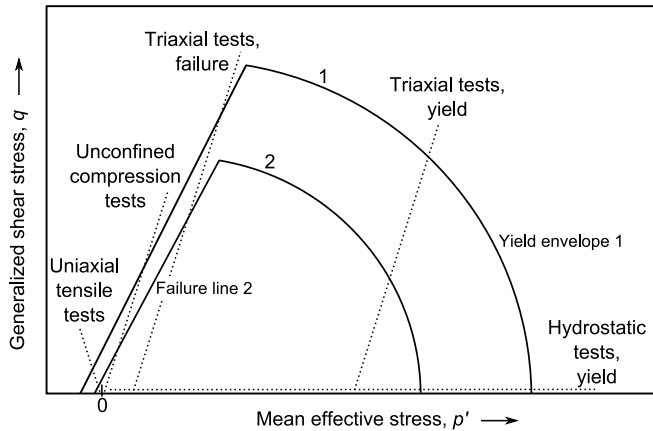
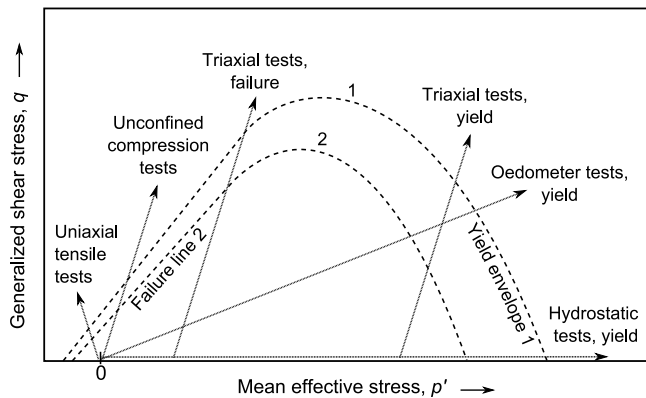


Figure 2.2:
 p' - q diagram with smooth transition.



In Kågeson-Loe et al. (1993) deformation of the chalk fabric shows two distinct phases where the material deformation behaviour changes: The first is the start of accelerated deformation and marks the limit of the elastic response. The second marks the onset of significant volumetric strains due to permanent plastic deformation. Others regard the two yield phases as one, i.e. a region or transition between the elastic and plastic behaviour (Michelson, 1917, Andersen, 1995, Engstrøm, 1992). In this thesis, the first yield point is the one meant whenever a value for the yield point or yield strength is stated.

The porosity-strength connection depends on rock type in Smits et al. (1988). They also find a correlation between the Brinell hardness of the rock and the pore collapse stress. Engstrøm (1992) shows porosity and strength correlates for North Sea chalk and data from the Joint Chalk Research programme show similar trend (Hickman, 2004, p. 34). This indicates better packing correlates with higher strength or that the lower porosity for stronger materials is due to higher cementation or a combination of the two. Ruddy et al. (1989) report the history dependent behaviour of chalk has to do with a previously compacted chalk behaves as a stronger chalk due to its decreased porosity.

Powell and Lovell (1994) conclude simple grain displacement dominate the deformation of the chalk matrix. Based on 1600 SEM images of dry chalk they document no compelling evidence of crushing of individual calcite grains and see no evidence of overall grain size reduction other than what results from breakdown of bioclasts. This is also the case observed by Johnson and Rhett (1986), Addis and Jones (1990), Holloway-Strong et al. (2007). Andersen et al. (1992) propose a physical model where the deformation is controlled by cascades of failure–redistribution–failure of the load bearing and weakly cemented arches and beams in the chalk microstructure.

One other characteristic of chalk behaviour, which is related to the breaking of intergranular cement, is the recording of acoustic emission during loading to failure. Recording of acoustic emission in high porosity Danian chalk shows very little acoustic activity (Scott Jr. et al., 2001). Thus the failure type is apparently different from what is observed in higher indurated rocks. Johnson et al. (1989) notice that the similarity between hydrostatic and uniaxial-strain tests indicate that similar processes of grain framework modifications occur for these stress paths.

Two intrinsic parameters can be used to describe the failure properties of a rock: The angle of internal friction, ϕ , and the internal cohesion, c . The friction angle is defined as $\arctan(\mu)$, where μ is the coefficient of internal friction and the cohesion is the inherent shear stress (Fjær et al., 2008).

The conceptual plots on Figure 2.1 and Figure 2.2 illustrate the stress paths for the traditional rock mechanical tests: 1) A Brazilian test determining the indirect tensile strength. 2) The unconfined compression test giving the shear

failure values. 3) The triaxial test giving either failure or yield depending on the stress path which is usually performed with a hydrostatic uploading followed by a deviatoric phase. 4) The hydrostatic test determining the yield point which is defined at the onset of a higher deformation rate, i.e. pore collapse, and where all principal effective stresses are equal. 5) The oedometer test with fixed horizontal confinement also stating a yield point. These standard rock mechanical testing procedures are described in the ISRM standards (Ulusay and Hudson, 2007).

The indirect tensile strength is here interpreted as being equivalent to the uniaxial tensile strength and is therefore plotted on the negative p' axis. In Mellor and Hawkes (1971) tests on limestone and granite show a good one-to-one correlation between Brazilian indirect tensile strength and traditional uniaxial tensile strength. According to Risnes et al. (2000) the Brazilian test compared to the direct uniaxial tensile test gives strength values that are 30% lower. They argue that the true tensile strength could be higher although they also state these considerations are approximate.

At failure the intermediate stress, σ_2 , is zero for the Brazilian test as stated in (Jaeger et al., 2007) and the failure point can therefore not be plotted directly in the p' - q diagram since the Lode angle is not zero. I choose to interpret the Brazilian test result as similar to the direct tensile strength to get a stress representation in a reasonable manner. There exist biaxial stress results for concrete (Lade, 1982, Xiaoping et al., 1989) where the extensional behaviour of the material is investigated and from that $\sigma_{t, \text{Brazilian}} = \sigma_t$ as a close approximation.

Finally, it is relevant to point to the fact that chalk might be considered as a material that is non-linear elastic (Talesnick and Shehadeh, 2007). Although the Stevns chalk in Figure 2.3 behaves close to linear besides some bedding effects as an example.

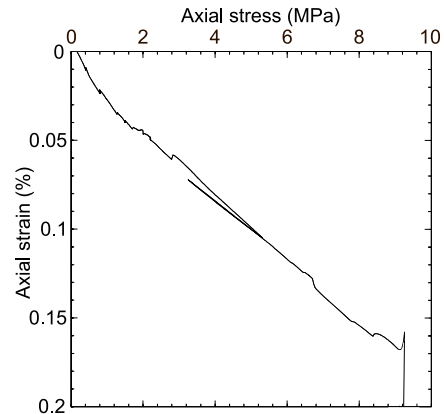


Figure 2.3:

Triaxial example of loading behaviour with reloading branch for oil-saturated Stevns chalk, 1 MPa confining pressure and with fast loading rate.

With the laboratory prerequisites covered it is now time to look at which phenomena affect the chalk properties.

2.2 Previously Proposed Mechanisms for the Fluid and Temperature Effects

As mentioned in Chapter 1 the chalk is stronger when oil-saturated than water-saturated and the temperature weakens the fluid saturated chalk. This is thoroughly covered in the literature and this review will start with some of these observations and proceed with an overview of the mechanisms proposed to explain the weakening.

The first to consider temperature effects in chalk is Charlez et al. (1992) investigating offshore chalk up to 120 °C. The shear mechanism is temperature independent while the yield strength decreases to less than a third in going from 20 °C to 120 °C. They also determine the thermal expansion coefficient.

Early observations of the influence by different fluids on rock strength valid for limestones, marbles, and sandstones are Boozer et al. (1963), Rutter (1972), Vukuturi et al. (1974). The earliest encountered references to the weakening in chalk are Meigh and Early in 1957 and Bell in 1977, who observe weakening by water on outcrop chalks with a reduction of strength of up to 70%. Johnson et al. (1989) observe no influence of injection of seawater in reservoir chalk brought to the in-situ brine- and oil-saturation.

Apparently, the friction angle is independent of pore fluid in Pasachalk (2000; 2003). Opposing this is that Gutierrez et al. (2000) found higher angles for oil-saturated chalk than water-saturated from a simple tilt test on a large number of chalk samples submerged in either oil or water. Madland et al. (2002) find that heating results in weakening for water, dry, and glycol-saturated chalk. Madland (2005) finds decreasing cohesion for water-saturated chalk than oil-saturated as well as a decreasing cohesion with higher temperature and no distinctive trend for the angle of friction.

Risnes et al. (1998) observe that the extensional failure preloaded beyond yield falls close to the same failure line for methanol, water, and oil and they conclude the failure is independent of fluid type. Consequently, changing the fluid have a negligible effect on the extensional failure of the particulate chalk. A closer look at the failure points reveals a trend with the oil to lie further from the failure line than methanol, which in turn lie closer to the line while water is on the line. The preloading will make the chalk reach a lower porosity if stressed to the same stress level as compared with a chalk that has a higher yield strength. Hence a water-saturated chalk reaches a lower porosity than an oil-saturated chalk and is expected to respond with higher failure strength. Consequently, despite the extensional failure points lie close together it still resembles the same strengthening pattern as observed elsewhere.

One often encountered mechanism stated to explain the water-weakening is *capillary effects*, where local water menisci around the grain contacts strengthen

the chalk for dry and oil-saturated specimens, while they disappear for fully water-saturated chalk. This is similar to the behaviour of partially saturated soil and has been investigated on partially saturated chalk. Consequently, [Papamichos et al. \(1997\)](#) and [Collin et al. \(2002; 2008\)](#) implement the mechanism numerically. [Hickman \(2004\)](#) presents an extensive overview of chalk constitutive models and uses a common state variable, which includes both the situation with two phase saturated chalk and with fully saturated chalk.

Also, lowering the pressure by applying a *suction* to the oil-filled pore space causes a strengthening with higher suction first described experimentally in chalk by [Delage et al. in 1996](#) and the mechanism is mentioned by [Schroeder and Shao \(1996\)](#), [Schroeder et al. \(1998\)](#). The two Pasachalk projects present more experimental verification ([Pasachalk, 2000; 2003](#)). The data obtained are further dealt with and modelled numerically by [De Gennaro et al. \(2003; 2004; 2005a;b\)](#), [Priol et al. \(2005; 2007\)](#), [Taibi et al. \(2009\)](#).

Chemical effects is another explanation for the weakening. In 1983 [Newman](#) reports water weakening on high porosity offshore chalk and relates it to the chemical composition of the seawater. The proposed mechanism is dissolution and at high stresses pressure solution. A chemo-mechanical coupling is proposed by [Hellmann et al. \(2002\)](#) and [Pietruszczak et al. \(2006\)](#), where the mechanism for the chalk weakening is *intergranular pressure solution*. This process consists of dissolution of the chalk at grain contacts followed by diffusion of the dissolved fraction away from the grain contact area to grain surface affected by lower stresses. A good example of this is deformation of porous sucrose and KCl which are highly soluble in water and show exponential dependence from temperature and linear dependence from stress on the creep response ([Pharr and Ashby, 1983](#)). The experimental basis in [Hellmann et al. \(2002\)](#) is long term creep experiments (nearly two years) where the temperature effect is low. A fluid effect with strain rates was found to correlate with calcite solubility.

[Zhang and Spiers \(2005a;b\)](#) observe that higher phosphate content in the pore water results in lower strain rate and oil-saturated samples show low strain rates. One of the latest observations in this category are by [Croizé et al.](#), who in 2010 account of pressure solution on the edge of a calcite crystal wetted with water. [Zhang et al. \(2010\)](#) also deliver results on the time and temperature dependent intergranular pressure solution in water-saturated granular calcite. [Korsnes](#) measures weakening effects in tests in 2006, 2007, 2008a at different temperatures and with different chemical composition of the pore water, where most of the tests are performed with continuous flooding in order to amplify the chemical effects. Their hypothesis is that a *substitution* of Ca^{2+} by Mg^{2+} takes place and causes diffusion at grain contacts. Similarly, [Austad et al. \(2008\)](#) also argue for the substitution mechanism and comment that the different size

of the Ca^{2+} and Mg^{2+} causes stress on the chalk surface at grain contacts causing the mechanical strength of the chalk to be decreased. A coupled damage, dissolution-diffusion model (Hu and Hueckel, 2007) is a similar theory. Purely chemical dissolution/precipitation at grain contacts is proposed by Heggheim et al. (2005) based on mechanical tests on chalk specimens aged at 130 °C with different water solutions.

Risnes et al. briefly considers a strictly physical model dependent on the zeta potential of the chalk surface affecting the repulsive forces from the double layers on chalk grains (Risnes et al., 2000, Risnes, 2001). Risnes et al. (2003) correlate the strength of chalk with the *water activity* in the pore fluid. Interestingly, the water activity is correlated with the dielectric permittivity of the fluid for concentrated electrolyte solutions (Lyashchenko and Karataeva, 2007). The water activity for glycol and water mixtures correlates with strength and cohesion of chalk in Risnes et al. (2005). They present a new *adsorption pressure model*. The model is based on the energy needed to remove adsorbed water from the grain surfaces and this converts to an adsorption pressure that correlates with the cohesion of the chalk. They include the water activity of the pore fluid because less water molecules affect the adsorption layer.

Another often stated mechanism is the reduction in the *free surface energy* by an adsorbed fluid on the solid part leading to a weakening of the material. In other words, a surface active fluid makes the likelihood of crack propagation higher. Boozer et al. (1963) investigate the time and temperature effects on sandstone and limestone saturated with different fluids. They relate the strength decrease to lowering of the free surface energy.

Later, Rutter (1972; 1974) observe water-weakening in outcrop limestone of low porosity at different temperatures with no sign of pressure solution and so Rutter proposes that the mechanism behind the weakening is a *Rehbinder effect*. The Rehbinder effect is a surface effect where a reduction in the free surface energy is an effect of dislocations that emerge at the crystal-fluid interface and leads to a higher probability of crack initiation. *Microcracking* may be a dominant effect according to Baud et al. (2009) for dry and wet limestone of porosity higher than 30%. They also suggest that the weakening effect correlates with a reduction in the surface energy for both triaxial and hydrostatic conditions.

Finally, another angle to what influence the mechanical behaviour of chalk is that a thin, hydrophobic film suppresses the water-weakening (Rhett and Lord, 2001). Similarly, the heterogeneity on the nanoscale found by Hassenkam et al. (2009) and that organic coating on the coccolith fragments could be the mechanism affecting the measured elasticity and surface properties.

2.3 Evidence Opposing the Mechanisms

That capillary effects may not be the cause for the water weakening in fully saturated chalk is demonstrated by a test series on water–ethylene glycol mixtures with water completely miscible in glycol (Risnes et al., 2005). Also Lord et al. (1998) reason that the amount of adsorbed water is not enough for the capillary effects to exist in dry chalk. Johnson et al. (1989) notice no effect of water flooding of reservoir cores at 131 °C with reservoir water content.

Intergranular pressure solution leads to an increase in the contact area between the chalk grains with time and can hardly result in weakening. Hickman (2004) also comment on the time a possible chemical process needs in order to take effect, compared with the fact that water-flooding of chalk shows an immediate response (Schroeder et al., 1998). This instantaneous deformation in chalk by water injection is also observed for chalk specimens by Homand and Shao (2000) and in fractures by Gutierrez et al. (2000). Madland (2005, p. 37) refute the pressure solution as the sole mechanism based on the weakening effect of aging the chalk specimens (Heggheim et al., 2005). Adam et al. (2009) find the frame weakening process in acoustic measurements is reversible and consequently state this is due to no dissolution by the brine.

The new adsorption theory by Risnes et al. (2005) does not conform to the modelling result by Cooke et al. (2010)*, where methanol also adsorb to the calcite surface. Additionally, according to the model the larger hydration pressure would cause a larger weakening compared to water.

The very little acoustic activity recorded by Scott Jr. et al. (2001) might indicate the failure type is apparently different from what is observed in higher indurated rocks and so relating the reduction in free surface energy to the probability of initiation of cracks might not be the full explanation specifically for water-weakening in chalk.

These considerations are the reason for the focus of this thesis on other mechanisms than the ones just discussed. The review of the literature above addresses the failure and pore collapse properties although the time-dependent mechanisms are an integral part of the mechanical behaviour. The next section looks into this.

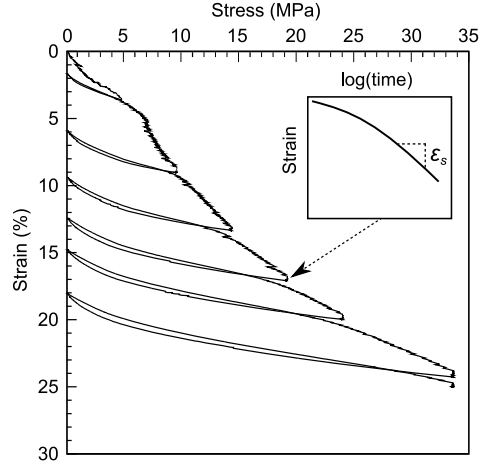
2.4 Time-Dependent Behaviour

In time-dependent behaviour the material responds weaker for a slow loading or deformation rate than for a higher. A creep phase with constant stress, where the material is allowed to deform, is similar to going from a fast loading rate

*They “calculated the energy gained by the adsorption of a methanol molecule on the surface to be almost twice that gained by the comparable adsorption of water”.

to a slow and makes the material respond as a weaker material and hence with a higher deformation. Figure 2.4 has an example of this in the small inset. The influence of viscoplastic strains beyond yield for the reloading branches is obvious when comparing with Figure 2.3 on page 12.

Figure 2.4: Oedometer example of reloading behaviour for oil-saturated Stevns chalk subjected to a slow applied strain rate. There is a creep phase before each reloading branch and observed hardening for the high stress region.



Dividing into transient–steady state–accelerating creep regimes is first mentioned by Andrade (1910) for metal wires under constant tensional load. These regimes are commonly used in compression tests in rock mechanics (Fjær et al., 2008, Jaeger et al., 2007) with steady state and accelerating creep regimes present at higher confining stresses. Boresi and Schmidt (2003, p. 632) comment on the later use of these regimes as valid for constant tensile stress. Pharr and Ashby (1983) observe tertiary creep on porous KCl in water or methanol solutions. Their suggestion, that the temperature influenced creep rate is correlated with the fluid viscosity and KCl solubility, is noteworthy. Johnson and Rhett (1986) and later Andersen et al. (1992) observe no tertiary creep (accelerated creep leading to failure) – only transient creep.

The viscoplastic nature of porous soft rock calls for using the time dependent concepts from soil mechanics. The definition of creep index or secondary strain ϵ_s is (Mesri and Godlewski, 1977)

$$\epsilon_s = \frac{d\epsilon}{d(\log(t))}, \quad (2.3)$$

where ϵ is strain and t is time. ϵ_s is termed C_α when addressed to the void ratio. Conventionally, ϵ_s is determined by plotting the strain vs. logarithmic time for a creep phase and approximate the last part of the curve with a linear regression.

The definition of compression index Q is (Mesri and Godlewski, 1977)

$$Q = \frac{d\epsilon}{d(\log(\sigma))}, \quad (2.4)$$

where σ is stress. Q is termed C_c when addressed to the void ratio. For soils, Mesri and Godlewski (1977) find the relation

$$\frac{\epsilon_s}{Q} = \frac{d(\log(\sigma))}{d(\log(t))} = b, \quad (2.5)$$

where b is termed the b-factor or C_α/C_c . The factor b is a constant for any particular soil for all combinations of time, effective stress and strain level (Mesri and Godlewski, 1977). In 1986 de Waal finds this relationship is also valid for sandstones. For a sample run at interchanging strain rates as illustrated in Figure 2.5, the relation is (de Waal, 1986)

$$\frac{\sigma'_{\text{axial},1}}{\sigma'_{\text{axial},2}} = \left(\frac{\frac{d\epsilon_{\text{axial},1}}{dt}}{\frac{d\epsilon_{\text{axial},2}}{dt}} \right)^b, \quad (2.6)$$

where $\sigma_{\text{axial},1}$ is the effective axial stress related to a point on the stress–strain curve with an applied strain rate of $d\epsilon_{\text{axial},1}/dt$ and b is the material dependent b-factor. Smits et al. (1988) find higher b-factor for water-saturated Danian outcrop chalk than dry and kerosene-saturated, while water-saturated North Sea chalk falls in between.

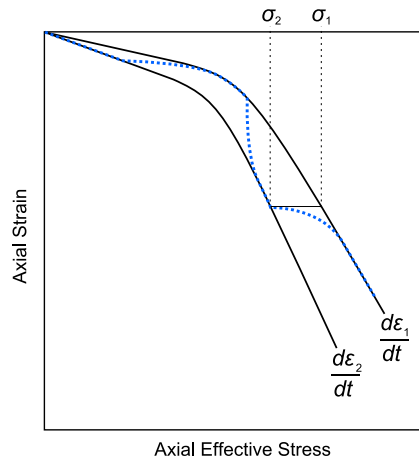


Figure 2.5:

Conceptual sketch of strain rate dependence in soft rock. The blue line represents the stress–strain path following two interchanging strain rates. Strain rate 1 is higher than strain rate 2. The material responds as a stronger material when applying the higher strain rate 1. Based on de Waal (1986).

An extensive laboratory test series on Liège chalk with different fluids and without any flow through shows fluid dependence for the strain rate and yield strength correlation in Figure 2.6 (Pasachalk, 2003). The span of the strain rates applied is large.

Figure 2.6:

CRS oedometer data set from Pasachalk (2003), De Gennaro and Pereira (2008) on Liège chalk. There is a correlation between applied strain rate and yield strength depending on the content of the pores. The oil is Soltrol170. Regression lines:

Dry:

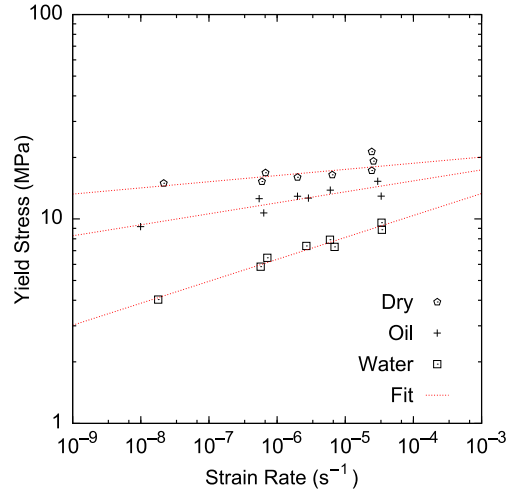
$$\ln(y) = 0.03013 \cdot \ln(x) + 3.208.$$

Oil:

$$\ln(y) = 0.0537 \cdot \ln(x) + 3.226.$$

Water:

$$\ln(y) = 0.1073 \cdot \ln(x) + 3.330.$$



Observing the fluid, temperature, and time effects listed above, where both the material and the fluid properties are seen to change the behaviour of the chalk, leads to a focus on the solid-fluid friction. On the other hand, Johnson et al. (1989) do not observe drainage of the chalk to influence the creep process.

2.5 Solid-Fluid Friction

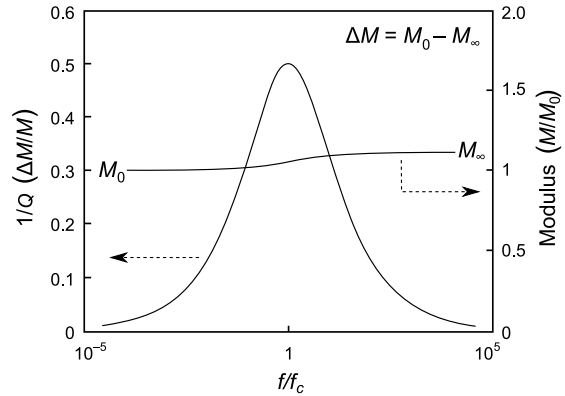
Bourbié et al. (1987, p. 79) comment on the dissipative nature build into the Biot theory and generalise the Biot critical frequency as a measure of the friction on the small scale – put concisely: the solid-fluid friction. The definition of the Biot critical frequency, f_c , (often also termed characteristic, cross-over, or reference frequency) is

$$f_c = \frac{\varphi \eta}{2\pi \rho_f k}, \quad (2.7)$$

where φ is porosity, η is the fluid absolute viscosity, ρ_f is fluid density, and k is absolute permeability. The Biot critical frequency marks the limit between a low frequency regime with the pore fluid following viscous forces and a high frequency regime with inertial forces dominating the fluid motion (Biot, 1956a;b). These regimes have been verified experimentally by Johnson et al. (1987).

The drag that the solid motion makes on the fluid and whether this is in the viscous or inertial regime is basically a matter of friction between the liquid and the solid. Bourbié et al. (1987, p. 80) list the critical frequency for various materials and pore fluids. Fabricius et al. (2010) find the amount of softening of elastic modulus to be correlated with the reference frequency.

Figure 2.7:
The Biot critical frequency and quality factor for seismic wave propagation. From [Mavko et al. \(2009, p. 311\)](#).



The dissipative mechanism is exemplified in Figure 2.7, where the reciprocal quality factor Q_{seismic}^{-1} is related to the phase delay between the stress and strain for a propagating seismic wave ([Mavko et al., 2009, p. 123](#)). The applied frequency for a seismic wave results in the highest attenuation at the Biot critical frequency. As a consequence, a higher fluid kinematic viscosity results in a higher frequency that has the highest attenuation and a lower fluid kinematic viscosity will give a lower frequency at which the highest attenuation is present.

In this thesis, it is proposed that the solid-fluid friction is a controlling parameter for the failure or pore collapse in chalk. When assuming that a certain energy needs to be applied to a specimen to reach the point in which the specimen will go into failure or into pore collapse, a higher solid-fluid friction will dissipate more energy compared to a lower friction and consequently the chalk in the case of high solid-fluid friction will need more energy to be applied to it before the specimen enters the failure/pore collapse. This is the background for using the Biot critical frequency for the failure and pore collapse in rock mechanical tests on high-porosity, low-cementation chalk.

The next chapters use the Biot critical frequency as a central measure for the solid-fluid friction in chalk.

Chapter 3

Methods

This chapter describes the methods used in order to apply the Biot critical frequency. Encountering a difference in the permeability of the chalk dependent on whether it is fully oil-saturated or water-saturated leads to the concept of an electrical skin depth, which is described herein. The section following after this covers the supplementary test series. A further investigation with previously published data is the time-dependence of the material with the stress and strain rate incorporated together with a dimensionless friction factor. Finally, I present extended methods to comprise the creep index and b-factor.

3.1 Biot Critical Frequency

The procedure for calculating the Biot critical frequency in Equation 2.7 for each test result in Table 2.1 (on page 8) is to take the corresponding fluid viscosity and density from Table 2.2 (on page 9) together with the available porosity and permeability for the specific chalk. Table 3.1 gives examples of final values of the critical frequency for different fluids. Figure 3.1 is a graphical representation showing the impact by changing the input parameters for the Biot critical frequency. This is done keeping other parameters constant and with a dependency between porosity and permeability through Kozeny's equation (Equation 3.1).

For a number of tests the actual permeability of the tested chalk is not known but the exact porosity is stated. One way of obtaining the permeability when the porosity is known is to use Kozeny's equation for laminar flow in a porous medium (Mortensen et al., 1998):

$$k = c \frac{\varphi^3}{(1 - \varphi)^2 S_s^2} = c \frac{\varphi^3}{(1 - \varphi)^2 (S_a \rho_s)^2}, \quad (3.1)$$

$$c = \left(4 \cos \left(\frac{1}{3} \arccos \left(\varphi \frac{8^2}{\pi^3} - 1 \right) + \frac{4}{3} \pi \right) + 4 \right)^{-1}, \quad (3.2)$$

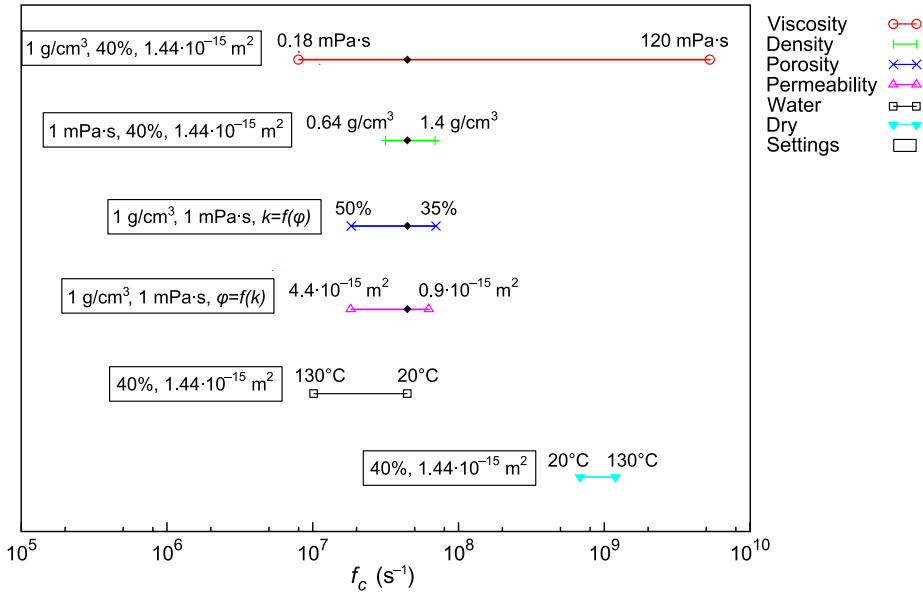


Figure 3.1: Overview of the possible ranges of $f_c = \frac{\varphi\eta}{2\pi\rho_f k}$ for an idealised fluid and rock system which vary in the physical parameters η , ρ_f , φ or k with the density or viscosity of water where possible (water-saturated chalk at 20°C with 40% porosity and $1.44 \cdot 10^{-15} \text{ m}^2$ permeability marked with \blacklozenge). The dry case is separate because the very low gas density and viscosity combines to a high value of f_c . Note the increasing critical frequency with temperature for dry rock opposed to the case of a fluid saturated rock (Table 3.1).

with c stated here for 3D circular interconnected tubes, φ is the porosity, S_s is specific surface as grain surface area to grain volume, S_a is specific surface area in surface area per solid mass, ρ_s is solid (grain) density*. Andreassen and Fabricius (2010b, Paper I) describes the procedure to back-calculate the specific surface area, and obtain S_a of $2.0 \text{ m}^2/\text{g}$ for Liège chalk, $1.6 \text{ m}^2/\text{g}$ for Aalborg chalk, and $2.0 \text{ m}^2/\text{g}$ for Stevns chalk, which are the values used in Equation 3.1.

As mentioned above, one step more is needed for the water-saturated chalk, which is to consider the influence of the dissolved ions affected by the charge that the chalk surface possesses. This is dealt with in the next section.

3.1.1 Electrical Skin Depth

As the use of the screening length concept has been progressively refined, the methods described in the appended papers are not fully consistent for the viscous skin depth term in all the papers and Figure 1 in Paper III. The chalk system is

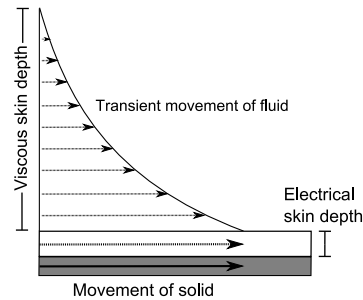
* 2.7 g/cm^3 is used for the solid density of chalk.

Table 3.1: Biot critical frequencies for various fluids and air based on density and viscosity information in Table 2.2. Calculated for a chalk with 40% porosity and $1.44 \cdot 10^{-15} \text{ m}^2$ permeability while assuming a strain rate of 1%/hour or stress rate of 0.01 MPa/hour. See Section 3.3.1 on page 26 for the functions of critical frequency and applied rate.

Fluid	Temperature (°C)	f_c (s ⁻¹)	$f(\bar{f}_c, \dot{\epsilon})$ or $f(\bar{f}_c, \dot{\sigma})$	$f(f_c, \dot{\epsilon})$	$f(f_c, \dot{\sigma})$
Water	130	$1.01 \cdot 10^7$	1.8	0.22	0.15
Methanol	130	$1.17 \cdot 10^7$	2.1	0.24	0.17
Decane	130	$1.97 \cdot 10^7$	3.7	0.33	0.25
Formamide	130	$2.60 \cdot 10^7$	4.7	0.38	0.30
Water	20	$4.44 \cdot 10^7$	6.8	0.48	0.40
Glycol	130	$5.10 \cdot 10^7$	7.4	0.51	0.43
Soltrol	20	$1.70 \cdot 10^8$	12.7	0.69	0.63
Dry	20	$6.78 \cdot 10^8$	17.9	0.83	0.79
Glycol	20	$8.66 \cdot 10^8$	18.6	0.85	0.81
Dry	130	$1.19 \cdot 10^9$	19.5	0.87	0.84
Liq. paraffin	20	$6.00 \cdot 10^9$	22.7	0.94	0.92

complex and the mechanisms applied here should be taken as an overall picture of the near wall situation. Lyklema (1991) should be consulted for qualified knowledge. The concepts are necessary in order to quantify the effects and Figure 3.2 sketches the implied mechanisms.

Figure 3.2: Sketch of viscous and electrical skin depths, partly from Bourbié et al. (1987).



In the fluid saturated pores, the electrical skin depth to the solid surface is in principle acting as a reduction of the porosity and also affects the calculated permeability, as the skin layer becomes thinner with increasing number of ions dissolved in the water. In accordance with the Debye-Hückel theory, I use the screening length κ^{-1} for an electrolyte (Lyklema, 1991) to quantify this effect,

$$\kappa^{-1} = \left(\frac{\epsilon_o \epsilon_r k_B T}{2 N_A e^2 I} \right)^{1/2}, \quad (3.3)$$

Table 3.2: Chemical composition of the tap water, equilibrated water, and synthetic seawater used in the test series (Schroeder, 2002, Korsnes et al., 2006).

	Tap water (10^{-3} mol/L)	Eq. water (10^{-3} mol/L)	Ssw-2 (mol/L)	Ssw (mol/L)	Ssw-u (mol/L)	Ssw-u2 (mol/L)
SiO_3^{2-}	0.255	0.070				
HCO_3^-	5.610	1.10	0.002	0.002	0.002	0.002
Cl^-	1.42	0.810	0.467	0.525	0.583	0.567
SO_4^{2-}	0.90	0.175	0.048	0.024	0	0
Mg^{2+}	0.621	0.02	0.045	0.045	0.045	0
Ca^{2+}	4.184	0.434	0.013	0.013	0.013	0.013
Na^+	0.892	1.27	0.44	0.45	0.46	0.533
K^+	0.059	0.02	0.01	0.01	0.01	0.01
Fe^{3+}	0	0.01				

Table 3.3: Debye screening length using Table 3.2 and Equation 3.3.

	Ssw (nm)	Ssw-2 (nm)	Ssw-u (nm)	Ssw-u2 (nm)	Eq. water (nm)	Dist. water [¶] (nm)	Tap water (nm)
20 °C	0.350	0.347	0.354	0.372	5.52	5.52	2.42
50 °C	0.349	0.346	0.353	0.371	5.42	5.42	2.37
70 °C	0.334	0.331	0.338	0.355	5.17	5.17	2.26
90 °C	0.320	0.316	0.323	0.340	4.94	4.94	2.16
130 °C	0.293	0.290	0.296	0.311	4.50	4.50	1.97

[¶]Distilled water is assumed to equilibrate instantaneously with the chalk and reach a similar electrical skin as eq. water.

where ϵ_0 is the permittivity of vacuum, ϵ_r is the relative dielectric permittivity, k_B is Boltzmann's constant, T is the absolute temperature, N_A is the Avogadro number, e is the elementary charge, and I is the ionic strength of the electrolyte. Table 3.2 states the chemical composition of all the relevant types of water and Table 3.3 lists the subsequent Debye lengths.

As the ionic content goes to zero the screening length approaches infinity and using the screening length as a skin depth hindering the permeability in this situation cannot be true. It is necessary to assume that distilled water equilibrate fast or instantaneously with the calcite and therefore reach the ionic content equal to equilibrated water.

The reduction in porosity, φ_{reduced} , is then calculated from the effective specific surface,

$$\varphi_{\text{reduced}} = \varphi - (1 - \varphi) \kappa^{-1} S_a \rho_s. \quad (3.4)$$

The small differences in screening lengths for the synthetic seawaters in Table 3.3 result in small differences for the calculated critical frequency (Andreassen and Fabricius, 2010b, Paper I).

Introducing a dimensionless critical frequency is possible and water at 20 °C is chosen as reference fluid. The reference material is Liège chalk, and accordingly a dimensionless critical frequency becomes (Andreassen and Fabricius, 2010a, Paper III).

$$\tilde{f}_c = \frac{f_c}{f_{\text{ref}}} = \frac{\pi f_c \delta_L^2 \rho_{\text{water}}}{\eta_{\text{water}}}, \quad (3.5)$$

where the reference viscous skin depth δ_L is chosen to be 0.74 μm , which is the average pore diameter for Liège chalk (De Gennaro et al., 2004). The value of f_{ref} is then 583 260 s^{-1} .

3.2 Supplementary Experimental Test Series

The supplementary test series on Stevns chalk establish the unconfined compression strength (UCS) and indirect tensile strength (Brazilian) on chalk with various pore fluids and in the dry state. The specimens are cut from two blocks of Stevns chalk with small differences in classification properties (Table 3.4). They are both white, porous muddy chalk with some bryozoans and of induration H2. The test set-up is a conventional closed cell in a constant rate of strain equipment (Figure 3.3).

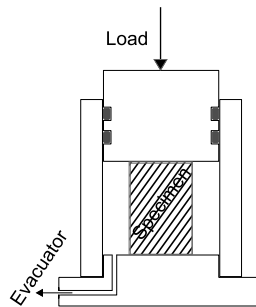


Figure 3.3:
Sketch of the equipment.

This equipment makes it possible to apply a low absolute pressure with the use of an evacuator supplying a suction of 0.09 MPa equal to an absolute pressure of 0.013 MPa in the cell. The cell diameter is 60 mm and the specimen diameter is 50 mm or 54 mm. Table 3.4 lists the classification properties of the tested specimens. Observed ring friction is a cause of the movement of the top pressure head against the inner cell wall and is subtracted from the actuator force read

Table 3.4: Supplementary experimental test series with unconfined compression tests (ucs) and Brazilian tests at 25 °C. The specimen label states the specimen diameter. The low pressure tests are on dry chalk.

Specimen	Fluid	Height (cm)	Diameter (cm)	Sat. mass (g)	Dry mass (g)	φ (%)	ρ_{bulk} (g/cm ³)	ρ_{dry} (g/cm ³)	f_c (s ⁻¹)
UCS									
SC54 A	Water	6.919	5.410	296.96	221.24	48.7	1.867	1.391	2.10·10 ⁷
SC50 C	Water	6.579	5.007	250.77	194.61	44.6	1.936	1.502	3.05·10 ⁷
SC50-2 C	Water	7.074	4.983	265.44	207.44	44.5	1.924	1.504	3.06·10 ⁷
ST50	Isopar-L	6.902	4.999	249.49	205.11	44.1	1.841	1.514	6.72·10 ⁷
SC54 B	Dry	7.031	5.407	229.42	228.49	47.8	1.421	1.416	3.48·10 ⁸
SC50 B	Dry	6.715	5.023	197.11	197.03	45.4	1.481	1.481	4.29·10 ⁸
SC50-2 B	Dry	7.014	5.017	209.71	209.68	44.2	1.512	1.512	4.75·10 ⁸
SC50 A	Low pres.	6.532	5.023	192.86	192.78	45.0	1.490	1.490	1.45·10 ⁹
SC50-2 A	Low pres.	7.002	5.019	207.99	207.95	44.6	1.501	1.501	1.50·10 ⁹
Brazilian									
SC54 D	Water	2.617	5.429	113.57	85.27	48.1	1.875	1.408	2.22·10 ⁷
ST50	Isopar-L	2.883	5.012	103.45	84.64	45.1	1.819	1.488	6.19·10 ⁷
SC54 C	Dry	2.815	5.395	90.06	90.03	48.4	1.399	1.399	3.30·10 ⁸
SC50-2 B	Dry	2.700	5.004	79.73	79.72	44.6	1.502	1.502	4.59·10 ⁸

out. An LVDT records the external deformation. [Andreassen et al. \(2011, Paper II\)](#) list the calculation of the density and viscosity of air at the relevant pressure for an evacuated specimen. This gives a density of $4.28 \cdot 10^{-4}$ g/cm³ and an absolute viscosity for air of 0.0216 mPa·s (at absolute pressure of up to 36 kPa).

The results of these tests are presented in Chapter 4. The following section applies the Biot critical frequency for time-dependent behaviour.

3.3 Time-Dependent Behaviour

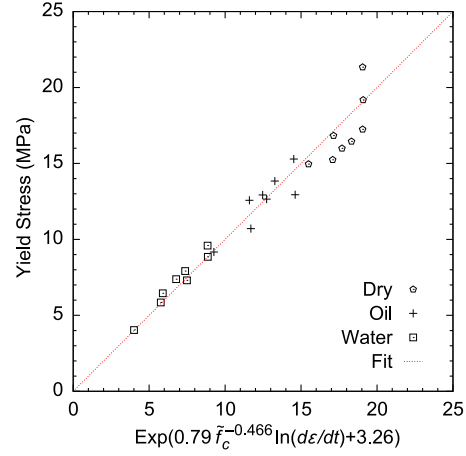
In the appended papers the incorporation of the stress and strain rate is approached in several different manners. One is chosen to be described here containing one refinement, although the others are briefly mentioned in Section 3.3.2. In order to relate the different rate equations, this also covers a comparison chart. Then follows a method based on the interpretation of creep index values to obtain the b-factor.

3.3.1 Incorporating Stress and Strain Rate

For the data set in Figure 2.6 (on page 19) the slopes of the pore fluid specific regression lines are fitted to the dimensionless critical frequency (Equation 3.5)

Figure 3.4:

The dimensionless critical frequency on time-dependent data set from [Pasachalk \(2003\)](#), [De Gennaro and Pereira \(2008\)](#). There exists a correlation between the yield strength and strain rate irrespective of pore fluid.



calculated for each pore fluid and for the dry state. The correlation on [Figure 3.4](#) between the yield strength and the applied strain rate is

$$\begin{aligned} \ln(\sigma_{\text{yield}}) &= 0.79 \tilde{f}_c^{-0.466} \ln\left(\frac{d\epsilon}{dt}\right) + 3.26, & \Rightarrow \\ f(\tilde{f}_c, \dot{\epsilon}) &= \exp\left(0.79 \tilde{f}_c^{-0.466} \ln\left(\frac{d\epsilon}{dt}\right) + 3.26\right), \end{aligned} \quad (3.6)$$

with σ_{yield} in MPa, and the strain rate in s^{-1} .

An attempt to obtain the stress rate dependence from [Pasachalk \(2003\)](#) data did not yield a consistent result. There was nearly no rate dependence for oil-saturated specimens, so instead the rate dependence was obtained based on hydrostatic test results in [Table 2.1](#) (on page 8) run under stress rates. The procedure consisted of determining the modulus for tests with stress-strain curves included. Then an effective strain rate was calculated based on the modulus and the stated stress rate. An average of the strain rate to stress rate ratios is 0.0004 and assuming a similar phenomenological behaviour as in [Equation 3.6](#) gives[†]

$$\begin{aligned} \ln(\sigma_{\text{yield}}) &= 0.79 \tilde{f}_c^{-0.466} \ln\left(0.0004 \frac{d\sigma}{dt}\right) + 3.26, & \Rightarrow \\ f(\tilde{f}_c, \dot{\sigma}) &= \exp\left(0.79 \tilde{f}_c^{-0.466} \ln\left(0.0004 \frac{d\sigma}{dt}\right) + 3.26\right), \end{aligned} \quad (3.7)$$

with σ_{yield} in MPa, and the stress rate in MPa/s. This procedure is discussed later.

[†]Using $\dot{\epsilon} = A_1 \dot{\sigma}$ with $A_1 = 0.15 \text{ MPa}^{-1}$ for the elastic behaviour. Procedure from [de Waal \(1986, p. 73\)](#).

The rate dependence bears similarities with the Mesri and Godlewski (1977) and de Waal (1986) material property the b-factor. From the above rate equation (Equation 3.6) and Equation 2.6 (on page 18)

$$\ln\left(\frac{\frac{\sigma_1}{\exp(3.26)}}{\frac{\sigma_2}{\exp(3.26)}}\right) = 0.79\tilde{f}_c^{-0.466} \ln\left(\frac{\frac{d\epsilon_1}{dt}}{\frac{d\epsilon_2}{dt}}\right), \quad \text{so}$$

$$b = 0.79\tilde{f}_c^{-0.466}. \quad (3.8)$$

3.3.2 Previously Applied Stress and Strain Rate Functions

The functions have the same structure although they have different ranges. The two approaches are from Andreassen and Fabricius (2010c, Paper IV) and Andreassen et al. (2010, Paper V). Figure 3.5 shows the ranges involved, which are exemplified with water at 20 °C. The range for the stress rate ($1700\tilde{f}_c^{-0.5} \ln(\dot{\sigma})$) is unrealistically broad and this function is termed obsolete by now.

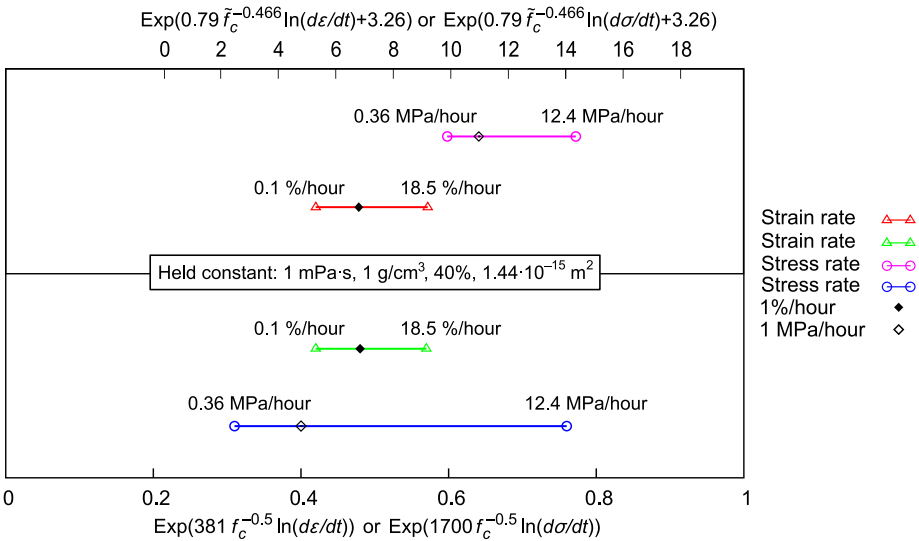


Figure 3.5: Overview of the possible ranges from the rate influence on the functions of f_c , \tilde{f}_c , $\dot{\epsilon}$ or $\dot{\sigma}$ for a water-saturated chalk with 40% porosity and $1.44 \cdot 10^{-15} \text{ m}^2$ permeability. Upper half: Strain rate in s^{-1} . Stress rate in MPa/s. Note the factor of 0.0004 (in MPa^{-1} , Equation 3.7) is not included here for the stress rate term. Lower half: Strain rate in s^{-1} . Stress rate in 10^{-1} GPa/s . f_c in s^{-1} .

3.3.3 Creep

The creep index of a material together with the compression index gives the b-factor (Equation 2.5 on page 18) and hence this is investigated in order to be able to compare results with Equation 3.8. An extensive data set on creep of

chalk is given in Priol et al. (2007). Figure 3.6 gives the creep index values from this data set and fitting with the Biot critical frequency yields

$$\epsilon_s = 0.08 \tilde{f}_c^{-1} \sigma_{\text{axial}} + c, \quad (3.9)$$

with ϵ_s in fractions, and the factor 0.08 in MPa^{-1} . The constant c is small and not similar for the three fluid saturations. This is because the correlations are based on creep index values beyond yield and the yield point is different for each fluid. The creep index values are for the transient creep region.

Figure 3.7 shows the compression index for the same data set. The oil regression line is steeper than the water regression line while the yield strength is higher for oil-saturated chalk than for the dry state and the water-saturated chalk. The end of next chapter presents the b-factor results but first the main results from the analysis are presented at the beginning of the next chapter.

Figure 3.6:

Stress and fluid dependent creep index values. High pressure oedometer data set recalculated from Priol et al. (2007). The outlier for oil is omitted from the fit. Regression lines:

Water:

$$y = 8.07 \cdot 10^{-4} \cdot x - 1.84 \cdot 10^{-3}$$

Oil:

$$y = 2.59 \cdot 10^{-4} \cdot x - 7.48 \cdot 10^{-4}$$

Dry:

$$y = 5.67 \cdot 10^{-5} \cdot x + 7.03 \cdot 10^{-4}$$

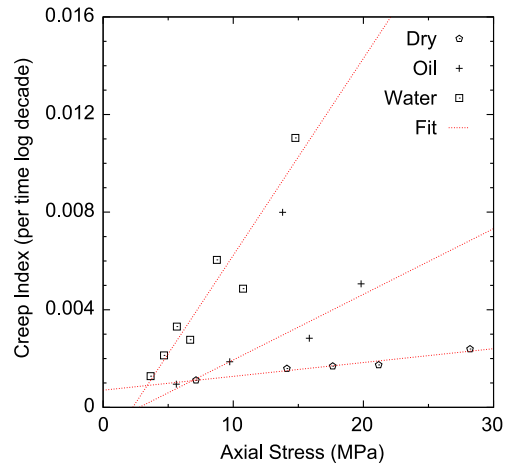


Figure 3.7:

Stress and strain path for the high pressure oedometer data set in Figure 3.6, recalculated from Priol et al. (2007). Regression lines:

Water:

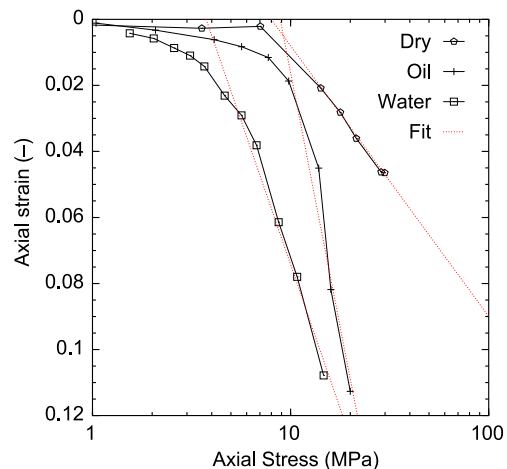
$$Q = 0.1923 \text{ per stress log decade.}$$

Oil:

$$Q = 0.308 \text{ per stress log decade.}$$

Dry:

$$Q = 0.0845 \text{ per stress log decade.}$$



Chapter 4

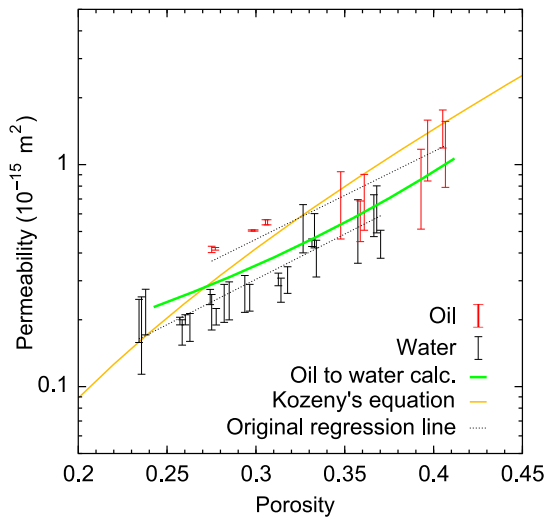
Results

The results are collected here from the analysis and investigation of the correlation between critical frequency and the failure and pore collapse properties. This chapter also includes the supplementary test series and comprises the results from the calculations on the time-dependent behaviour. First, a section presenting a test of the electrical skin depth concept.

4.1 Electrical Skin Depth

There exist fluid effects on the permeability observed in the Pasachalk project (Pasachalk, 2000, p. 22) on a large number of specimens. The water flow gives a lower permeability than oil flow (Figure 4.1). An electrical skin depth consisting of ions in the water being hindered to move by the calcite surface charge would result in the same observation. Based on the permeability trend line

Figure 4.1: Test of the skin depth hypothesis using a water film thickness of 5.52 nm. Each bar represents a large number of permeability test results for Liège chalk. The calculated water permeability from the oil regression line falls closely to the measured water permeability. Dataset from the Pasachalk (2000) project.



and the skin depth obtained from the Debye length for equilibrated water at 20 °C, Equation 3.4 and Equation 3.1 result in the green curve on Figure 4.1. Consequently, the behaviour is reproduced by assuming an electrical skin depth. Including Kozeny's relation (Equation 3.1) between porosity and permeability on the same plot is to show the general theoretical prediction.

4.2 Biot Critical Frequency in Failure and Pore Collapse

The main result of this thesis is the p' - q plot in Figure 4.2. The plot comprises the laboratory results collected (listed in Table 2.1) and totals 636 test results. The failure-yield with dashed lines are drawn to provide a guide to the eye as to where an envelope relating to similar strengths would be expected to plot. Andreassen and Fabricius (2010b, Paper I) states the equation for the envelope.

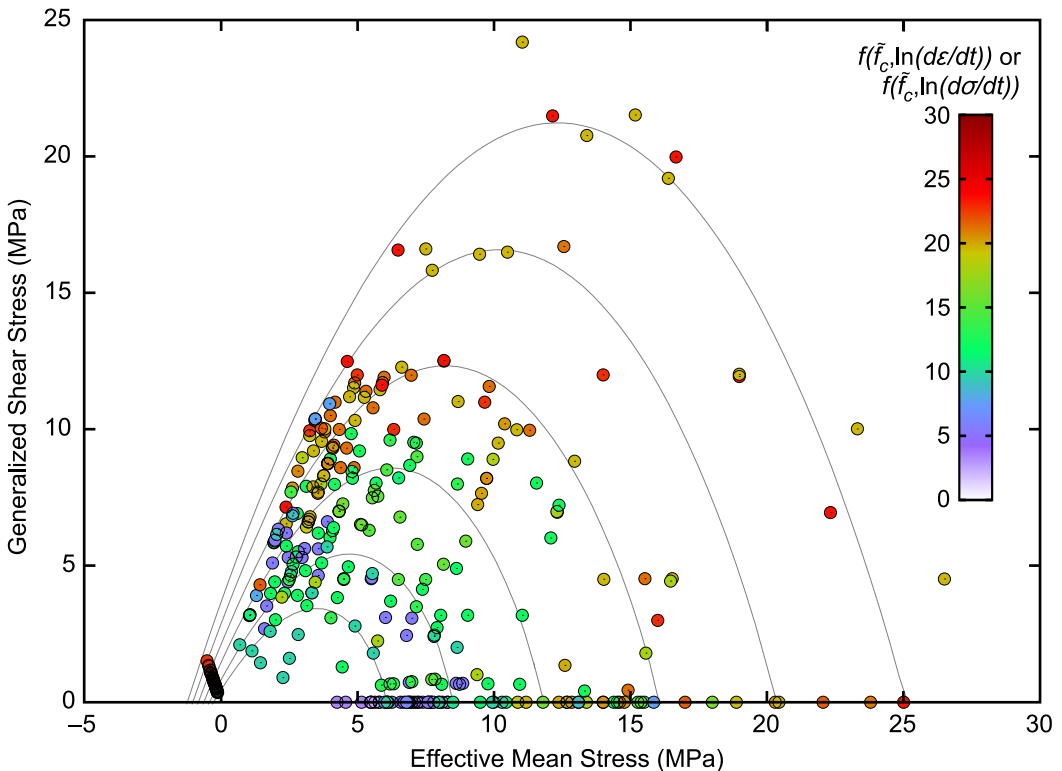
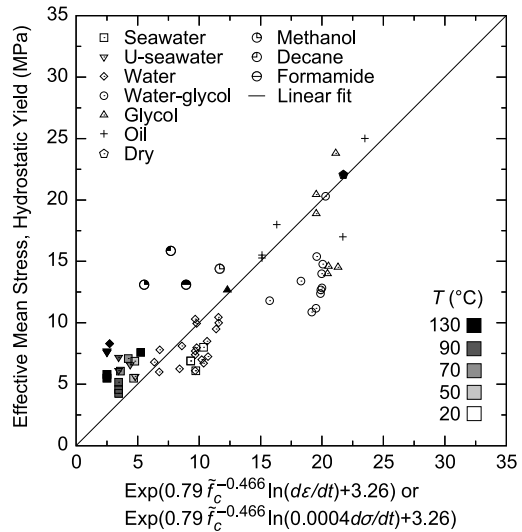


Figure 4.2: Main result in a p' - q plot covering all gathered data. Each circle is one result from either a Brazil, unconfined compression, triaxial or hydrostatic test and either a failure or yield strength. The function of Biot critical frequency and strain or stress rate (Equation 3.6 and 3.7) yields the colour grading. Note that the failure-yield envelopes drawn at regular intervals are only guide to the interpretation.

An overall connection between higher strength from the test results correlates with the higher function values, although a scattering is clearly present.

Extracting three sets of data for a closer look gives Figure 4.3 for the hydrostatic tests, Figure 4.5 for the Brazilian tests, and Figure 4.6 for the UCS tests. This makes it possible to include both temperature and fluid information in the plots. There exists a trend with higher strength correlated with higher value of

Figure 4.3:
Yield strength for both strain and stress rate controlled hydrostatic tests with specification of pore fluid and temperature.



the Biot critical function combined with the stress or strain rate. The methanol- and decane-saturated chalk have a high strength and do not fit the overall correlation. The decane-saturated result is from the data series by [Rhett and Lord \(2001\)](#) at 130 °C. Another data series on dodecane-saturated chalk from [Schroeder and Shao \(1996\)](#) gives a weaker strength at 20 °C. As dodecane and decane both are paraffins with viscosity and density not far from each other the observed difference in strengths causes concerns.

Figure 4.4:
Location of the water-glycol mixtures with marked mol% water for a subset of the hydrostatic tests in Figure 4.3.

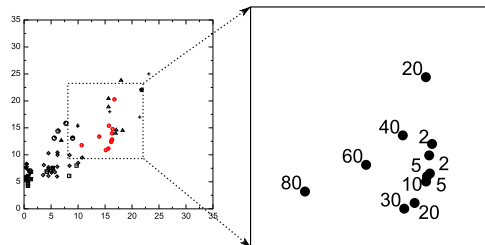
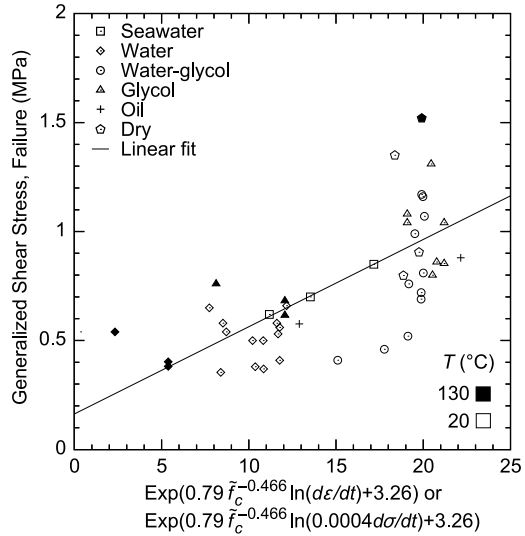


Figure 4.4 gives the specific locations of the two test series by [Risnes et al. \(2005\)](#) with different water-glycol mol% mixtures. This is a good example of

the variability stemming from test series on two different chalk blocks, with the 20–40–60–80 series giving a stronger response. The increasing water fraction affects the fluid viscosity and density and in turn this fits the overall correlation between strength and Biot critical frequency and rate function. The low water fractions weaken the chalk comparatively more than the higher water fractions.

Figure 4.5:
Failure strength for both strain and stress rate controlled Brazilian tests with specification of pore fluid and temperature.
Regression line: $y = 0.04x + 0.25$.



Additionally, the data from [Korsnes et al. \(2006; 2008a\)](#) (the high temperature tests with water having different chemical composition located at the bottom and to the far left) plots with a very low $f(\tilde{f}_c, \dot{\epsilon})$ value because the tests were performed at a low strain rate. These test series and [Korsnes et al. \(2008b\)](#) are the only ones performed with continuous fluid flow making the tests not fully comparable with the other tests.

The mapping between the yield strength and $f(\tilde{f}_c, \dot{\epsilon})$ or $f(\tilde{f}_c, \dot{\sigma})$ is 1:1 for the hydrostatic plot. For the Brazilian and unconfined compression plots the function on the x -axis is the same but the q value (y -axis) is different. Therefore, it is not a 1:1 fitting line in [Figure 4.5](#) and [4.6](#).

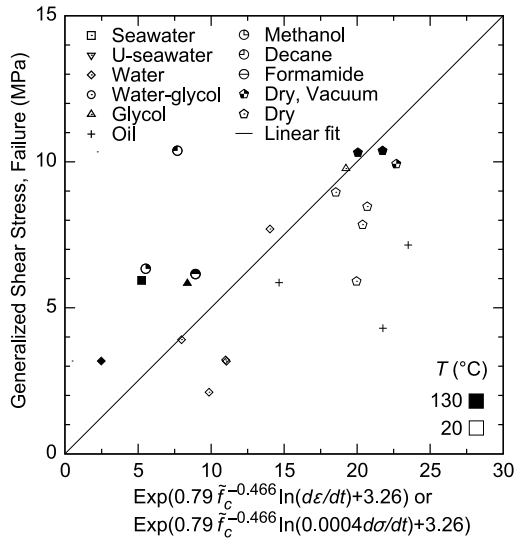
For the Brazilian test results there is a good correlation for the three results with high content of salts, 100–250 g/l NaCl and 50–700 g/l $\text{CaCl}_2 \cdot 2\text{H}_2\text{O}$ ([Risnes et al., 2003](#)). The salt content changes the viscosity and density of the fluid and hence the $f(\tilde{f}_c, \dot{\epsilon})$ value.

The unconfined compression tests clearly show the strengthening with temperature for dry chalk. Glycol-saturated chalk show weakening from 20 °C to 130 °C. Further comments on this plot are brought in the next section with incorporation of the supplementary test series.

Figure 4.6:

Failure strength for both strain and stress rate controlled unconfined compression tests with specification of pore fluid and temperature. The two failure points for the high viscosity oil-saturated chalk are outliers from their respective test series and may represent very weak chalk specimens.

Regression line: $y = 0.5x$.



4.3 Supplementary Experimental Test Series

Figure 4.7 gives an overview of the observed failure planes for the supplementary test series. The locations of the failure planes indicate longitudinal splitting type failure (Jaeger et al., 2007). One test result (SC50 A) is an outlier showing weak failure

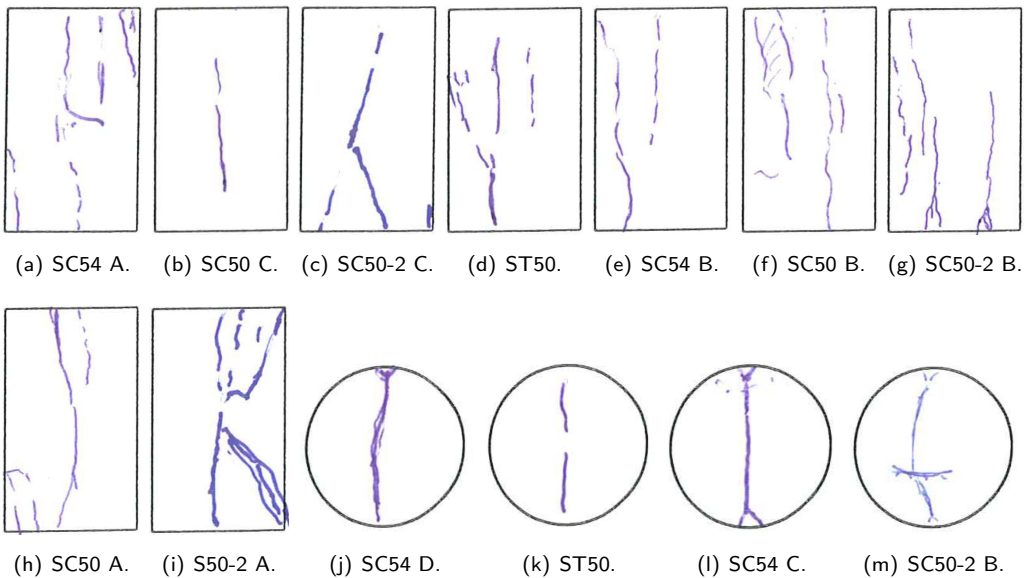
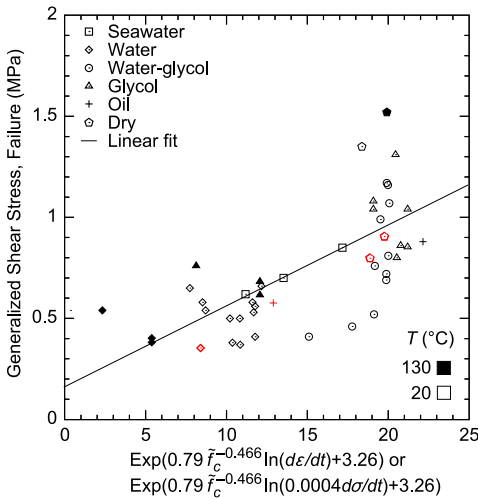


Figure 4.7: Sketches of failure planes for the supplementary test series. Sketch (h) show chipping at the bottom edge leading to premature failure. Sketches (j) to (m) are the Brazilian tests.

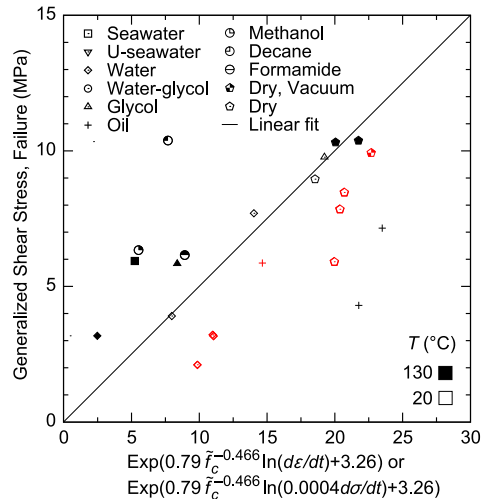
Specimen	Fluid	σ_c (MPa)	$\dot{\epsilon}$ (%/hour)
— UCS —			
SC54 A	Water	2.1	3.4
SC50 C	Water	3.2	1.8
SC50-2 C	Water	3.2	1.9
ST50	Isopar-L	5.9	2.8
SC54 B	Dry	5.9	3.0
SC50 B	Dry	7.9	2.4
SC50-2 B	Dry	8.5	3.0
SC50 A	Dry, low pres.	4.4	1.8
SC50-2 A	Dry, low pres.	9.9	2.3
— Brazilian —			
SC54 D	Water	0.35	
ST50	Isopar-L	0.58	
SC54 C	Dry	0.80	
SC50-2 B	Dry	0.91	

Table 4.1: The results for the supplementary experimental test series.

behaviour due to chipping at the bottom edge and the further analysis omits this result. The failure strengths and corresponding strain rates measured from the strain read-out follow in Table 4.1.



(a) Brazilian results. Similar to Figure 4.5.



(b) UCS results. Similar to Figure 4.6.

Figure 4.8: The supplementary test results in red. A good fit exists between the chalk failure strength and the critical frequency function.

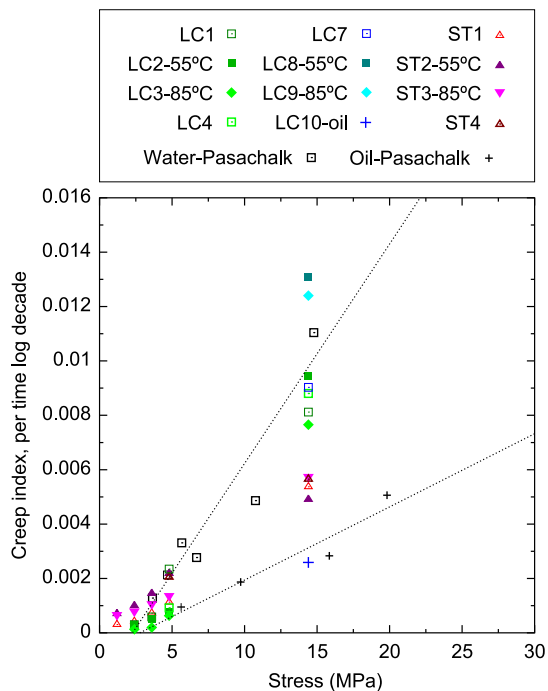
The data are marked with red in Figure 4.8 and they show a good correlation between $f(\tilde{f}_c, \dot{\epsilon})$ and failure strength. One dry specimen seems weak and falls below the two other results. The unconfined compression test under low absolute pressure responds stronger than dry chalk at ambient pressure. Stress concentration can according to Mogi (2007) decrease the measured strength of the chalk and this seems the case for the UCS results. The specimen lengths are not fulfilling the L/D -ratio of 2 because of the closed cell set-up and this should be taken into account when designing future test equipments.

4.4 Time-Dependent Behaviour and the b-Factor

An additional supplementary test series is Figure 4.9 for creep index at different temperatures and for two chalk types. The Liège chalk (LC) has an average porosity of 44.0% and the Stevns chalk (ST) has an average porosity of 38.8%. Appendix A presents the classification and creep index data. The creep index does not show a clear temperature weakening with the LC data at 85 °C having a lower creep index than the LC data at 55 °C. The ST data plot in one group but with a lower creep index in accordance with its lower porosity. The oil-saturated LC10 specimen conform to the previous Pasachalk oil-data (Figure 3.6).

Figure 4.9:

Oedometer creep data results on two chalk types: Stevns (ST) and Liège (LC). Classification data in Table A.1 on page 60. Pasachalk data series and regression lines for oil and water are the same as in Figure 3.6 (on page 29). All results are for water-saturated chalk except LC10 and the Oil-Pasachalk series.

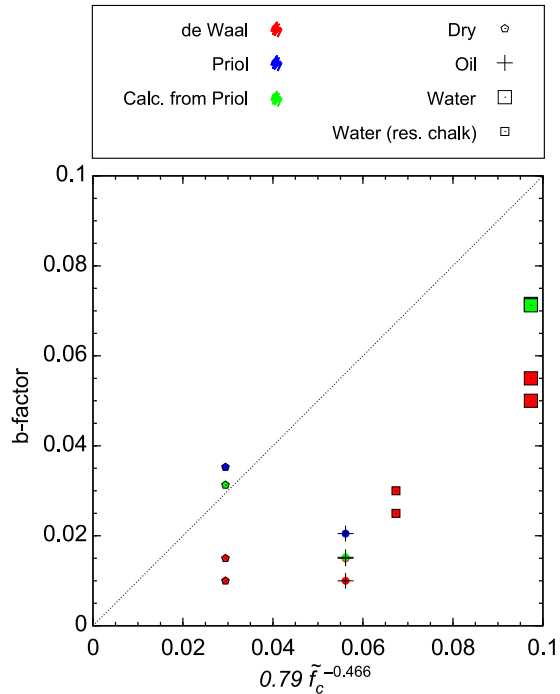


One other mechanism influences the chalk behaviour, the history of the loading affecting the current porosity and hence the strength of the chalk. This is seen from LC7, LC8, and LC9 with higher creep index values than LC1, LC2, LC3, and LC4, which have been subjected to more creep phases and so compacted more.

A test of the time dependent correlations is given in Figure 4.10. The material parameter b determined from the creep index of Figure 3.6 and the corresponding compression index of Figure 3.7 are one data set. Another is calculated from the compression index (Figure 3.7) and by using Equation 3.9. The last data set is from Smits et al. (1988), with an assumed porosity of 0.4 for the data for outcrop chalk and 0.3 for the North Sea reservoir chalk as these are not characterised in the reference. The b -factors increase with increasing value of $0.79\tilde{f}_c^{-0.466}$ independent of origin of the data whether the chalk is saturated with water, oil or dry (except for two data points). Remark that the trend do not conform to the 1:1 line.

Figure 4.10:

Those stated by Smits et al. (1988) for dry, oil, and water saturated outcrop chalk (porosity 0.4) and water saturated North Sea reservoir chalk (porosity 0.3) are marked with red. The creep data presented in Figure 3.6 and 3.7 combines in Equation 2.5 to give the b -factors with blue color. Using both Equation 2.5 and Equation 3.9 with the known Q values gives the b -factors with green color. Data from Priol et al. (2007) and de Waal (1986), Smits et al. (1988).



A general discussion of the different results continues in the next chapter.

Chapter 5

Discussion

A central discussion on the topic of applying the Biot critical frequency is whether the correlation observed imply causality, i.e. is the solid-fluid friction causing the strengthening or weakening of the chalk as proposed? This chapter also covers a discussion of the concept of electrical skin depth and the implications. Issues with the strain and stress rate dependence are mentioned together with short comments on the supplementary test series. Finally, the b-factor is discussed in terms of being a material parameter.

5.1 Causality

First, it is highlighted that the database of 636 results with more than 20 different fluid types (counting water with different chemical composition as one type each) is very broad and form an adequate base for investigation of which physical parameters influence the failure and pore collapse of chalk.

It is new that the fluid viscosity and density form part of the correlating parameters. The review in Chapter 2 shows that previously proposed mechanisms do not consider this. The porosity and hereby the permeability is known to correlate with the strength attributes.

The causality between using the Biot critical frequency compared to using other central properties is investigated on porosity divided by permeability and fluid viscosity divided by fluid density in [Andreassen and Fabricius \(2010b, Paper I\)](#). For the viscosity divided by the fluid density, there is an overall trend linking the results from different saturating fluids, whereas results with the same pore fluid give identical fractions. The porosity divided by permeability gives a weak trend. These two effects combine through the use of the Biot critical frequency and this signifies the need to incorporate all four properties: Porosity, permeability, fluid viscosity, and fluid density.

There exists a slow propagating wave for porous material subjected to an acoustic signal and therefore the critical frequency is a measure of the friction

on the fluid from the solid (Johnson et al., 1987). What is shown in this thesis is that there exists an overall correlation between this mechanism and the failure and pore collapse strengths. Strictly speaking, the correlation does not show in what manner the critical frequency influence the strength of chalk. The draining of the fluid from the pore space appears to be the cause and this lead to considerations of the impact from effective stress, drainage paths and specimen size.

It is interesting that the correlation is valid for both pore collapse and the shear failure. When assuming that a certain energy needs to be applied to a specimen to reach the point in which the specimen will go into failure or into pore collapse, a higher solid-fluid friction will dissipate more energy compared to a lower friction and consequently the chalk in the high-friction case will need more energy to be applied before the specimen enters the critical state.

5.2 Electrical Skin Depth

The concept of an electrical skin depth affecting the available porosity for fluid flow and hence the permeability is similar to a double layer or diffuse layer comprising both the ions adsorbed on the calcite surface and the ions screening the charge on the surface. The latter ions are not free to move as the ions in the rest of the fluid. It is assumed here that the screening length is similar to the stationary layer of fluid near the pore wall. The size of one water molecule is approx. 0.4 nm (density of water divided by its atomic weight) and it can be seen that the screening length in synthetic seawater is very close to one layer of water molecules (Table 3.3 on page 24). Accordingly, the concept of electrical skin depth is not a dominating effect for seawater but for equilibrated water it affects a chalk with 40% porosity to have an effective porosity of approx. 38% (Andreassen and Fabricius, 2010b, Paper I) and therefore is not negligible. It is not new to use the concept of a double layer for chalk but it is new to quantify it and use it in relation to permeability.

Often the wettability is used as an explanation for observed behaviour of the chalk, e.g. for the difference in permeability measured with water or oil in Figure 4.1. In this figure there are large ranges of measured permeabilities and overlap between the original regression lines although the trend is clear and support the validity of using the electrical skin depth in the calculation from permeability measured with oil to permeability measured with water.

Another consideration rising from the introduction of the electrical skin is the solid-fluid friction and whether it is influenced by this. Somehow, it should have a small influence but here it is assumed that the porosity reduction already incorporated is covering the magnitude of the influence.

Methanol poses a special case. According to Risnes and Flaageng (1999)

methanol-saturated chalk is approx. 50% stronger than water-saturated chalk. There appears to be a mix-up of Figure 6 and 8 in the paper. They report the compression test results as stronger than the yield results from triaxial tests with stress ratio of 0.9. Unfortunately, the existence of a mix-up has not been verified and thus the results are not included in this analysis. The value of critical frequency is low for methanol and do not predict methanol-saturated chalk to be stronger than water-saturated chalk. From another point of view, methanol is a polar fluid and adsorb to the calcite surface (Cooke et al., 2010) and consequently there must exist a double layer in the same manner as for water. Rhett and Lord (2001, p. 126) measure very little dissolution of calcium in pure methanol. If methanol has 1/10 of the ionic strength of equilibrated water the screening length concept would imply methanol to conform to the mechanical strength observations. Further experimental verification is indeed needed here in order to conclude if this counters the Biot critical correlation with strength.

Finally, the time effect is unaccounted for when assuming distilled water instantaneously reach ionic content similar to equilibrated water.

5.3 Strain and Stress Rate Dependence

Oedometer results determine the rate dependency applied in this thesis and consequently the function for all stress paths is based only on this. As a first approach this rests on Wood (1990, p. 420), who finds that when changing the stress path, the yield surface retains its shape, although the size of the yield surface depends on the rate. This needs to be further examined.

The stress rate dependence is not verified and establishing the relation based on the modulus is at best an estimate and at worst the difference to the strain rate dependence indicates that other mechanisms are at play. Using the previously applied stress rate by taking the level of the water-saturated stress-dependence gives a doubtful range of application, and so this term is obsolete. Investigation of the possible impact that other stress paths have is relevant in this connection.

The dimensionless critical frequency with rate dependence, where the chosen reference frequency is water at 20 °C, does not map low strain rates and high temperature well at the same time. A suggestion in order to mend this flaw is to choose another reference temperature.

5.4 Supplementary Test Series

The test series with the application of low pressure to dry specimens conform to the solid-fluid friction theory on strength of chalk. There is a good correlation

between failure and critical frequency for this single test series. The chalk with pore pressure below atmospheric pressure is stronger than the dry chalk at atmospheric pressure. Note verification normally require more than one test in order to be significant.

5.5 The Material Constant: The *b*-Factor

The derivation of the *b*-factor from the strain rate test series demonstrate the integrate implications from the Biot critical frequency concept. The *b*-factor seems to follow a lower trend in Figure 4.10 with some initial scattering. Again, this should be further investigated because the lower trend could mask an influence from other properties, e.g. cementation. Still, the deduction from the above is that the *b*-factor must be based on the solid-fluid friction according to the theoretical framework here.

5.6 Temperature Effects

To return to the effect sought after in the first place: The effect of temperature on the mechanical properties. The temperature influences the critical frequency because the fluid viscosity is highly sensitive to temperature. The influence by temperature on fluid density is comparatively smaller. The electrical skin depth has a direct absolute temperature dependence and can as such influence the water-saturated chalk. The rate dependence as well as the material constant from above result in temperature dependence owing to the critical frequency.

Actually, in the line of development of the critical frequency model there is not included consideration of the solid material response to change in temperature. Similarly, Charlez et al. (1992) neglect the thermal expansion of the matrix relative to the fluid expansion.

Many of the above topics points to a need for further investigations and suggestions for these are made in the recommendations for future work chapter following after a recap with conclusions.

Chapter 6

Conclusion

The Biot critical frequency can be used as a friction factor in fully saturated chalk. It is a measure to quantify the impact a fluid has on a low-cemented, high-porous chalk. I find that the critical frequency with rate dependence is correlated to both the failure and the yield results obtained from standard rock mechanical tests: Brazilian, unconfined compression, hydrostatic, and triaxial tests. Additionally, I find that the critical frequency with rate dependence is correlated to the creep index beyond yield and the material dependent b-factor.

I introduce an effective porosity calculated from the electrical skin depth ranging from the solid into the fluid. The electrical skin depth properly predicts the water permeability from measured oil permeability.

The critical frequency correctly estimates the decrease in strength properties with increasing temperature for fluid-saturated chalk and the increase for dry chalk strength with increasing temperature or at low pressure. The incorporation of rate dependence form a basis for comparing test results independent of time scale and pore space fluid. The b-factor is proposed to be dominated by the solid-fluid friction.

The original hypothesis on temperature influence of mechanical properties in chalk being related to an Arrhenius equation has been definitely substituted by a combined effect of the Biot critical frequency which includes temperature effects through the basic fluid parameters. A practical outcome is that using the critical frequency in reservoir engineering purposes makes it possible to scale laboratory test series with temperature and strain rates.

It is a new finding that the fluid viscosity and density form part of the correlating parameters. It is also new to include an electrical skin depth and refer the porosity reduction to this. Additionally, it is new to show an integration between strain rate and b-factor with specification of which physical properties affect these.

Chapter 7

Recommendations for Future Work

Below I give directions for further research and the list contains my suggestions on how to test the theory rigorously:

- The failure mechanism for the high-porosity, low-cementation chalk assumed to be of a different nature than more cemented material requires verification.
- The fluid effect remains to be analysed for the internal friction angle and cohesion. Even though this is contained in the p' - q shear failure it has not been formally compared across test series, which state them directly.
- It is necessary to improve the $f(\tilde{f}_c, \dot{\epsilon})$ and $f(\tilde{f}_c, \dot{\sigma})$ functions to better plot the high-temperature, low-strain rate data.
- To further investigate the use of the Biot critical frequency, it is essential to obtain results from low-cemented chalk with a larger interval of porosity and permeability.
- Explore both the strain and stress rate dependence for other stress paths.
- The unmatched strength to the critical frequency for methanol requires further investigation.
- I am curious to observe the critical frequency directly, and that can be done with measurement of the slow wave, but reportedly by [Bourbié et al. \(1987\)](#) the fluid should have low viscosity and the material high permeability.
- In the course of the review the zeta potential have been mentioned, which determines the slipping plane for the fluid, and therefore could be compared with the use of the screening length. A survey looking further into

this might provide more on the thickness of the double layer in chalk and its actual importance in rock mechanical phenomena.

- Numerical modelling of an appropriate constitutive relation incorporating the Biot critical frequency is suggested.
- A consequence analysis for reservoir modelling incorporating changes in pore fluids due to water or gas injection.
- It would be interesting if the theory could be applied on other geologic materials.

Bibliography

- Adam, L., Batzle, M., Lewallen, K. T., and van Wijk, K. (2009). Seismic wave attenuation in carbonates. *J. Geophys. Res.*, 114:B06208. [2.3](#)
- Addis, M. A. and Jones, M. E. (1990). Mechanical behaviour and strain rate dependance of high porosity chalk. In *Proceedings of the International Chalk Symposium held at Brighton Polytechnic on 4–7 September 1989*. Thomas Telford. [2.1](#), [2.1](#)
- Andersen, M. A. (1995). *Petroleum Research in North Sea Chalk. Joint Chalk Research, Phase IV*. RF — Rogaland Research, Prof. Olav Hanssensvei 15, P. O. Box 2503 Ullandhaug, N-4004 Stavanger, Norway. [1.1](#), [2.1](#)
- Andersen, M. A., Foged, N., and Pedersen, H. F. (1992). The rate-type compaction of a weak North Sea chalk. In *Rock Mechanics Proceedings of the 33rd U.S. Symposium*, pages 253–261. American Society of Civil Engineers. [2.1](#), [2.4](#)
- Andrade, E. N. d. C. (1910). The Viscous Flow in Metals and Allied Phenomena. In *Proc. R. Soc. A*, volume 84, pages 1–12, London. [2.4](#)
- Andreassen, K. and Fabricius, I. (2010a). Biot critical frequency applied as common friction factor for chalk with different pore fluids and temperatures. In *Paper ARMA 10-453 presented at the 44th US Rock Mechanics Symposium and 5th U.S.-Canada Rock Mechanics Symposium, Salt Lake City, Utah, June 27–30*. [3.1.1](#)
- Andreassen, K. A. and Fabricius, I. L. (2010b). Biot critical frequency applied to description of failure and yield of highly porous chalk with different pore fluids. *Geophysics*, 75(6):E205–E213. [2.1](#), [3.1](#), [3.1.1](#), [4.2](#), [5.1](#), [5.2](#)

- Andreassen, K. A. and Fabricius, I. L. (2010c). Water weakening of chalk explained from a fluid-solid friction factor. In *Paper presented at Rock Mechanics in the Nordic Countries Conference, 9–12 June, Kongsberg, Norway*. 3.3.2
- Andreassen, K. A., Fabricius, I. L., and Foged, N. N. (2010). Biot critical frequency applied as common friction factor for pore collapse and failure of chalk with different pore fluids and temperatures. In *SPE Paper MS-130447 presented at the SPE Europec/EAGE Annual Conference and Exhibition, Barcelona, Spain, 14–17 June*. 3.3.2
- Andreassen, K. A., Fabricius, I. L., and Foged, N. N. (2011). Biot critical frequency applied as common friction factor for pore collapse and failure of chalk with different pore fluids and temperatures. *SPE Journal*, SPE-130447-PA. Accepted for publication. 2.1, 3.2
- Ashby, M. F. and Jones, D. R. H. (1996). *Engineering materials – 1: An introduction to their properties and applications*. Pergamon Press, 2nd edition. 1.1.2
- Austad, T., Strand, S., Madland, M. V., Puntervold, T., and Korsnes, R. I. (2008). Seawater in chalk: An EOR and compaction fluid. *SPE Reservoir Evaluation & Engineering*, 11(4):648–654. 2.2
- Barr, G. (2003). *International critical tables, e-book, accessed 11 June 2009*, chapter Viscosity of aqueous solutions of non-electrolytes, page 22. Knovel. 2.2
- Baud, P., Vinciguerra, S., David, C., Cavallo, A., Walker, E., and Reuschlé, T. (2009). Compaction and failure in high porosity carbonates: Mechanical data and microstructural observations. *Pure and Applied Geophysics*, 166(5):869–898. 2.1, 2.2
- Bell, F. G. (1977). A note on the physical properties of the chalk. *Engineering Geology*, 11(3):217–225. 2.2
- Biot, M. A. (1956a). Theory of propagation of elastic waves in a fluid-saturated porous solid. I. Low-frequency range. *The Journal of the Acoustical Society of America*, 28(2):168–178. 2.5
- Biot, M. A. (1956b). Theory of propagation of elastic waves in a fluid-saturated porous solid. II. Higher frequency range. *The Journal of the Acoustical Society of America*, 28(2):179–191. 2.5
- Boozer, G. D., Hiller, K. H., and Serdengecti, S. (1963). Effects of pore fluids on the deformation behavior of rocks subjected to triaxial compression. In *Proc. 5th US Rock Mech. Symp., USA*, pages 579–625. 2.2

- Boresi, A. P. and Schmidt, R. J. (2003). *Advanced mechanics of materials*. John Wiley & Sons, 6th edition. 2.4
- Bourbié, T., Coussy, O., and Zinzner, B. (1987). *Acoustics of porous media*. Editions Technip. 2.5, 2.5, 3.2, 7
- Carter, N. L. and Kirby, S. H. (1978). Transient creep and semibrittle behavior of crystalline rocks. *Pure and Applied Geophysics*, 116:807–839. 1.1.2
- Charlez, P. A., Heugas, O., and Shao, J. (September 21–23, 1992). Effect of Temperature on Mechanical Properties of Chalk. *Fourth North Sea Chalk Symposium, Deauville, France*. 2.2, 5.6
- Collin, F., Cui, Y. J., Schroeder, Ch., and Charlier, R. (2002). Mechanical behaviour of lixhe chalk partly saturated by oil and water: experiment and modelling. *International Journal for Numerical and Analytical Methods in Geomechanics*, 26(9):897–924. 2.1, 2.2
- Collin, F., Gennaro, V. D., Delage, P., and Priol, G. (2008). An elasto-viscoplastic model for chalk including suction effects. In D. G. Toll, C. E. Augarde, D. G. and Wheeler, S. J., editors, *Unsaturated Soils. Advances in Geo-Engineering, Proceedings of the 1st European Conference, E-UNSAT 2008, Durham, United Kingdom, 2-4 July 2008*, chapter 85, pages 633–639. Taylor & Francis. 2.2
- Cooke, D. J., Gray, R. J., Sand, K. K., Stipp, S. L. S., and Elliott, J. A. (2010). Interaction of ethanol and water with the $\{10\bar{1}4\}$ surface of calcite. *Langmuir*, 26(18):14520–14529. 2.3, 5.2
- CRC (2008). CRC Handbook of Chemistry and Physics. e-book, <http://www.hbcponline.com/>, accessed 11 June 2009. 2.2
- Croizé, D., Renard, F., Bjørlykke, K., and Dysthe, D. K. (2010). Experimental calcite dissolution under stress: Evolution of grain contact microstructure during pressure solution creep. *Journal of Geophysical Research-Solid Earth*, 115:B09207. 2.2
- De Gennaro, V., Delage, P., Cui, Y. J., Schroeder, Ch., and Collin, F. (2003). Time-dependent behaviour of oil reservoir chalk: A multiphase approach. *Soils and Foundations, Journal of the Japanese Geotechnical Society*, 43(4):131–147. 2.2
- De Gennaro, V., Delage, P., and Priol, G. (2005a). Multiphase time dependent compression behaviour of two chalks. In Barla, G. and Barla, M., editors, *IACMAG*, volume 2. 2.2

- De Gennaro, V., Delage, P., Priol, G., Collin, F., and Cui, Y.-J. (2004). On the collapse behaviour of oil reservoir chalk. *Geotechnique*, 54(6):415–420. [1.1.2](#), [2.2](#), [3.1.1](#)
- De Gennaro, V. and Pereira, J. M. (2008). Viscoplastic modelling of unsaturated geomaterials. In *The 12th International Conference of International Association for Computer Methods and Advances in Geomechanics (IACMAG)*, Goa, India. [2.6](#), [3.4](#)
- De Gennaro, V., Sorgi, C., and Delage, P. (2005b). Air-water interaction and time dependent compressibility of a subterranean quarry chalk. In *Post-Mining 2005, November 16–17, France*. [2.2](#)
- de Waal, J. A. (1986). *On the rate type compaction behaviour of sandstone reservoir rock*. Ph.D. dissertation, Technische Hogeschool Delft, The Netherlands. [2.4](#), [2.5](#), [†](#), [3.3.1](#), [4.10](#)
- Delage, P., Schroeder, Ch., and Cui, Y. J. (1996). Subsidence and capillary effects in chalks. In *Eurock*, pages 1291–1298. [2.1](#), [2.1](#), [2.2](#)
- Dong, M. and Chatzis, I. (1995). The imbibition and flow of a wetting liquid along the corners of a square capillary tube. *Journal of Colloid and Interface Science*, 172(2):278–288. [2.1](#), [2.2](#)
- Engstrøm, F. (1992). Rock mechanical properties of Danish North Sea chalk. In *Fourth North Sea Chalk Symposium, September 21–23, Deauville, France*. [2.1](#)
- Fabre, D. and Gustkiewicz, J. (1997). Poroelastic properties of limestones and sandstones under hydrostatic conditions. *International Journal of Rock Mechanics and Mining Sciences*, 34(1):127–134. [2.1](#)
- Fabricius, I. L., Bächle, G. T., and Eberli, G. P. (2010). Elastic moduli of dry and watersaturated carbonates — effect of depositional texture, porosity and permeability. *Geophysics*, 75(3):N65–N78. [2.5](#)
- Fjær, E., Holt, R. M., Horsrud, P., Raaen, A. M., and Risnes, R. (2008). *Petroleum related rock mechanics*. Developments in Petroleum Science 53. Elsevier, 2nd edition. [2.1](#), [2.1](#), [2.4](#)
- Gutierrez, M., Øino, L. E., and Høeg, K. (2000). The effect of fluid content on the mechanical behaviour of fractures in chalk. *Rock Mechanics and Rock Engineering*, 33(2):93–117. [2.2](#), [2.3](#)
- Hassenkam, T., Skovbjerg, L. L., and Stipp, S. L. S. (2009). Probing the intrinsically oil-wet surfaces of pores in north sea chalk at subpore resolution. *Proceedings of the National Academy of Sciences*, 106(15):6071–6076. [2.2](#)

- Heggheim, T., Madland, M. V., Risnes, R., and Austad, T. (2005). A chemical induced enhanced weakening of chalk by seawater. *Journal of Petroleum Science and Engineering*, 46(3):171–184. [2.2](#), [2.3](#)
- Hellmann, R., Renders, P. J. N., Gratier, J. P., and Guiguet, R. (2002). Experimental pressure solution compaction of chalk in aqueous solutions Part 1. Deformation behavior and chemistry. In Hellmann, R. and Wood, S. A., editors, *Water-Rock Interactions, Ore Deposits, and Environmental Geochemistry, A Tribute to David A. Crerar, The Geochemical Society, Special publication No. 7*, pages 129–152. [1.1.2](#), [2.2](#)
- Hickman, R. J. (2004). *Formulation and Implementation of a Constitutive Model for Soft Rock*. Ph.D. dissertation, Virginia Polytechnic Institute and State University, Department of Civil Engineering. [2.1](#), [2.2](#), [2.3](#)
- Hickman, R. J., Gutierrez, M. S., Gennaro, V. D., and Delage, P. (2008). A model for pore-fluid-sensitive rock behavior using a weathering state parameter. *International Journal for Numerical and Analytical Methods in Geomechanics*, 32(16):1927–1953. [2.1](#)
- Hjuler, M. L. (2007). *Diagenesis of upper cretaceous onshore and offshore chalk from the North Sea area*. Ph.D. dissertation, Technical University of Denmark, Department of Environmental Engineering. [1.1.1](#), [1.4](#), [1.1.2](#)
- Hjuler, M. L. and Fabricius, I. L. (2009). Engineering properties of chalk related to diagenetic variations of upper cretaceous onshore and offshore chalk in the north sea area. *Journal of Petroleum Science and Engineering*, 68(3-4):151–170. [1.1.1](#)
- Holloway-Strong, M. U., Hughes, S. J., and Hellowell, E. E. (2007). Stress-deformation behavior of chalk. *International Journal of Geomechanics*, 7(6):403–409. [2.1](#)
- Homand, S. and Shao, J. F. (2000). Mechanical behaviour of a porous chalk and water/chalk interaction. Part I: Experimental study. *Oil & Gas Science and Technology – Rev. IFP*, 55(6):591–598. [2.3](#)
- Hu, L. B. and Hueckel, T. (2007). Coupled chemo-mechanics of intergranular contact: Toward a three-scale model. *Computers and Geotechnics*, 34(4):306–327. Chemo-Mechanical Interaction in Geomaterials. [2.2](#)
- Jaeger, J. C., Cook, N. G. W., and Zimmerman, R. W. (2007). *Fundamentals of rock mechanics*. Blackwell Publishing, 4th edition. [2.1](#), [2.4](#), [4.3](#)

- Johnson, D. L., Koplik, J., and Dashen, R. (1987). Theory of dynamic permeability and tortuosity in fluid-saturated porous media. *Journal of Fluid Mechanics Digital Archive*, 176(-1):379–402. 2.5, 5.1
- Johnson, J. P. and Rhett, D. W. (1986). Compaction behaviour of Ekofisk chalk as a function of stress. *Society of Petroleum Engineers*, SPE 15872:221–225. 2.1, 2.4
- Johnson, J. P., Rhett, D. W., and Siemers, W. T. (1989). Rock mechanics of the Ekofisk reservoir in the evaluation of subsidence. *Journal of Petroleum Technology*, SPE 17854:717–722. 1.1, 2.1, 2.2, 2.3, 2.4
- Kågeson-Loe, N. M., Jones, M. E., Petley, D. N., and Leddra, M. J. (1993). Fabric evolution during the deformation of chalk. *International Journal of Rock Mechanics and Mining Sciences & Geomechanics Abstracts*, 30(7):739–745. 2.1
- Knovel (1999). Chemical properties handbook. e-book, http://www.knovel.com/web/portal/browse/display?_EXT_KNOVEL_DISPLAY_bookid=49, accessed 11 June 2009. 2.2
- Korsnes, R. I. (2007). *Chemical induced water weakening of chalk by fluid-rock interactions. A mechanistic study*. Ph.D. dissertation, University of Stavanger, Department of Petroleum Engineering. 2.2
- Korsnes, R. I., Madland, M. V., and Austad, T. (2006). Impact of brine composition on the mechanical strength of chalk at high Temperature. In *Eurock 2006: Multiphysics Coupling and Long Term Behaviour in Rock Mechanics: Proceedings of the International Symposium of the International Society for Rock Mechanics, EUROCK 2006, 9–12 May 2006, Liège, Belgium*, pages 133–140. Taylor & Francis/Balkema. 2.1, 2.2, 3.2, 4.2
- Korsnes, R. I., Madland, M. V., Austad, T., Haver, S., and Røsland, G. (2008a). The effects of temperature on the water weakening of chalk by seawater. *Journal of Petroleum Science and Engineering*, 60(3-4):183–193. 2.1, 2.2, 4.2
- Korsnes, R. I., Wersland, E., Austad, T., and Madland, M. V. (2008b). Anisotropy in chalk studied by rock mechanics. *Journal of Petroleum Science and Engineering*, 62(1-2):28–35. 2.1, 4.2
- Krenk, S. (2000). Characteristic state plasticity for granular materials. Part I: Basic theory. *International Journal of Solids and Structures*, 37(43):6343–6360. 2.1
- Lade, P. V. (1982). Three-parameter failure criterion for concrete. *Journal of the Engineering Mechanics Division*, 108(5):850–863. 2.1

- Larsen, G., Frederiksen, J., Villumsen, A., Fredericia, J., Gravesen, P., Foged, N., Knudsen, B., and Baumann, J. (1995). *Vejledning i Ingeniørgeologisk prøvebeskrivelse*. Number 1 in dgf-bulletin. Danish Geotechnical Society. [1.1.1](#)
- Liow, J. L., Juusela, M., and Gray, N. B. (2001). Viscosity effects in the discharge of a two-layer liquid through an orifice. *14th Australasian Fluid Mechanics Conference, Adelaide, Australia, 10–14 December 2001*, pages 853–856. [2.1](#)
- Loe, N. M., Leddra, M. J., and Jones, M. E. (1992). Strain states during stress path testing of the Chalk. In *Rock Mechanics, Proceedings of the 33rd US Symposium*. Balkema, Rotterdam, pages 927–936. [2.1](#)
- Lord, C. J., Johlman, C. L., and Rhett, D. W. (1998). Is capillary suction a viable cohesive mechanism in chalk? In *SPE/ISRM Eurock, Norway*, pages 479–485. [2.3](#)
- Lyashchenko, A. and Karataeva, I. (2007). Relation of water activity to the static dielectric constant of concentrated electrolyte solutions. *Doklady Physical Chemistry*, 414(1):120–122. [2.2](#)
- Lyklema, J. (1991). *Fundamentals of Interface and Colloid Science*, volume I. Academic Press. [3.1.1](#), [3.1.1](#)
- Madland, M. V. (2005). *Water Weakening of Chalk: A Mechanistic Study*. Ph.D. dissertation, Faculty of Science and Technology, Department of Petroleum Engineering. Dr. Ing. thesis no. 11. [2.1](#), [2.2](#), [2.3](#)
- Madland, M. V., Finsnes, A., Alkafadgi, A., Risnes, R., and Austad, T. (2006). The influence of CO₂ gas and carbonate water on the mechanical stability of chalk. *Journal of Petroleum Science and Engineering*, 51(3–4):149–168. [2.1](#)
- Madland, M. V., Korsnes, R. I., and Risnes, R. (2002). Temperature effects in Brazilian, uniaxial and triaxial compressive tests with high porosity chalk. *SPE Annual Technical Conference and Exhibition, San Antonio, Texas, 29 September–2 October 2002*, 77761:1–11. [2.1](#), [2.2](#)
- Maury, V., Piau, J.-M., and Halle, G. (1996). Subsidence induced by water injection in water sensitive reservoir rocks: The example of Ekofisk. *Paper SPE 36890 presented at the European Petroleum Conference, 22–24 October 1996, Milan, Italy*, pages 153–169. [1.1](#)
- Mavko, G., Mukerji, T., and Dvorkin, J. (2009). *The Rock Physics Handbook: Tools for Seismic Analysis in Porous Media*. Cambridge University Press, Cambridge, 2nd edition. [2.2](#), [2.7](#), [2.5](#)

- Meigh, A. C. and Early, K. R. (1957). Some physical properties and engineering properties of chalk. In *Proc. 4th Int. Conf. Soil Mech. Found. Eng.*, volume 1, pages 68–73. [2.2](#)
- Mellor, M. and Hawkes, I. (1971). Measurement of tensile strength by diametral compression of discs and annuli. *Engineering Geology*, 5(3):173–225. [2.1](#)
- Mesri, G. and Godlewski, P. M. (1977). Time- and stress-compressibility inter-relationship. *Journal of the Geotechnical Engineering Division, Proceedings of the American Society of Civil Engineers*, 103, No. GT5:417–430. [2.4](#), [2.4](#), [2.4](#), [2.4](#), [3.3.1](#)
- Michelson, A. A. (1917). Laws of elasto-viscous flow. *Proceedings of the National Academy of Sciences of the United States of America*, 3(5):319–323. [2.1](#)
- Mogi, K. (2007). *Experimental rock mechanics Geomechanics research series*. Taylor & Francis. [4.3](#)
- Mortensen, J., Engstrøm, F., and Lind, I. (1998). The relation among porosity, permeability, and specific surface of chalk from the Gorm field, Danish North Sea. *SPE Reservoir Evaluation & Engineering*, 1(3):245–251. [3.1](#)
- Natural History Museum (2002). Science News. London. Located July 2002 on <http://www.nhm.ac.uk/science/news/coccolith.html>. Image. [1.2\(a\)](#)
- Newman, G. H. (1983). The effect of water chemistry on the laboratory compression and permeability characteristics of some North-Sea chalks. *Journal of Petroleum Technology*, 35(5):976–980. [2.2](#)
- NIST (2008). Thermophysical properties of fluid systems: webbook, accessed 23 october 2009; <http://webbook.nist.gov/chemistry/fluid/>. [2.2](#)
- Norwegian Petroleum Directorate (1997). Improved oil recovery (IOR): Different methods – What is the current status? Located July 2002 on <http://npd.no/Webdesk/netblast/pages/index.html?id=4370>. [1.1](#)
- Omdal, E., Madland, M. V., Kristiansen, T. G., Nagel, N. B., Korsnes, R. I., and Hiorth, A. (2010). Deformation behavior of chalk studied close to in situ reservoir conditions. *Rock Mechanics and Rock Engineering*, 43(5):557–580. [2.1](#)
- Palliser, C. and McKibbin, R. (1998). A model for deep geothermal brines, III: Thermodynamic properties – enthalpy and viscosity. *Transport in Porous Media*, 33(1):155–171. [2.2](#)

- Papamichos, E., Brignoli, M., and Santarelli, F. J. (1997). An experimental and theoretical study of a partially saturated collapsible rock. *Mechanics of Cohesive-frictional Materials*, 2(3):251–278. 2.2
- Pasachalk (2000). Schroeder, Ch., Illing, P., Charlier, R., Collin, F., Delage, P., Cui, Y-J., De Gennaro, V., De Leebeeck, A., Keül, P. and Bois, A.-P. (2000). mechanical behaviour of partially and multiphase saturated chalks fluid–skeleton interaction : Main factor of chalk oil reservoirs compaction and related subsidence. Technical report, Part 1. European Joule III contract No. JOF3CT970033. 2.2, 4.1, 4.1
- Pasachalk (2003). Mechanical behaviour of partially and multiphase saturated chalks fluid–skeleton interaction : Main factor of chalk oil reservoirs compaction and related subsidence. Technical report, Part 2. European Joule III contract No. ENK6-2000-00089. 2.2, 2.4, 2.6, 3.4, 3.3.1
- Pharr, G. M. and Ashby, M. F. (1983). On creep enhanced by a liquid phase. *Acta Metallurgica*, 31(1):129–138. 2.2, 2.4
- Pietruszczak, S., Lydzba, D., and Shao, J. F. (2006). Modelling of deformation response and chemo-mechanical coupling in chalk. *International Journal for Numerical and Analytical Methods in Geomechanics*, 30(10):997–1018. 2.2
- Powell, B. and Lovell, G. (1994). Mechanisms of chalk compaction. *Rock Mechanics in Petroleum Engineering*, pages 811–818. 2.1
- Priol, G., De Gennaro, V., Delage, P., and Cui, Y. (2005). *Unsaturated Soils: Advances in Testing, Modelling and Engineering Applications, On the suction and the time dependent behaviour of reservoir chalks of North Sea oilfields*, chapter 4, pages 43–54. A.A. Balkema Publishers. 2.2
- Priol, G., Gennaro, V. D., Delage, P., and Servant, T. (2007). Experimental investigation on the time dependent behaviour of a multiphase chalk. In *Experimental Unsaturated Soil Mechanics*, volume 112 of *Springer Proceedings in Physics*, pages 161–167. Springer Berlin Heidelberg. 2.2, 3.3.3, 3.6, 3.7, 4.10
- Rhett, D. W. and Lord, C. J. (2001). Water weakening in sedimentary rocks. In *DC Rocks 2001, The 38th US Symposium on Rock Mechanics (USRMS)*, pages 121–128. 2.1, 2.2, 4.2, 5.2
- Risnes, R. (2001). Deformation and yield in high porosity outcrop chalk. *Physics and Chemistry of the Earth, Part A: Solid Earth and Geodesy*, 26(1-2):53–57. 2.1, 2.2

- Risnes, R., Berg, T., Furuvald, A., and Paulsen, T. (2000). Tensional failure and solid-fluid interactions in high porosity chalk. In *The Fourth North American Rock mechanics Symposium, Seattle, USA, Pacific Rocks*. 2.1, 2.2
- Risnes, R. and Flaageng, O. (1999). Mechanical properties of chalk with emphasis on chalk-fluid interactions and micromechanical aspects. *Oil & Gas Science and Technology – Rev. IFP*, 54(6):751–758. 5.2
- Risnes, R., Garpestad, O. J., Gilje, M., Oland, L. T., Ovesen, M., and Vargervik, E. (1998). Strain hardening and extensional failure in high porosity chalk. *SPE/ISRM Rock Mechanics in Petroleum Engineering*. 2.1, 2.2
- Risnes, R., Haghighi, H., Korsnes, R. I., and Natvik, O. (2003). Chalk-fluid interactions with glycol and brines. *Tectonophysics*, 370(1-4):213–226. Physical Properties of Rocks and other Geomaterials, a Special Volume to honour Professor H. Kern. 2.1, 2.2, 2.2, 4.2
- Risnes, R. and Kleppa, E. (1996). Plastic behaviour of high porosity chalk in constant k-ratio tests. In *5th North Sea Chalk Symposium, Reims, France*. 2.1
- Risnes, R., Kristensen, C. N., and Andersen, M. (1996). Triaxial tests on high porosity chalk with different saturating fluids. In *5th North Sea Chalk Symposium, Reims, France*. 2.1, 2.2
- Risnes, R., Madland, M. V., Hole, M., and Kwabiah, N. K. (2005). Water weakening of chalk – mechanical effects of water-glycol mixtures. *Journal of Petroleum Science and Engineering*, 48(1-2):21–36. 2.1, 2.2, 2.3, 4.2
- Ruddy, I., Andersen, M. A., Pattillo, P. D., Bishlawi, M., and Foged, N. (1989). Rock compressibility, compaction, and subsidence in a high-porosity chalk reservoir - a case-study of Valhall field. *Journal of Petroleum Technology*, 41(7):741–746. 2.1
- Rutter, E. H. (1972). The influence of interstitial water on the rheological behaviour of calcite rocks. *Tectonophysics*, 14(1):13–33. 2.2
- Rutter, E. H. (1974). The influence of temperature, strain rate and interstitial water in the experimental deformation of calcite rocks. *International Journal of Geotectonics and Tectonophysics*, 22:311–334. 2.2
- Schroeder, Ch. (2002). *Du coccolithe au réservoir pétrolier. Approche phénoménologique du comportement mécanique de la craie en vue de sa modélisation à différentes échelles*. Ph.D. dissertation, Université de Liège, Faculté des Sciences Appliquées. 1.1.2, 3.2

- Schroeder, Ch., Bois, A.-P., Maury, V., and Halle, G. (1998). Water/chalk (or collapsible soil) interaction: Part II. Results of tests performed in laboratory on Lixhe chalk to calibrate water/chalk models. In *Proceedings Eurock, SPE/ISRM*, volume 98 (SPE 47587), pages 833–840, Trondheim, Norway. [2.2](#), [2.3](#)
- Schroeder, Ch. and Shao, J. (1996). Plastic deformation and capillary effects in chalks. In *5th North Sea Chalk Symposium, Reims, France*. [2.1](#), [2.1](#), [2.2](#), [4.2](#)
- Scott Jr., T. E., Abousleiman, Y., and Zaman, M. (2001). Acoustical imaging and mechanical properties of soft rock and marine sediments. Technical report, University of Oklahoma (US). Quarterly Technical Progress Report No. 15302R04. [2.1](#), [2.3](#)
- Smits, R. M. M., de Waal, J. A., and van Kooten, J. F. C. (1988). Prediction of abrupt reservoir compaction and surface subsidence caused by pore collapse in carbonates. *SPE Formation Evaluation*, 3(2):340–346. [2.1](#), [2.4](#), [4.4](#), [4.10](#)
- Sulak, R. M. and Danielsen, J. (1989). Reservoir aspects of Ekofisk subsidence. *Journal of Petroleum Technology*, 41(7):709–716. [1.3](#)
- Sylte, J. E., Thomas, L. K., Rhett, D. W., Bruning, D. D., and Nagel, N. B. (1999). Water induced compaction in the Ekofisk field. In *Paper SPE 56426 presented at the SPE Annual Technical Conference and Exhibition, 3–6 October 1999, Houston, Texas*. [1.1](#)
- Taibi, S., Duperret, A., and Fleureau, J.-M. (2009). The effect of suction on the hydro-mechanical behaviour of chalk rocks. *Engineering Geology*, 106:40–50. [2.2](#)
- Talesnick, M. and Shehadeh, S. (2007). The effect of water content on the mechanical response of a high-porosity chalk. *International Journal of Rock Mechanics and Mining Sciences*, 44(4):584 – 600. [1.1.2](#), [2.1](#)
- Ulusay, R. and Hudson, J. A. (2007). *The complete ISRM suggested methods for rock characterization, testing and monitoring: 1974-2006*. International Society for Rock Mechanics, Commission on Testing Methods. [2.1](#)
- Viksund, B. G. (1998). *Fluid flow in fractured chalk models at different wettabilities*. Ph.D. dissertation, University of Bergen, Norway. [1.1.1](#)
- Vukuturi, V. S., Lama, R. D., and Saluja, S. S. (1974). *Handbook on Mechanics Properties of Rocks*, volume I. Trans Tech Publications. [2.2](#)
- Wood, D. M. (1990). *Soil Behaviour and Critical State Soil Mechanics*. Cambridge University Press. [5.3](#)

- Xiaoping, Y., Ottosen, N. S., Thelandersson, S., and Nielsen, M. P. (1989). Review of constructive models for concrete. Technical report, JRC Scientific and Technical Reports (EUR collection). [2.1](#)
- Zhang, X. and Spiers, C. J. (2005a). Compaction of granular calcite by pressure solution at room temperature and effects of pore fluid chemistry. *International Journal of Rock Mechanics and Mining Sciences*, 42(7-8):950–960. *Rock Physics and Geomechanics*. [2.2](#)
- Zhang, X. and Spiers, C. J. (2005b). Effects of phosphate ions on intergranular pressure solution in calcite: An experimental study. *Geochimica et Cosmochimica Acta*, 69(24):5681–5691. [2.2](#)
- Zhang, X., Spiers, C. J., and Peach, C. J. (2010). Compaction creep of wet granular calcite by pressure solution at 28 degrees C to 150 degrees C. *Journal of Geophysical Research-Solid Earth*, 115:B09217. [2.2](#)

Appendix A

Supplementary creep tests

The laboratory tests described here was performed in corporation with Bertold Plischke and Niels Foged as a preliminary investigation on the temperature influence on time effects in chalk.

The test series consists of oedometer tests in a constant-rate-of-strain equipment placed in a container with a heating bath connected through a circulating pump. The temperature was raised at the beginning of the test and then kept constant. The water was saturated with chalk powder at room temperature and the specimens were submerged in this equilibrated water under evacuation when saturating the specimen. The saturation was determined by means of boyancy in the same equilibrated water or oil in the case of LC10. These measurements result in Table [A.1](#).

The friction between the inner cell wall and pressure head was corrected for. The loading rate was generally 1%/hour and creep phases were held at regular intervals resulting in Table [A.2](#).

From these results the temperature influence was not observed to follow an Arrhenius equation.

Table A.1: Supplementary creep tests at room and higher temperature.

Specimen	Fluid	T (°C)	Height (cm)	$W^{\#}$ (%)	$\varphi_{\text{original}}$ (%)	φ_{after} (%)	ρ_{bulk} (g/cm ³)	ρ_{dry} (g/cm ³)	S_{original} (%)	S_{after} (%)
ST1	Water	23	3.000	19.3	37.23	33.91	2.021	1.695	87.7	90.3
ST2	Water	55	3.000	23.5	39.70	31.68	2.019	1.635	96.8	100.9
ST3	Water	85	3.000	24.3	39.33	34.71	2.035	1.638	95.6	101.0
ST4	Water	23	3.033	20.5	38.03	32.23	2.017	1.673	90.2	96.1
LC1	Water	23	3.007	28.5	44.15	39.47	1.946	1.514	97.8	99.8
LC2	Water	55	3.013	27.6	43.81	39.39	1.943	1.523	95.9	98.0
LC3	Water	85	3.004	28.7	43.70	39.90	1.963	1.526	100.1	99.8
LC4	Water	23	3.010	27.1	44.62	39.78	1.908	1.501	91.2	98.7
LC7	Water	23	2.910	28.0	44.00	38.92	1.942	1.518	96.6	98.6
LC8	Water	55	3.000	27.6	43.02	38.83	1.970	1.544	99.0	99.6
LC9	Water	85	3.000	26.7	42.97	39.66	1.958	1.545	95.9	98.8
LC10	Isopar-L	23	1.997	24.4	43.45	–	1.860	1.535	98.7	–

#Original water content.

Table A.2: Creep index for the supplementary creep tests in Table A.1.

Specimen	Fluid	T (°C)	ϵ_s (10^{-3} fraction pr. time log decade)					
			1.2 MPa	2.4 MPa	3.6 MPa	4.8 MPa	9.6 MPa	14.4 MPa
ST1	Water	23	0.308	0.419	0.727	1.126		5.373
ST2	Water	55	0.706	0.999	1.451	2.186		4.907
ST3	Water	85	0.665	0.796	1.065	1.366		5.748
ST4	Water	23				2.051	4.679	5.653
LC1	Water	23		0.302	0.583	2.346	7.166	8.119
LC2	Water	55		0.304	0.524	0.778	6.753	9.432
LC3	Water	85		0.130	0.198	0.629	4.777	7.656
LC4	Water	23				0.919	7.230	8.803
LC7	Water	23						9.030
LC8	Water	55						13.08
LC9	Water	85						12.40
LC10	Isopar-L	23						2.590

Appendix B

Errata

List of known errors in the appended papers with the corrections marked in red and underlined:

- **Paper I** – Table 4. The Debye lengths are here calculated without taking the temperature dependence of the permittivity into account. Table **3.3** on page **24** lists the correct Debye lengths. Consequently, the reduced porosity and permeability should be recalculated based on these Debye lengths.
- **Paper II** – Equation 3, **Paper III** – Equation 11, **Paper IV** – Equation 9, and **Paper V** – Equation 3 should be

$$c = \left(4 \cos \left(\frac{1}{3} \arccos \left(\varphi \frac{8^2}{\pi^3} - 1 \right) + \frac{4}{3} \pi \right) + 4 \right)^{-1}$$

- In **Paper III**, Figure 6, the regression lines should be

$$\begin{aligned} \text{Dry: } y &= 5.67 \cdot 10^{-4} \cdot \underline{x} + 7.03 \cdot 10^{-4}, \\ \text{Oil: } y &= 2.59 \cdot 10^{-4} \cdot \underline{x} - 7.48 \cdot 10^{-4}, \\ \text{Water: } y &= 8.07 \cdot 10^{-4} \cdot \underline{x} - 1.84 \cdot 10^{-3}. \end{aligned}$$

- **Paper III**, Figure 7, “...when calculating the data points in figure **8**” should be “figure **10**”.
- In **Paper III**, Figure 9, the equations on the x -axis should be

$$\exp \left(0.79 \tilde{f}_c \ln \left(\frac{d\epsilon}{dt} \right) \underline{+3.3} \right) \text{ or } \exp \left(0.79 \tilde{f}_c \ln \left(\frac{d\sigma}{dt} \right) \underline{+3.3} \right).$$

Appendix C

Paper I

Andreassen, K.A., and Fabricius, I.L. (2010).

Biot Critical Frequency Applied to Description of Failure and Yield of Highly Porous Chalk with Different Pore Fluids.

Geophysics, 75(6):E205–E213.

Biot critical frequency applied to description of failure and yield of highly porous chalk with different pore fluids

Katrine Alling Andreassen¹ and Ida Lykke Fabricius²

ABSTRACT

Injection of water into chalk hydrocarbon reservoirs has led to mechanical yield and failure. Laboratory experiments on chalk samples correspondingly show that the mechanical properties of porous chalk depend on pore fluid and temperature. In case of water-saturated samples, the concentration and nature of dissolved salts have an effect. Water has a significant softening effect on elastic properties of chalk as calculated from wave data, and the softening increases with increasing critical frequency as defined by Biot. The critical frequency is the highest frequency where elastic wave propagation is controlled by solid-fluid friction. The reference frequency is thus a measure of this friction, and we propose that the fluid effect on mechanical properties of chalk may be the result of liquid-solid friction. We reviewed 622 published experiments on mechanical properties of porous

chalk. The data include chalk samples that were tested at temperatures from 20 °C to 130 °C with the following pore fluids: fresh water, synthetic seawater, glycol, and oil of varying viscosity. The critical frequency is calculated for each experiment. For each specimen, we calculate the thickness to the slipping plane outside the Stern layer on the pore surface. For electrolytes, the thickness of this layer is calculated based on Debye-Hückel theory. The layer reduces the porosity available for fluid flow. We find that the Biot critical frequency based on pore scale data can be used to explain effects on the macro scale. We find that the effective yield stress and also the effective stress of failure in tension as well as in compression are log-linearly related to log reference frequency. This opens the possibility to predict yield and failure under reservoir conditions from mechanical tests made under laboratory conditions. It also opens the possibility of predicting the effects of water flooding on chalk stability.

INTRODUCTION

In petroleum engineering, improved oil recovery by water injection is an important mechanism for achieving an increased production of hydrocarbons. The Ekofisk field located in the North Sea responded to water injection by subsidence although preliminary laboratory tests did not show any mechanical effect of injected seawater, (Johnson et al., 1989). It was also surprising that the water injection made the Ekofisk field subside in spite of no apparent pressure decrease, see e.g., Maury et al. (1996) or Sylte et al. (1999). These observations sparked an extensive interest in the water weakening phenomenon. Several explanations have been proposed through the years.

One often-stated mechanism is capillary effects, where local water menisci around the grain contacts strengthens the chalk for dry and oil-saturated specimens, whereas they disappear for fully water-saturated chalk. This is similar to the behavior of partially saturated

soil and has been investigated by Delage et al. (1996) and Papamichos et al. (1997) on partially saturated chalk. Also, lowering the pressure by applying a suction to the pore space causes a strengthening of the chalk (De Gennaro et al., 2004; Taibi et al., 2009). In the numerical constitutive modeling of chalk by Hickman et al. (2008), a common state variable is introduced that includes both the situation with two phase saturated chalk and the one with fully saturated chalk. That capillary effects is not the only cause for the water weakening in fully saturated chalk is demonstrated by a test series on water-ethylene glycol mixtures with glycol completely miscible in water (Risnes et al., 2005). Also Lord et al. (1998) reason that there is not enough adsorbed water for the capillary effects to exist in dry chalk.

Chemical effects is another explanation for the weakening. Newman (1983) found water weakening on high-porosity offshore chalk and related it to the chemical composition of the seawater. The pro-

Manuscript received by the Editor 16 December 2009; revised manuscript received 12 April 2010; published online 30 November 2010.

¹Technical University of Denmark, Department of Civil Engineering, Kongens Lyngby, Denmark. E-mail: kao@byg.dtu.dk.

²Technical University of Denmark, Department of Environmental Engineering, Kongens Lyngby, Denmark. E-mail: ilf@env.dtu.dk.

© 2010 Society of Exploration Geophysicists. All rights reserved.

posed mechanism is dissolution and, at high stresses, pressure solution. A chemo-mechanical coupling is proposed by Hellmann et al. (2002) and Pietruszczak et al. (2006), where the mechanism for the chalk weakening is intergranular pressure solution. This process consists of dissolution of the chalk at grain contacts followed by diffusion of the dissolved fraction away from the grain contact area to grain surface affected by lower stresses. This mechanism though leads to an increase in the contact area between the chalk grains with time and can hardly result in weakening. Risnes et al. (2003) correlate the strength of chalk with the water activity in the pore fluid. A large test series on chalk is reported by Madland et al. (2002). They find that heating results in weakening. Korsnes et al. (2006, 2008a) measure weakening effects in tests at different temperatures and with different composition of the pore water, where most of the tests are performed with continuous flooding to amplify the chemical effects. Their hypothesis is that a substitution of Ca^{2+} by Mg^{2+} takes place and causes diffusion at grain contacts. A coupled damage, dissolution-diffusion model (Hu and Hueckel, 2007) is a similar theory. Purely chemical dissolution/precipitation at grain contacts is proposed by Heggeheim et al. (2005). Instantaneous deformation in chalk by water injection is observed for chalk specimens by both Schroeder et al. (1998) and Homand and Shao (2000), and in fractures by Gutierrez et al. (2000). Pressure solution or a dissolution-diffusion mechanism seem speculative explanations to the water weakening.

Another often-stated mechanism is the reduction in the free surface energy by an adsorbed fluid on the solid part leading to a weakening of the material. In other words, a surface active fluid makes the likelihood of crack propagation higher. Experimentally, the water-weakening effect is observed by Rutter (1972, 1974) in outcrop limestone of low porosity at different temperatures with no sign of pressure solution and so the author proposes that the mechanism behind the weakening is a Rebinder effect. The Rebinder effect is a surface effect where a reduction in the free surface energy is an effect of dislocations that emerge at the crystal-fluid interface and leads to a higher probability of crack initiation. For seismic waves in granular media, Sharma and Tutuncu (1994) show grain contact adhesion hysteresis leads to energy dissipation. This concept is also valid for different pore fluids (Tutuncu et al., 1995). Microcracking may be a dominant effect according to Baud et al. (2009) for dry and wet limestone of porosity higher than 0.30. They also suggest that the weakening effect correlates with a reduction in the surface energy for both triaxial and hydrostatic conditions. One other characteristic of chalk behavior, which is not related to the weakening but to the breaking of intergranular cement, could be the recording of acoustic emission during loading to failure. Recording of acoustic emission in high-porosity Danian chalk, though, shows very little acoustic activity (Scott Jr. et al., 2001). Thus, the failure type is apparently different from what is observed in higher indurated rocks, and therefore, relating the reduction in free surface energy to the probability of initiation of cracks might not be the full explanation specifically for water weakening in chalk. This indicates that a focus on mechanisms other than the three mentioned above is necessary.

From a simple tilt test on a large number of chalk samples submerged in either oil or water, Gutierrez et al. (2000) found higher friction for oil-saturated chalk than water-saturated. This observation causes our focus on fluid-solid friction as a possible mechanism for weakening; therefore, we turn to the theory of wave propagation in porous media with the critical frequency as a central measure. Bourbié et al. (1987) and Mavko et al. (1998) list critical frequencies

for various materials and fluids where an increasing crossover frequency from water to oil is observed depending on the type of rock studied. On a large set of carbonate rock samples, Fabricius et al. (2010) found the amount of softening of elastic modulus to be correlated with the reference frequency.

Published laboratory data thus indicate a weakening effect of water and a smaller weakening effect of other fluids on high-porosity chalk as well as a weakening effect of temperature. On the basis of these observations, the present study is aimed at a combined interpretation of the results of rock mechanical tests on chalk with different pore fluids and at various temperatures. Pore fluids are characterized by their density and viscosity and chalk samples by their porosity and permeability. These properties are combined in the critical frequency defined by Biot (1956a, b).

The definition of the Biot critical frequency, f_c , (often also termed characteristic, crossover, or reference frequency) is

$$f_c = \frac{\phi \eta}{2\pi \rho_n k}, \quad (1)$$

where ϕ is porosity, η is the fluid absolute viscosity, ρ_n is fluid density, and k is absolute permeability. The Biot critical frequency marks the limit between a low-frequency regime with the pore fluid following viscous forces and a high-frequency regime with inertial forces dominating the fluid motion (Biot, 1956a, b). These regimes have been verified experimentally by Johnson et al. (1987).

For an applied elastic wave velocity, the drag that the solid motion makes on the fluid and whether this is in the viscous or inertial regime is basically a matter of friction between the liquid and the solid (Johnson et al., 1987). In the case of rock mechanical testing, the phenomenon changes to the drag the solid phase makes on the fluid while the fluid drains from the specimen due to the applied load. The critical frequency is here interpreted as a friction factor in the same manner as Reynolds number. Reynolds number Re is usually seen with a friction proportional to $64/Re$ valid for laminar flow. The Reynolds number also relates to the transition from a flow regime dominated by viscous forces to a flow regime dominated by inertial forces.

We propose that the solid-fluid friction is a controlling parameter for the failure or pore collapse in chalk. When assuming that a certain energy needs to be applied to a specimen to reach the point in which the specimen will go into failure or into pore collapse, a higher solid-fluid friction will dissipate more energy compared to a lower friction and consequently the chalk in the high-friction case will need more energy to be applied before the specimen enters the failure/pore collapse. This is the background for using the Biot critical frequency for the failure and pore collapse in rock mechanical tests.

The critical frequency will be applied as a general measure of strength characterizing the chalk/fluid medium. The main difference across all the test set-ups found in the literature is the changing pore fluid properties although there is both scattering of results and overlap of the span of the data. The test series reported in the literature are normally performed with a specific hypothesis to be tested, e.g., whether temperature weakens seawater-saturated chalk or if viscosity of the pore fluids is the determining strengthening parameter. This review combines the data so that a general interpretation is possible.

METHODS

To narrow the focus, this investigation is limited to high-porosity chalk. The low cementation should cause the fluid effects to domi-

Biot critical frequency for chalk

E207

nate with respect to the frame response of the chalk. There are 622 tests included in the study. The tests are made on outcrop chalk from three different localities: Liège or Lixhe chalk from a quarry in Belgium, Aalborg chalk from a quarry in western Denmark, and Stevns Chalk from a quarry in eastern Denmark. The physical properties vary among the outcrop chalks, with Liège being characterized by a porosity of generally 0.40 and a permeability of 1.5 mDarcy ($1.48 \cdot 10^{-15} \text{ m}^2$). Stevns chalk has a porosity of generally 0.45 and a permeability of 3.5 mDarcy ($3.45 \cdot 10^{-15} \text{ m}^2$), whereas Aalborg chalk generally has 0.45 porosity and a slightly higher general permeability of 4 mDarcy ($3.95 \cdot 10^{-15} \text{ m}^2$). These values are not exact and vary among the chalk blocks sampled for testing. Further characterization of these chalk lithologies is found in [Hjuler \(2007\)](#) and [Hjuler and Fabricius \(2009\)](#). All the selected outcrop chalks have induration H2, are water wet, and are weakly cemented. The selected tests have a narrow interval of applied deformation rate, $2.8 \cdot 10^{-7} \text{ s}^{-1}$ to $2.8 \cdot 10^{-6} \text{ s}^{-1}$, with an average of $1.6 \cdot 10^{-6} \text{ s}^{-1}$ (0.1%/hour to 1%/hour, average 0.58%/hour) to reduce the influence of time effects.

Table 1 lists all references to the test results comprised in this review. All the relevant information regarding the tested specimens, pore fluid, stress path, etc., was recorded and placed in a large spreadsheet for ease of handling. The rock mechanical tests include four types: (1) A Brazilian test determining the indirect tensile strength, (2) the unconfined compression test giving the shear failure values, (3) the triaxial test giving either failure or yield depending on the stress path that is usually performed with a hydrostatic uploading followed by a deviatoric phase, and (4) the hydrostatic test determining the yield point that is defined at the onset of a higher deformation rate, i.e., pore collapse, and where all principal effective stresses are equal. These standard rock mechanical testing procedures are described in [Jaeger et al. \(2007\)](#).

The abbreviations used for the seawater of different chemical composition are: SSW for standard seawater, SSW-U for seawater

without sulphate, SSW-U2 for seawater without magnesium and sulphate, SSW-2 for seawater with double the concentration of sulphate ([Korsnes et al., 2006](#)).

Information from the different mechanical test types are combined by summarizing stress states at failure or for the pore collapse (yield) in a p' - q plot, ([Fjær et al., 2008](#)), with

$$p' = \frac{1}{3}(\sigma'_1 + \sigma'_2 + \sigma'_3), \text{ and} \quad (2)$$

$$q = \frac{1}{\sqrt{2}}\sqrt{(\sigma'_1 - \sigma'_2)^2 + (\sigma'_2 - \sigma'_3)^2 + (\sigma'_1 - \sigma'_3)^2}, \quad (3)$$

where $\sigma'_1, \sigma'_2, \sigma'_3$ are the principal effective stresses. σ'_1 is the largest, vertical stress, σ'_2 the intermediate, horizontal stress, and σ'_3 is the smallest, horizontal stress. Figure 1 illustrates the concept of the p' - q diagram.

The indirect tensile strength (Brazilian test) is here interpreted as being equivalent to the uniaxial tensile strength ([Mellor and Hawkes, 1971](#)) and is therefore plotted on the negative p' axis. We do this because the stress state for the Brazilian test does not involve equal, intermediate, and minor stress although this has been assumed in earlier publications. The intermediate stress σ_2 is zero as stated in [Jaeger et al. \(2007\)](#) and can therefore not be plotted directly in the same stress plane as the p' - q plane. The interpretation of the Brazilian test result as the uniaxial tensile strength is needed to correct for this.

Table 2 lists all the density and viscosity data found in tabulated references and sorted according to pore pressure and temperature.

For a number of tests the actual permeability of the tested chalk is not known but the exact porosity is stated. To determine the permeability when the porosity is known, we use Kozeny's equation for laminar flow in a porous medium ([Mortensen et al., 1998](#)):

Table 1. Overview of test results included in this review and their references. UCS: Unconfined compression test. SSW(-U/U2/2): Synthetic seawater of different chemical composition. Glycol: Ethylene glycol.

Test type	Fluid	Temperature (°C)	Chalk type	Tests	Reference
Brazilian	Eq. water, seawater, oil	Room	Liège	8 ^c	Risnes et al. (1996)
Triax, hydrostatic	Water, seawater, oil, liquid paraffin, dry	Room	Liège	58	Schroeder and Shao (1996)^a
Triax, hydrostatic	Eq. water, oil	Room	Liège	19	Homand and Shao (2000)
Triax, Brazilian, UCS	Water, glycol	20, 130	Liège, Aalborg	194	Madland et al. (2002)
Brazilian, triax	Eq. water, glycol, high salinity SSW	Room	Liège, Aalborg	59 ^c	Risnes et al. (2003)
Triax, Brazilian, hydrostatic	Water, glycol, mixture hereof	Room	Liège	191	Risnes et al. (2005)
Hydrostatic	Distilled water, SSW, SSW-2, SSW-U, SSW-U2	130	Stevns	10	Korsnes et al. (2006)
Hydrostatic	Tap water	20	Aalborg	3 ^b	Madland et al. (2006)
Hydrostatic	Distilled water, SSW, SSW-U	Room, 50, 70, 90	Stevns	17	Korsnes et al. (2008a)
Hydrostatic, Brazilian	Tap water	Room	Liège, Stevns	63	Korsnes et al. (2008b)

^a[Delage et al. \(1996\)](#) contains similar data set.

^bExcluded CO₂ saturated samples.

^cExcluded triax and hydrostatic tests run at higher deformation rate than $2.8 \times 10^{-6} \text{ s}^{-1}$ (1%/hour).

E208

Andreassen and Fabricius

$$k = c \frac{\phi^3}{(1-\phi)^2 S_s^2} = c \frac{\phi^3}{(1-\phi)^2 (S_a \rho_s)^2}, \quad (4)$$

$$c = \left(4 \cos \left(\frac{1}{3} \arccos \left(\phi \frac{8^2}{\pi^3} - 1 \right) + \frac{4}{3} \pi \right) + 4 \right)^{-1}, \quad (5)$$

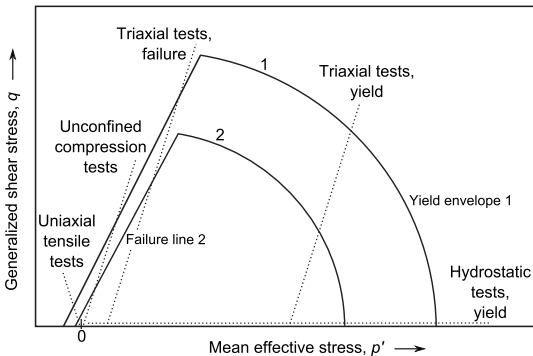


Figure 1. Conceptual sketch of the stress paths for rock mechanical tests. The curve representing failure line and yield envelope with label 1 signifies a stronger medium than the curve with label 2. The Brazilian test giving the indirect tensile strength should be similar to the strength found from the uniaxial tensile test.

with c stated here for 3D circular interconnected tubes, ϕ is the porosity, S_s is specific surface as grain surface area to grain volume, S_a is specific surface area in surface area per solid mass, ρ_s is solid (grain) density. We used $2.7 \cdot 10^3 \text{ kg/m}^3$ for the solid density of the chalk. Measured specific surface area by BET (N_2 adsorption) is $1.7 \text{ m}^2/\text{g}$ for Liège chalk, $3.6 \text{ m}^2/\text{g}$ for Aalborg chalk, and $1.7 \text{ m}^2/\text{g}$ for Stevns chalk (Hjuler and Fabricius, 2009). Others have found $2.0 \text{ m}^2/\text{g}$ for Liège chalk (Madland et al., 2006), and $2.2 \text{ m}^2/\text{g}$ to $4 \text{ m}^2/\text{g}$ for Stevns chalk (Olsen et al., 2008). Some data where porosity and permeability are both known, a backcalculation is applied to obtain the effective specific surface that is relevant to the flow. The reason behind applying the effective specific surface, S_{as} , is that we assume it to be a material property for each chalk locality and, therefore, does not change between different chalk blocks. The procedure is implemented due to the missing permeability for individual specimens and is expected to give only an indication of the true permeability. It will always be better to measure the permeability by flow through the specimens. Applying this backcalculation yields an effective specific surface, S_{as} of $2.0 \text{ m}^2/\text{g}$ for Liège chalk, $1.6 \text{ m}^2/\text{g}$ for Aalborg chalk, and $2.0 \text{ m}^2/\text{g}$ for Stevns chalk, which are the values used in equation 4. The few test results with an actual measured permeability gives a difference of 0.4% to 30% (median 13%) to the calculated permeability.

In the fluid saturated pores, the viscous skin depth to the solid surface is in principle acting as a reduction of the porosity and also affects the calculated permeability. It is relevant to take this phenomenon into account as the skin layer becomes thinner with increasing number of ions dissolved in the water. In accordance with the Debye-Hückel theory, we use the screening length κ^{-1} for an electrolyte (Lyklema, 1991) to quantify this effect,

Table 2. Physical properties of the pore fluids and air used in this review when determining the critical frequency.

Fluid	Temperature °C	Pressure ^a MPa	Density 10^3 kg/m^3	Viscosity $10^{-3} \text{ Pa} \cdot \text{s}$	Reference
Water	20	0	0.9982072	1.001604	[1]
	20	0.2	0.9982987	1.001519	[1]
	20	0.3	0.9983445	1.001476	[1]
	130	0.3	0.9349022	0.2129295	[1]
	130	0.8	0.9351622	0.2130594	[1]
Brine	20	0	1.0210639	1.070581	[1]
	50	0.7	1.0113678	0.6018571	[2]
	70	0.7	1.0013154	0.4446152	[2]
	90	0.7	0.9891664	0.3461644	[2]
	130	0.7	0.9594769	0.2344113	[2]
	130	0.8	0.9595247	0.2344399	[2]
Glycol	20	0	1.1134009	21.81278	[3]
	130	0	1.0310034	1.188431	[3]
Oil ^b	20	0	Varying with oil type	Varying with oil type	Varying with oil type
Air ^c	20	0	0.001192921	0.01829175	[4]
	130	0	0.000863188	0.02324175	[4]

[1]NIST (2008), Mavko et al. (1998), [2]NIST (2008), Palliser and McKibbin (1998), [3]Yaws (1999), [4]Lide (2008).

^aNot including the atmospheric pressure.

^bUsually specified or taken from the producent's datasheet.

^cFor tests on dry specimens.

$$\kappa^{-1} = \left(\frac{\epsilon_0 \epsilon_r k_B T}{2 N_A e^2 I} \right)^{1/2}, \quad (6)$$

ϵ_0 is the permittivity of vacuum, ϵ_r is the relative dielectric permittivity, k_B is Boltzmann's constant, T is the absolute temperature, N_A is the Avogadro number, e is the elementary charge, and I is the ionic strength of the electrolyte. Table 3 states the composition of all the relevant types of water.

The Debye screening length is not the exact viscous skin depth. In some cases, the thickness of the skin layer is found to be 3 to 5 times the Debye length (Masliyah and Bhattacharjee, 2006); in other cases, it is found to be smaller than the skin depth (Israelachvili, 1991). For simplicity, we choose to use the Debye length directly as a measure of the skin depth. The reduction in porosity is then calculated from the effective specific surface,

$$\phi_{\text{reduced}} = \phi - (1 - \phi) \kappa^{-1} S_a \rho_s. \quad (7)$$

Distilled water is taken to equilibrate instantaneously with the chalk and, therefore, reaches the same ionic strength as equilibrated water.

Assumed critical frequency isolines for the failure and yield envelope curve are represented by a linear failure curve and a circular yield envelope as in Hickman et al. (2008).

RESULTS AND DISCUSSION

Figure 2 shows the summarized result of all data with guidelines of a hypothetical failure–yield curve with regular intervals to visualize envelopes with each having the same critical frequency. To help in the reading of the figure, critical frequencies calculated for the different fluids are placed in Table 4. These are examples calculated for a characteristic chalk with a porosity of 0.40 and an original absolute permeability of $1.44 \cdot 10^{-15} \text{ m}^2$. The table shows that taking the vis-

cous skin depth into consideration introduces a decrease in the critical frequency for the seawater compared with distilled or tap water; however, this is a second-order effect compared with the effect of porosity and permeability on the critical frequency.

The level of critical frequency increases as failure values and yield values increase in the same manner as higher inferred friction is supposed to give a stronger response. Some of the regions on Figure 2 are singled out according to test procedure and plotted versus reference frequency: the hydrostatic tests in Figure 3, the Brazilian tests in Figure 4, and the unconfined compression tests in Figure 5. The latter only includes a small dataset but is still in accordance with the slope observed on the graphs of the hydrostatic and Brazilian tests.

Temperature has a large effect on the viscosity especially for ethylene glycol, and this tendency can be observed in all three plots above. The water-saturated results show a less distinct temperature weakening due to the natural scattering and lesser decrease in viscosity with temperature. The changes in the ratio of air viscosity to air density by going from 20 °C to 130 °C causes the critical frequency to increase with temperature only for dry media. For the Brazilian and unconfined compression tests, a temperature effect is only found as an increase for dry samples in accordance with our hypothesis. Another supporting observation in the Brazilian plot on Figure 4 is that the relatively strong samples with high salinity seawater containing 250 g/l NaCl and 700 g/l $\text{CaCl}_2 \cdot 2\text{H}_2\text{O}$ have a relatively high critical frequency due to the high viscosity of the brine.

The causality between using the Biot critical frequency compared to using other central properties is investigated on porosity divided by permeability in Figure 6 and viscosity divided by fluid density in Figure 7. For the porosity divided by the permeability, there exists a weak trend (Figure 6). For the viscosity divided by the fluid density, there is an overall trend linking the results from different saturating fluids, whereas results with the same pore fluid give identical fractions (Figure 7). These two effects combine through the use of the Biot critical frequency and this signifies the need to incorporate all four properties that gives the good correlation in Figure 3.

Table 3. Chemical composition of the tap water, equilibrated water, and synthetic seawater used in the experiments, (Schroeder, 2002; Korsnes et al., 2006).

	Tap water 10^{-3} mol/L	Eq. water 10^{-3} mol/L	SSW-2 mol/L	SSW-L mol/L	SSW-U mol/L	SSW-U2 mol/L
SiO_3^{2-}	0.255	0.070				
HCO_3^-	5.610	1.10	0.002	0.002	0.002	0.002
Cl^-	1.42	0.810	0.467	0.525	0.583	0.567
SO_4^{2-}	0.90	0.175	0.048	0.024	0	0
Mg^{2+}	0.621	0.02	0.045	0.045	0.045	0
Ca^{2+}	4.184	0.434	0.013	0.013	0.013	0.013
Na^+	0.892	1.27	0.44	0.45	0.46	0.533
K^+	0.059	0.02	0.01	0.01	0.01	0.01
Fe^{3+}	0	0.01				

To further investigate the use of the Biot critical frequency, it is necessary to obtain results from low-cemented chalk with a larger interval of porosity and permeability. This can verify the hypothesis of using the Biot critical frequency as a measure for the failure and pore collapse. Chalk is a unique material and applying the critical frequency concept on other materials may require adaptation to suit their special features, e.g., high electrical properties of clay and its very high surface area or the varying cementation of sandstone.

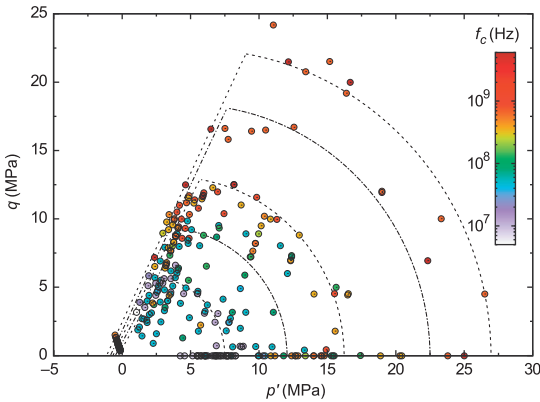


Figure 2. Mean effective stress and generalized shear stress with the critical frequency stated by color-coding. Isolines with assumed equal levels of critical frequency are drawn at regular intervals to guide the interpretation. Each colored circle represents a result from one test — either a Brazilian, unconfined compression, or triaxial test and either a failure or yield point. See the conceptual p' - q sketch (Figure 1) for location of stress paths for the standard rock mechanical tests. Outliers exist but are generally attributed to weak samples.

When comparing Figures 3–5 for each of the three rock mechanical test types, there exists a similarity with the common exponent 4.3 for the regression line expressions. The similarity points to a fractal or self-organized criticality relation (Bak et al., 1987; Paczuski et al., 1996). To know the actual mechanism behind the self-organized criticality is not required, which is an advantage for the present use. It has been applied in rock mechanics by Desai (2001) and symbolizes scale-free behavior due to the system being in a critical state. Both failure and pore collapse of chalk signifies a critical state. Self-organized criticality is hence tested for all the hydrostatic yield results from Figure 3. For a system to have self-organized criticality, it must plot linearly between the logarithm of the distribution of a parameter and the logarithm of the size of the same parameter. Figure 8 reveals that the distribution of hydrostatic yield strengths does not conform to the requirement. In Figure 9 self-organized criticality exists for the distribution of Biot critical frequency over several orders of magnitude. The drop below the initial linear log-log relation shows a need for more test results for chalk with a high Biot critical frequency.

Using the Biot critical frequency as a predictive factor for reservoir chalk is possible although it is necessary to assume full saturation with one pore fluid. The temperature incorporates conveniently through the fluid density and absolute fluid viscosity. The prediction is useful as a first estimate or to give the upper and lower bounds for a chalk with a known interval of properties.

Capillary effects, dissolution, and reduction in free surface energy are all mechanisms that might come into play for the microscopic behavior of the chalk; however, for the macroscopic behavior our results indicate that the fluid-solid friction represented by the critical frequency is the dominating first-order effect.

Table 4. Calculated critical frequency for a typical chalk of 0.40 porosity, effective specific surface of 2.0 m²/g, and a permeability of 1.44 · 10⁻¹⁵ m² at 20 °C and atmospheric pore pressure, (Equation 1). The viscous skin depth from Equation 6 and the resulting effective porosity and permeability are calculated from Equation 4 and Equation 7.

Fluid	20 °C					130 °C ^a				
	η 10 ⁻³ Pa·s	κ^{-1} 10 ⁻⁹ m	ϕ_{reduced}	k_{eff} 10 ⁻¹⁵ m ²	f_c Hz	η 10 ⁻³ Pa·s	κ^{-1} 10 ⁻⁹ m	ϕ_{reduced}	k_{eff} 10 ⁻¹⁵ m ²	f_c Hz
SSW-2 ^b	1.0706	0.3720	0.3988	1.420	4.686 · 10 ⁷	0.2344	0.4362	0.3986	1.417	1.094 · 10 ⁷
SSW ^b	1.0706	0.3759	0.3988	1.420	4.686 · 10 ⁷	0.2344	0.4408	0.3986	1.417	1.094 · 10 ⁷
SSW-U ^b	1.0706	0.3800	0.3988	1.420	4.687 · 10 ⁷	0.2344	0.4456	0.3986	1.416	1.094 · 10 ⁷
SSW-U2 ^b	1.0706	0.3995	0.3987	1.419	4.689 · 10 ⁷	0.2344	0.4685	0.3985	1.415	1.095 · 10 ⁷
Tap water	1.0016	2.417	0.3922	1.316	4.760 · 10 ⁷	0.2129	2.8344	0.39082	1.295	1.094 · 10 ⁷
Distilled water	1.0016	5.522	0.3821	1.170	5.216 · 10 ⁷	0.2129	6.4756	0.3790	1.128	1.218 · 10 ⁷
Eq. water	1.0016	5.522	0.3821	1.170	5.216 · 10 ⁷	0.2129	6.4756	0.3790	1.128	1.218 · 10 ⁷
Oil ^c	3.01	0	0.400	1.440	1.700 · 10 ⁸					
Dry	0.01829	0	0.400	1.440	6.779 · 10 ⁸	0.02324	0	0.400	1.440	1.190 · 10 ⁹
Ethylene glycol	21.813	0	0.400	1.440	8.661 · 10 ⁸	1.1884	0	0.400	1.440	5.096 · 10 ⁷
Oil ^d	120	0	0.400	1.440	6.004 · 10 ⁹					

^aAt an absolute pressure of 0.2 MPa not including the atmospheric pressure.

^b $\rho_n = 1.0211 \cdot 10^3 \text{ kg/m}^3$ at 20 °C and $\rho_n = 0.9595 \cdot 10^3 \text{ kg/m}^3$ at 130 °C.

^c $\rho_n = 0.7826 \cdot 10^3 \text{ kg/m}^3$,

^d $\rho_n = 0.88 \cdot 10^3 \text{ kg/m}^3$.

Biot critical frequency for chalk

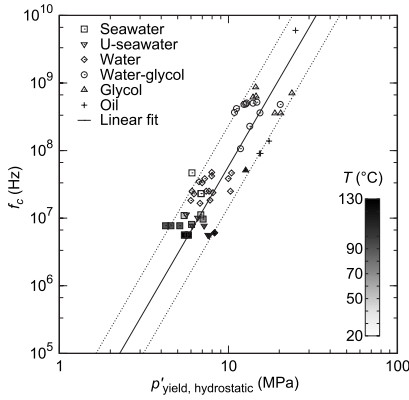


Figure 3. Mean effective stress and critical frequency for the yield points in hydrostatic tests. U-seawater: Seawater without either sulphate or magnesium or both. Water-glycol: Different mol% of water and ethylene glycol solutions. Oil: At 20 °C and with different viscosity. Coefficient of determination $r^2 = 0.75$, $n = 62$. Fitted with $y = 2.9 \cdot 10^3 x^{4.3}$.

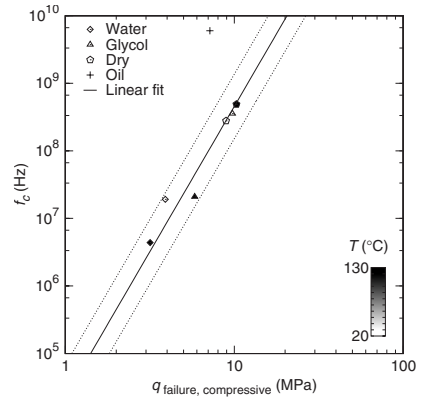


Figure 5. Generalized shear stress and critical frequency for the failure points in unconfined compression tests. Oil: Liquid paraffin at 20 °C is an outlier and is not included in the fit. Coefficient of determination $r^2 = 0.94$, $n = 6$. Fitted with $y = 22.6 \cdot 10^3 x^{4.3}$.

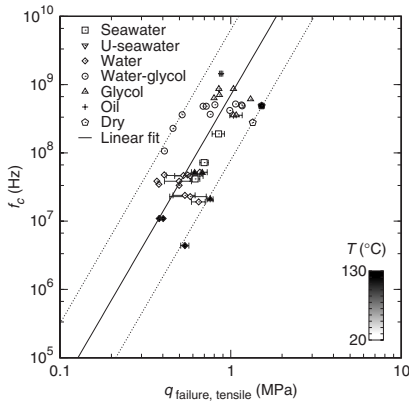


Figure 4. Generalized shear stress and critical frequency for the failure points in Brazilian tests. The errorbars show the span from multiple tests in a test series. U-seawater: Seawater without either sulphate or magnesium or both. Water-glycol: Different mol% of water and ethylene glycol solutions. Seawater: High salinity synthetic seawater. Oil: At 20 °C and with different viscosity. Coefficient of determination $r^2 = 0.50$, $n = 358$. Fitted with $y = 7.0 \cdot 10^3 x^{4.3}$.

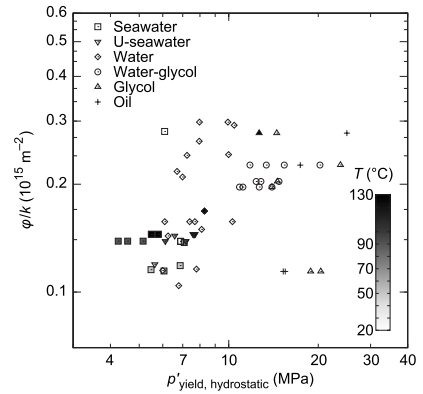


Figure 6. Causality test of porosity divided by permeability. A weak trend exists with higher porosity-permeability fraction indicating higher strength. Note that the x-axis range is different than in Figure 3.

E212

Andreassen and Fabricius

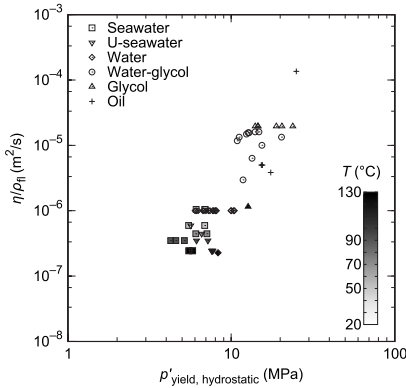


Figure 7. Causality test of fluid viscosity divided by fluid density. A dominating correlation exists across the different saturating fluid results while results with the same saturating fluid obviously give the same viscosity-density fraction and so have the same y value. The water-glycol mixtures have different fluid viscosity and density and follow the general trend.

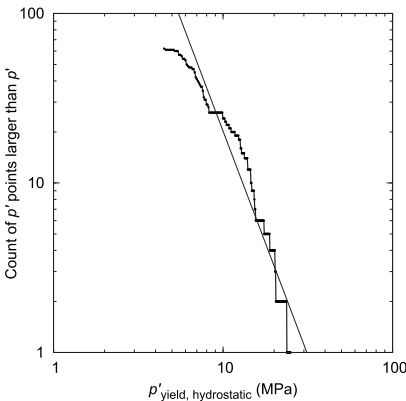


Figure 8. The distribution of hydrostatic yield results from Figure 3. Self-organized criticality is not fulfilled as it requires linear relation in a log-log plot. The fitting line is $y = 8826x^{-2.64}$.

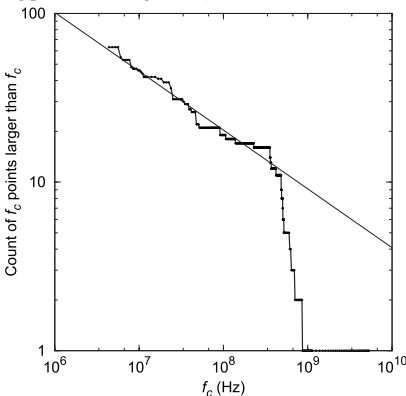


Figure 9. The Biot critical frequency for the hydrostatic yield results from Figure 3 exhibits a self-organized criticality behavior. For the high-frequency region, the counts drop below the fitting line and indicate a need for more data to verify the behavior. The fitting line is $y = 12530x^{-0.349}$.

CONCLUSIONS

The Biot critical frequency can be used as a friction factor in fully saturated chalk. This allows us to predict the effect of changing the pore fluid properties. We find that the critical frequency is correlated to both the failure and the yield results obtained from standard rock mechanical tests: Brazilian, unconfined compression, hydrostatic, and triaxial tests. We introduce an effective porosity calculated from the viscous skin depth ranging from the solid into the fluid. The critical frequency correctly estimates the decrease in strength properties with increasing temperature for fluid-saturated chalk and an increase for dry chalk strength with increasing temperature.

These findings open the perspective in relation to water flooding of chalk reservoirs: that results in compaction and failure behavior from experiments done at laboratory conditions can be generalized to reservoir conditions.

ACKNOWLEDGMENTS

We would like to thank all the authors who have made their extensive laboratory results available in the literature. A special thanks to Ole Heddal for help with the stress plots and good discussions on the interpretation of the Brazilian test. We are grateful to the Associate Editor, Ira Ojala, and two anonymous reviewers for giving inspiring comments.

REFERENCES

- Bak, P., C. Tang, and K. Wiesenfeld, 1987, Self-organized criticality: An explanation of the $1/f$ noise: *Physical Review Letters*, **59**, no. 4, 381–384, doi: 10.1103/PhysRevLett.59.381.
- Baud, P., S. Vinciguerra, C. David, A. Cavallo, E. Walker, and T. Reuschlé, 2009, Compaction and failure in high porosity carbonates: Mechanical data and microstructural observations: *Pure and Applied Geophysics*, **166**, no. 5–7, 869–898, doi: 10.1007/s00024-009-0493-2.
- Biot, M. A., 1956a, Theory of propagation of elastic waves in a fluid-saturated porous solid. I. Low-frequency range: *The Journal of the Acoustical Society of America*, **28**, no. 2, 168–178, doi: 10.1121/1.1908239.
- , 1956b, Theory of propagation of elastic waves in a fluid-saturated porous solid. II. Higher frequency range: *The Journal of the Acoustical Society of America*, **28**, no. 2, 179–191, doi: 10.1121/1.1908241.
- Bourbié, T., O. Coussy, and B. Zinzner, 1987, *Acoustics of porous media*: Editions Technip.
- De Gennaro, V., P. Delage, G. Priol, F. Collin, and Y. J. Cui, 2004, On the collapse behaviour of oil reservoir chalk: *Geotechnique*, **54**, no. 6, 415–420, doi: 10.1680/geot.2004.54.6.415.
- Delage, P., Ch. Schroeder, and Y. J. Cui, 1996, Subsidence and capillary effects in chalks: *Eurock*, 1291–1298.
- Desai, C. S., 2001, *Mechanics of materials and interfaces: The disturbed state concept*: CRC Press.
- Fabricius, I. L., G. T. Bächle, and G. P. Eberli, 2010, Elastic moduli of dry and watersaturated carbonates — effect of depositional texture, porosity and permeability: *Geophysics*, **75**, no. 3, N65–N78, doi: 10.1190/1.3374690.
- Fjar, E., R. M. Holt, P. Horsrud, A. M. Raaen, and R. Risnes, 2008, *Petroleum related rock mechanics*, 2nd ed.: Elsevier, volume, 53, of *Developments in Petroleum Science*.
- Gutierrez, M., L. E. Øino, and K. Høeg, 2000, The effect of fluid content on the mechanical behaviour of fractures in chalk: *Rock Mechanics and Rock Engineering*, **33**, 93–117, doi: 10.1007/s006030050037.
- Heggheim, T., M. V. Madland, R. Risnes, and T. Austad, 2005, A chemical induced enhanced weakening of chalk by seawater: *Journal of Petroleum Science Engineering*, **46**, no. 3, 171–184, doi: 10.1016/j.petrol.2004.12.001.
- Hellmann, R., P. J. N. Renders, J. P. Gratier, and R. Guiguet, 2002, Experimental pressure solution compaction of chalk in aqueous solutions Part 1. Deformation behavior and chemistry: *Water-Rock Interactions, Ore Deposits, and Environmental Geochemistry, A Tribute to David A. Crerar*, 129–152.
- Hickman, R. J., M. S. Gutierrez, V. De Gennaro, and P. Delage, 2008, A model for pore-fluid-sensitive rock behavior using a weathering state parameter: *International Journal for Numerical and Analytical Methods in Geomechanics*, **32**, no. 16, 1927–1953, doi: 10.1002/nag.703.

Biot critical frequency for chalk

E213

- Hjuler, M. L., 2007, Diagenesis of upper cretaceous onshore and offshore chalk from the North Sea area: Ph.D. thesis, Technical University of Denmark.
- Hjuler, M. L., and I. L. Fabricius, 2009, Engineering properties of chalk related to diagenetic variations of upper cretaceous onshore and offshore chalk in the north sea area: *Journal of Petroleum Science Engineering*, **68**, no. 3–4, 151–170, doi: 10.1016/j.petrol.2009.06.005.
- Homand, S., and J. F. Shao, 2000, Mechanical behaviour of a porous chalk and water/chalk interaction. Part I: Experimental study: *Oil & Gas Science and Technology — Rev: IFP*, **55**, 599–609, doi: 10.2516/ogst:2000045.
- Hu, L. B., and T. Hueckel, 2007, Coupled chemo-mechanics of intergranular contact: Toward a three-scale model: *Computers and Geotechnics*, **34**, no. 4, 306–327, doi: 10.1016/j.compgeo.2007.02.009.
- Israelachvili, J. N., 1991, Intermolecular and surface forces: Academic Press.
- Jaeger, J. C., N. G. W. Cook, and R. W. Zimmerman, 2007, Fundamentals of rock mechanics, 4 ed.: Blackwell Publishing.
- Johnson, D. L., J. Koplik, and R. Dashen, 1987, Theory of dynamic permeability and tortuosity in fluid-saturated porous media: *Journal of Fluid Mechanics*, **176**, 379–402.
- Johnson, J. P., D. W. Rhett, and W. T. Siemers, 1989, Rock mechanics of the Ekofisk reservoir in the evaluation of subsidence: *Journal of Petroleum Technology*, **41**, no. 7, 717–722.
- Korsnes, R. I., M. V. Madland, and T. Austad, 2006, Impact of brine composition on the mechanical strength of chalk at high temperature: Eurock, Proceedings of the International Symposium of the International Society for Rock Mechanics, 9–12 May 2006, Belgium, Taylor & Francis/Balkema, 133–140.
- Korsnes, R. I., M. V. Madland, T. Austad, S. Haver, and G. Røslund, 2008a, The effects of temperature on the water weakening of chalk by seawater: *Journal of Petroleum Science Engineering*, **60**, no. 3–4, 183–193, doi: 10.1016/j.petrol.2007.06.001.
- Korsnes, R. I., E. Wersland, T. Austad, and M. V. Madland, 2008b, Anisotropy in chalk studied by rock mechanics: *Journal of Petroleum Science Engineering*, **62**, no. 1–2, 28–35, doi: 10.1016/j.petrol.2008.06.004.
- Lide, D. R., ed., 2008, CRC handbook of chemistry and physics, 89th ed.: Taylor and Francis Group, e-book, accessed 11 June 2009; <http://www.hbcpnline.com/>.
- Lord, C. J., C. L. Johlman, and D. W. Rhett, 1998, Is capillary suction a viable cohesive mechanism in chalk?: *SPE/ISRM Eurock*, Norway, 479–485.
- Lyklema, J., 1991, Fundamentals of interface and colloid science: Academic Press, Volume I.
- Madland, M. V., A. Finsnes, A. Alkafadgi, R. Risnes, and T. Austad, 2006, The influence of CO₂ gas and carbonate water on the mechanical stability of chalk: *Journal of Petroleum Science Engineering*, **51**, no. 3–4, 149–168, doi: 10.1016/j.petrol.2006.01.002.
- Madland, M. V., R. I. Korsnes, and R. Risnes, 2002, Temperature effects in Brazilian, uniaxial and triaxial compressive tests with high porosity chalk: *SPE Paper 77761*.
- Masliyah, J. H., and S. Bhattacharjee, 2006, *Electrokinetic and colloid transport phenomena*: Wiley-Interscience.
- Maury, V., J.-M. Piau, and G. Halle, 1996, Subsidence induced by water injection in water sensitive reservoir rocks: The example of Ekofisk: *European Petroleum Conference*, 22–24 October, Italy.
- Mavko, G., T. Mukerji, and J. Dvorkin, 1998, *The rock physics handbook: Tools for seismic analysis in porous media*: Cambridge University Press.
- Mellor, M., and I. Hawkes, 1971, Measurement of tensile strength by diametral compression of discs and annuli: *Engineering Geology*, **5**, no. 3, 173–225, doi: 10.1016/0013-7952(71)90001-9.
- Mortensen, J., F. Engstrøm, and I. Lind, 1998, The relation among porosity, permeability, and specific surface of chalk from the Gorm field, Danish North Sea: *SPE Reservoir Evaluation & Engineering*, **1**, no. 3, 245–251, doi: 10.2118/31062-PA.
- Newman, G. H., 1983, The effect of water chemistry on the laboratory compression and permeability characteristics of some North-Sea chalks: *Journal of Petroleum Technology*, **35**, no. 5, 976–980, doi: 10.2118/10203-PA.
- NIST, 2008, Thermophysical properties of fluid systems: webbook, accessed 23 October 2009; <http://webbook.nist.gov/chemistry/fluid/>.
- Olsen, C., T. Hongdul, and I. Lykke Fabricius, 2008, Prediction of Archie's cementation factor from porosity and permeability through specific surface: *Geophysics*, **73**, no. 2, E81–E87, doi: 10.1190/1.2837303.
- Paczuski, M., S. Maslov, and P. Bak, 1996, Avalanche dynamics in evolution, growth, and depinning models: *Physical Review E, Statistical Physics, Plasmas, Fluids, and Related Interdisciplinary Topics*, **53**, no. 1, 414–443, doi: 10.1103/PhysRevE.53.414.PubMed.
- Palliser, C., and R. McKibbin, 1998, A model for deep geothermal brines. III: Thermodynamic properties — enthalpy and viscosity: *Transport in Porous Media*, **33**, no. 1/2, 155–171, doi: 10.1023/A:1006549810989.
- Papamichos, E., M. Brignoli, and F. J. Santarelli, 1997, An experimental and theoretical study of a partially saturated collapsible rock: *Mechanics of Cohesive-Frictional Materials*, **2**, no. 3, 251–278.
- Pietruszczak, S., D. Lydzba, and J. F. Shao, 2006, Modelling of deformation response and chemo-mechanical coupling in chalk: *International Journal for Numerical and Analytical Methods in Geomechanics*, **30**, no. 10, 997–1018, doi: 10.1002/nag.510.
- Risnes, R., H. Haghghi, R. I. Korsnes, and O. Natvik, 2003, Chalk-fluid interactions with glycol and brines: *Tectonophysics*, **370**, no. 1–4, 213–226, doi: 10.1016/S0040-1951(03)00187-2.
- Risnes, R., C. N. Kristensen, and M. Andersen, 1996, Triaxial tests on high porosity chalk with different saturating fluids: 5th North Sea Chalk Symposium, France.
- Risnes, R., M. V. Madland, M. Hole, and N. K. Kwabiah, 2005, Water weakening of chalk — Mechanical effects of water-glycol mixtures: *Journal of Petroleum Science Engineering*, **48**, no. 1–2, 21–36, doi: 10.1016/j.petrol.2005.04.004.
- Rutter, E. H., 1972, The influence of interstitial water on the rheological behaviour of calcite rocks: *Tectonophysics*, **14**, no. 1, 13–33, doi: 10.1016/0040-1951(72)90003-0.
- , 1974, The influence of temperature, strain rate and interstitial water in the experimental deformation of calcite rocks: *Tectonophysics*, **22**, 311–334.
- Schroeder, Ch., 2002, Du coccolithe au réservoir pétrolier. Approche phénoménologique du comportement mécanique de la craie en vue de sa modélisation à différentes échelles: Ph.D. thesis, Université de Liège.
- Schroeder, Ch., A.-P. Bois, V. Maury, and G. Hallé, 1998, Water/chalk (or collapsible soil) interaction: Part II. Results of tests performed in laboratory on Lixhe chalk to calibrate water/chalk models: *SPE Paper 47587*.
- Schroeder, Ch., and J. Shao, 1996, Plastic deformation and capillary effects in chalks: 5th North Sea Chalk Symposium, France.
- Scott, T. E. Jr., Y. Abousleiman, and M. Zaman, 2001, Acoustical imaging and mechanical properties of soft rock and marine sediments: Technical report, University of Oklahoma (US), accessed 26 November 2009; <http://www.osti.gov/bridge/purl.cover.jsp?purl=/813446-LT1oqi/native/>.
- Sharma, M. M., and A. N. Tutuncu, 1994, Grain contact adhesion hysteresis: a mechanism for attenuation of seismic waves: *Geophysical Research Letters*, **21**, no. 21, 2323–2326, doi: 10.1029/94GL02056.
- Sylte, J. E., L. K. Thomas, D. W. Rhett, D. D. Bruning, and N. B. Nagel, 1999, Water induced compaction in the Ekofisk field: *SPE Paper 56426*.
- Taibi, S., A. Duperré, and J.-M. Fleureau, 2009, The effect of suction on the hydro-mechanical behaviour of chalk rocks: *Engineering Geology*, **106**, no. 1–2, 40–50, doi: 10.1016/j.enggeo.2009.02.012.
- Tutuncu, A. N., M. M. Sharma, and A. L. Podio, 1995, An experimental investigation of the role of pore fluids on the nonlinear hysteretic behavior of Berea Sandstone: 65th Annual International Meeting, SEG, Expanded Abstracts, 886–889.
- Yaws, C., ed., 1999, *Chemical properties handbook*: McGraw-Hill, e-book, accessed 11 June 2009; http://www.knovel.com/web/portal/browse/display?_EXT_KNOVEL_DISPLAY_bookid=49.

Appendix D

Paper II

Andreassen, K.A., Fabricius, I.L., and Foged, N.N. (accepted for publication).

Biot Critical Frequency Applied as Common Friction Factor for Pore Collapse and Failure of Chalk with Different Pore Fluids and Temperatures.

SPE Journal.



Biot Critical Frequency Applied as Common Friction Factor for Pore Collapse and Failure of Chalk with Different Pore Fluids and Temperatures

Katrine Alling Andreassen, SPE, Ida Lykke Fabricius, SPE, and Niels Nielsen Foged, SPE, Technical University of Denmark

Abstract

A fluid effect towards higher strengths for oil saturated chalk compared to water saturated chalk has previously been identified and labeled the water weakening phenomenon, but has not been further characterized physically. The hypothesis of this paper is that the Biot critical frequency with a strain or stress rate dependence can be used to explain this behavior on the pore scale and be extrapolated to the macroscale failure and pore collapse properties. A large set of previously published laboratory test results on chalk with different pore fluids was collected and as supplement we present a new test series on Stevns chalk with unconfined compression and Brazilian strength results.

Introduction

The weakening effect of water in chalk is significant for North Sea chalk reservoir subsidence and several experimental studies have focused on the subject. This paper reviews results from these test series in order to match the theoretical considerations and find the governing physical properties. The mechanisms stated to explain the water weakening are several. Delage et al. (1996) consider capillary suction to strengthen the menisci at grain contacts. In Rehbinder's effect dislocations gather until the stress concentration is sufficient to break the grain contact. This depends on the free surface energy (Boozer et al. 1963) and water reduces the surface energy (Adam et al. 2009). Hellmann et al. (2002) observe pressure dissolution in long term creep tests. Finally, complex physico-chemical mechanisms like the adsorption pressure model by Risnes et al. (2003) are also relevant.

Some of the mechanisms have been questioned. A test series by Risnes et al. (2005) with water and ethylene glycol mixtures show similar behavior as partially saturated chalk and because water and glycol are fully miscible no menisci and hence capillary suction should be present. Additionally, pressure dissolution is not an instantaneous process and this is in contradiction with the observation that water flooded chalk show fast response by collapsing (Schroeder et al. 1998).

Gutierrez et al. (2000) found higher friction for oil saturated chalk (42°) than water saturated (38°) in simple tilt tests on a large test series on chalk samples submerged in either oil or water. The chalk studied is Lägerdorf chalk from a quarry in northwest Germany. While the solid-solid friction is one location for the friction forces in the submerged simple tilt test, the fluid-solid friction should thus be considered as well. This moves our focus to fluid-solid friction as a possible mechanism for weakening when assuming no alteration of the chalk frame and consequently no change in solid-solid friction for oil saturated chalk compared to water saturated chalk. So we turn to the theory of wave propagation in porous media with the critical

frequency as a central topic. Bourbié et al. (1987) and Mavko et al. (2009) list critical frequencies for various materials and fluids where an increasing critical frequency from water to oil is observed depending on the type of rock studied. On a large set of dry and water saturated carbonate rock samples, Fabricius et al. (2010) found the amount of softening of elastic modulus to be correlated with the critical frequency.

The Biot critical frequency, f_c , is defined as

$$f_c = \frac{\varphi\eta}{2\pi\rho_f k}, \dots\dots\dots(1)$$

where φ is porosity, η is absolute viscosity of the pore fluid, ρ_f is fluid density, and k is absolute permeability. Biot's critical frequency marks the limit between a low frequency regime with the pore fluid following viscous forces and a high frequency regime with inertial forces dominating the fluid motion (Biot 1956a, 1956b). The drag that the solid motion makes on the fluid and whether this is in the viscous or inertial regime are basically matters of friction between the liquid and the solid. The critical frequency is thus here interpreted as a friction factor, as described in Andreassen and Fabricius (2010). Note that the Biot critical frequency throughout this paper is a calculated parameter and not a measured property.

When applying stress to a rock with high porosity and low cementation, a significant part of the resulting deformation is displacement of pore fluid. The displacement of fluid involves flow in the open pore space. Therefore any change in the open pore volume caused by changing the pore fluid is important. The viscous skin depth, δ , as defined by Johnson et al. (1987) determines the fluid depth affected by an oscillatory transverse movement of solid with frequency, f :

$$\delta = \sqrt{\frac{2\eta}{\rho_f 2\pi f}}, \dots\dots\dots(2)$$

During rock mechanical testing f approaches zero so δ should make no distinction among fluids. As described below, electrical forces may nevertheless create a skin in some pore fluids.

Another phenomenon is the rate dependence on strength in porous media. The higher applied strain or stress rate the stronger the rock. The knowledge of this effect links laboratory testing of chalk to reservoir behavior at field scale, as illustrated initially in 1989 by Ruddy et al. The subject is well covered experimentally by Schroeder (2002) and PASACHALK2 (2003).

To challenge our hypothesis described above we performed a supplementary test series on Stevns chalk with different pore fluids and on dry chalk at atmospheric pressure and with applied vacuum. The reason is that the lower pressure changes the density of air while the viscosity is mostly independent on pressure and so the calculated Biot critical frequency changes. Consequently, we expect an increase in chalk strength under vacuum.

Methods

This investigation is limited to soft high porosity chalk. The low cementation should cause the fluid effects to dominate over effects of the chalk frame. The tests are made on outcrop chalk from three different localities: Liège or Lixhe chalk from a quarry in Belgium, Aalborg chalk from a quarry in western Denmark, and Stevns chalk from a quarry in eastern Denmark. The physical properties vary among the outcrop chinks, with Liège being characterized by a porosity of generally 40% and a permeability of $1.5 \times 10^{-15} \text{ m}^2$. Stevns chalk has a porosity of generally 45% and a permeability of $3.5 \times 10^{-15} \text{ m}^2$. The supplementary test series on Stevns chalk represents an average porosity of 45.8%. Aalborg chalk generally has a porosity of 45% and a slightly higher general permeability of $4 \times 10^{-15} \text{ m}^2$. Further characterization of these chalk lithologies is given in Hjuler and Fabricius (2009). All the selected outcrop chinks have induration H2 and are thus only weakly cemented. **Table 1** lists the references included in this review. For some of the references the permeability is stated as a general value while the

porosity is given exactly. In order to take this problem into account, the permeability, k , in these cases is calculated from the porosity, ϕ , with the Kozeny equation, which for chalk predicts experimental permeability data well (Mortensen et al. 1998):

$$k = c \frac{\phi^3}{(1-\phi)^2 S_s^2} = c \frac{\phi^3}{(1-\phi)^2 (S_a \rho_s)^2}, \text{ and}$$

$$c = \left(4 \cos \left(\frac{1}{3} \arccos \left(\phi \frac{8^2}{\pi^3} - 1 \right) + \frac{4}{3} \phi \right) + 4 \right)^{-1}, \dots\dots\dots(3)$$

where Kozenys factor c is stated for 3D circular interconnected tubes, and the solid density, ρ_s , of chalk is 2.71 g/cm³. The specific surface, S_s , is assumed to be a material property for each chalk locality and therefore does not change between different chalk blocks. Measured specific surface area, S_a , by BET (N₂ adsorption) is 1.7 m²/g for Liège chalk, 3.6 m²/g for Aalborg chalk, and 1.7 m²/g for Stevns chalk (Hjuler and Fabricius 2009). To confirm that these numbers represent the effective specific surface which is relevant to the flow, a back-calculation is applied to link permeability calculated from porosity (Eq. 3) and measured permeability. The back-calculation gives an effective specific surface of 2.0 m²/g for Liège chalk, 1.6 m²/g for Aalborg chalk, and 2.0 m²/g for Stevns chalk. These values are then used in Eq. 3 for samples where only porosity is known.

Experimental set-up. The supplementary test series on Stevns chalk comprise unconfined compression strength (UCS) and indirect tensile strength (Brazilian) with various pore fluids and dry chalk. Specimens are cut from two blocks of Stevns chalk with small differences in classification properties, while they are both white, porous muddy chalk with some bryozoans. The test set-up is a conventional closed cell in a constant rate of strain equipment (**Fig. 1**). This equipment makes it possible to apply a vacuum with the use of an evacuator supplying a suction of 0.09 MPa equal to an absolute pressure of 0.013 MPa in the cell. The cell diameter is 60 mm and the specimen diameter is 50 mm or 54 mm. **Table 2** lists the classification properties of the tested specimens. The average height of the UCS specimens is 69 mm and the average thickness of the Brazilian specimens is 28 mm. Observed ring friction is a cause of the movement of the top pressure head against the inner cell wall and is subtracted from the actuator force read out. A LVDT records the external deformation.

Calculation of the Biot critical frequency requires the fluid or gas density and viscosity, see Andreassen and Fabricius 2010 for a collection of fluid densities and absolute viscosities at the different temperatures and pressures relevant for the test series in Table 1. The pressure of air relates to the mean free path λ of molecules in a gas (Serway et al. 2000) through

$$\lambda = \frac{RT}{\sqrt{2} \pi d^2 N_A P}, \dots\dots\dots(4)$$

where R is the universal gas constant, T is absolute temperature, d is diameter of molecules, N_A is Avogadro's number, and P is the absolute pressure. The diameter of air molecules is on average 4.12 nm (Porterfield and Kruse 1995). The viscosity of a gas depends on the mean free path of the molecules, mean velocity of the molecules, and on the density of the gas. As the mean free path is inversely dependent on the density the viscosity is independent on pressure (Maxwell 1866). At low pressure we assume that the mean free path equals the average pore diameter for the porous chalk (Fabricius 2010). Thus Eq. 4 corresponds to an absolute pressure of 36 kPa for a chalk with a pore diameter of 0.74 μm. Assuming that the mean free path remains constant for this and lower pressures and a perfect gas gives

$$\rho_{\text{gas}} = \frac{P}{R_{\text{specific}} T}, \dots\dots\dots(5)$$

That is a density of 4.28 × 10⁻⁴ g/cm³ when R_{specific} for dry air is 287.058 J kg⁻¹ K⁻¹. The absolute viscosity for air (assuming 80% nitrogen and 20% oxygen) at an absolute pressure of up to 36 kPa is 0.0216 mPa·s (NIST 2008).

Electrical skin depth. As the purpose of this review is to combine the results regardless of pore fluid we need to take the electrical charge of the chalk surface into account and whether this affects the fluid close to the solid surface. Water with dissolved ions is an electrolyte and the solid surface influence the charge balance to the distance where the ions totally screen the surface charge. Ions positioned further than this distance from the surface, will not be influenced. For oil there is no effect. If the water influenced by the charge is held back compared to the flow in the pores it is a viscous effect and we term it the electrical skin depth in order to avoid confusion with the viscous skin depth in accordance with the use by Johnson et al. (1987). The Debye-Hückel theory gives the screening length, κ^{-1} , for an electrolyte (Lyklema 1991) as

$$\kappa^{-1} = \left(\frac{\varepsilon_0 \varepsilon_r k_B T}{2 N_A e^2 I} \right)^{1/2}, \dots\dots\dots (6)$$

where ε_0 is the permittivity of vacuum, ε_r is relative dielectric permittivity, k_B is Boltzmann's constant, and e is the elementary charge. The number of ions and ionic strength, I , are determined from the chemical composition of the water. The screening length indicates when the charge of the chalk surface is screened by the ions in the electrolyte. We test if this may estimate the skin depth κ^{-1} by comparing a series of permeability data on Liège chalk (**Fig. 2**). Schroeder (2002) lists the composition for Liège tap water and equilibrated water and this in turn gives a Debye screening length of $\kappa^{-1} = 2.42$ nm for tap water and $\kappa^{-1} = 5.52$ nm for equilibrated water. We then approximate the skin depth with κ^{-1} . It acts as a reduction of the porosity and it also affects the permeability. This is quantified with respect to the specific surface by

$$\varphi_{\text{reduced}} = \varphi - (1 - \varphi) \kappa^{-1} S_a \rho_s, \dots\dots\dots (7)$$

and with the use of Kozenys equation this can in principle transfer a permeability measured on an oil saturated specimen to a permeability valid for the specimen being water saturated. The specific surface is not known and is found for regular intervals of porosity from the actual permeability read from the oil regression line. We assume that the specific surface is practically unaffected by the skin and use the Debye length of equilibrated water inserted in Eq. 6 and Eq. 7 for calculating reduced porosity, φ_{reduced} caused by replacing oil with water. Through Eq. 5 we then model permeability in water saturated state and obtain the calculated "Oil to water calc." line in Fig. 2. It shows the permeability measured on Liège chalk for specimens saturated with oil or water. The result is a permeability line in good proximity to the measured permeability for water saturated specimens and supports the hypothesis that skin depth may be approximated by κ^{-1} .

Rate dependence. From De Gennaro and Pereira (2008) and Priol et al. (2007) a dataset on oedometer tests on Liège chalk gives the strain rate ($d\varepsilon/dt$) dependence of the stress at yield, σ_{yield} , illustrated in **Fig. 3**. Fitting the slope of the regression lines to the Biot critical frequency for the dry, water and oil saturated states gives the correlation

$$\ln(\sigma_{\text{yield}}) = 381 f_c^{-0.5} \ln\left(\frac{d\varepsilon}{dt}\right), \dots\dots\dots (8)$$

where $d\varepsilon/dt$ in principle should be divided by a reference rate and the multiplied constant should have the unit $\text{s}^{0.5} \times \text{MPa}$ in order to arrive at a correct unit for the yield. For simplicity we choose to keep the above format with the strain rate required as s^{-1} and the Biot critical frequency as s^{-1} , which gives values in the 0–1 range for the hypothetical σ_{yield} as seen on **Fig. 4**.

PASACHALK2 (2003) presents data from a series of hydrostatic tests with stress rate dependence. This is a different stress path than for the data set giving Eq. 8 but Wood (1990) finds that the yield surface retains its shape, although the size of the yield surface depends on the rate. Fitting with the Biot critical frequency by using the same formulation as above but by only fitting for the multiplication factor gives

$$\ln(\sigma_{\text{yield}}) = 1700 f_c^{-0.5} \ln\left(\frac{d\sigma}{dt}\right), \dots\dots\dots(9)$$

where the stress rate, $d\sigma/dt$, is given in 10^{-1} GPa/s and the critical frequency is in s^{-1} .

Stress plots. The mean effective stress p' , and the generalized shear stress, q , definitions are (Fjær et al. 2008):

$$p' = \frac{1}{3}(\sigma'_1 + \sigma'_2 + \sigma'_3), \text{ and}$$

$$q = \frac{1}{\sqrt{2}}\sqrt{(\sigma'_1 - \sigma'_2)^2 + (\sigma'_2 - \sigma'_3)^2 + (\sigma'_1 - \sigma'_3)^2}. \dots\dots\dots(10)$$

This defines the axes in a traditional way of representing failure and yield results for different rock mechanical tests. Krenk (2000) defines an expression to draw a combined failure and yield envelope for each material:

$$q = q_{\text{max}} \left(1 - \left(\frac{p' - p_a}{p_{\text{max}}}\right)^n\right) (p' - p_a). \dots\dots\dots(11)$$

The conceptual plot on **Fig. 5** illustrates the stress paths for the traditional rock mechanical tests: Brazilian indirect tensile strength test, unconfined compression test, hydrostatic test, and triaxial test. The indirect tensile strength is here interpreted as being equivalent to the uniaxial tensile strength (Mellor and Hawkes 1971) and is therefore plotted on the negative p' axis. At failure the intermediate stress, σ_2 , is zero as stated in Jaeger et al. (2007) and the failure point can therefore not be plotted directly in the p' - q diagram since the Lode angle is not zero. We choose to interpret the Brazilian test result as similar to the direct tensile strength to get a stress representation in a reasonable manner. There exist biaxial stress results for concrete (Lade 1982; Xiaoping et al. 1989) where the extensional behavior of the material is investigated and from that $\sigma_{t, \text{Brazilian}} = \sigma_t$ as a close approximation.

Results

Table 3 lists the supplementary experimental test results. Combining for each test result the strain or stress rate dependencies with the Biot critical frequency result in the color-scaled generalized shear stress versus effective mean stress plot shown in **Fig. 6**. We find that data points with red shading represent higher yield stress or stress at failure than points with green or blue shading following an overall ranking according to the function $f(f_c \ln(de/dt))$ (Eq. 8) and function $f(f_c \ln(d\sigma/dt))$ (Eq. 9). The two functions thus correlate with the chalk strength.

Results from hydrostatic, Brazilian, and unconfined compression tests are singled out and presented in **Fig. 7, Fig. 8, and Fig. 9**. These also illustrate the effect of pore fluid type and temperature. The larger symbols (with a cross in them) in the plots represent the supplementary experimental test series from Table 3. Note that one specimen exhibited premature failure due to chipping at the bottom edge of the specimen and therefore is excluded.

Discussion

All the test results for high porosity and weakly cemented chalk from the references listed in Table 1 and the supplementary test series show a consistent pattern regardless of material properties, test type, pore fluid, and temperature. Hence when we interpret the Biot critical frequency as a friction factor for the fluid-solid friction and find the above pattern we assume that the solid-solid friction is independent on fluid. Note that the increased temperature weakens the fluid saturated chalk. Although some 20°C to 130°C data are from within the same test series, e.g. glycol on Fig. 8, and can be seen to follow the correlation, others are performed on different chalk series and have different porosities or strain rates, e.g. the methanol and seawater series on Fig. 7. These latter sets should not be compared with each other to simply look for temperature effects but only with

the general correlation, which they fit. The U-seawater is artificial seawater without either sulphate or magnesium, for further details see Korsnes et al. (2006).

To illustrate the implications of our work, we apply the regression lines from Fig. 7, Fig. 8 and Fig. 9 to experimental data on Valhall chalk (Ruddy et al. 1989). When we use the estimated parameters in **Table 4** we obtain a yield strength of 5.5 MPa at field conditions for chalk saturated with light crude oil. Comparing this with the laboratory determined yield strength range of 5.5 to 6.9 MPa (average 6.2 MPa) from Ruddy et al. (1989) shows the influence of temperature and strain rate. This result was obtained by taking into account the field rate of $2.8 \times 10^{-10} \text{ s}^{-1}$ (0.0001%/hour) and a temperature of 90°C. The calculation uses the following approximate values: The density for brine at 90°C is 1.01 g/cm³ and the viscosity is 0.37 mPa·s. For a light crude oil at the same temperature the density is 0.82 g/cm³ and the viscosity is 0.67 mPa·s. The porosity of 45% used in Table 4 is similar to Valhall and chosen for comparison.

The plots of the failure-yield envelopes and the specific rock mechanical test results illustrate the Biot critical frequency coupled with the rate dependence. There is a clear correlation among the data, and we propose that the scatter in the results may be due to the disregarded cementation and normal variability of geologic materials.

The correlation is less distinct for the Brazilian plot on Fig. 8 but focusing on trends of temperature effect gives correlations for glycol and water which are similar. The seawater results (squares in Fig. 8) in accordance with the correlation represent high salinity seawater where the high content of salts, 100–250 g/l NaCl and 50–700 g/l CaCl₂·2H₂O (Risnes et al. 2003) has a large effect on the density and viscosity. The Biot critical frequency increases with temperature for dry media and the dry Brazilian and unconfined compression test results show an increase in failure strength with temperature (Fig. 8 and Fig. 9).

Upscaling from laboratory results to reservoir application at reservoir conditions (stress level, field deformation rate and field temperatures for a light crude oil with low viscosity and density) is exemplified in Table 4 when stating initial input parameters and using the correlations. This is just one example and show the possible improvement which the present model could contribute with.

Conclusion

The Biot critical frequency can be used as a friction factor in fully saturated chalk with a rate-dependent term included. This allows us to predict the effect of changing the pore fluid properties. We find that the critical frequency is correlated to both the failure and the yield results obtained from standard rock mechanical tests: Brazilian, unconfined compression, hydrostatic, and triaxial tests. These correlations are used to extrapolate from laboratory conditions to reservoir conditions, which are exemplified for brine and a light crude oil for reservoir chalk at 90°C. A perspective for the use of this friction factor is in relation to water flooding of chalk reservoirs, where we may predict the consequence of replacing the natural pore fluids with injected water.

A systematic observed difference in absolute permeability measured with oil and with water has by earlier workers been explained as a consequence of wettability. We find that the high permeability measured by oil is the “true” absolute permeability, whereas the lower permeability measured with water can be explained by a narrowing of the effective pores caused by the space taken up by the electrical skin. The skin depth is here approximated by the Debye length for an electrolyte.

Nomenclature

e = elementary charge, q, C

f_c = Biot critical frequency, 1/t, s⁻¹

f = frequency of elastic wave, 1/t, s⁻¹

- I = ionic strength of electrolyte, n/L^3 , mol/L
 k = absolute permeability (fluid flow), L^2 , m^2
 k_B = Boltzmann's constant, $mL^2/t^2 \theta$, JK^{-1}
 N_A = Avogadro number, n^{-1} , mol^{-1}
 P = Pressure, m/Lt^2 , MPa
 p' = effective mean stress, m/Lt^2 , MPa
 q = generalized shear stress, m/Lt^2 , MPa
 R_{specific} = specific gas constant, $L^2/t^2 \theta$, $JK^{-1}kg^{-1}$
 S_s = specific surface area (grain surface area to grain volume), L^2/L^3 , m^2/m^3
 S_a = specific surface area (grain surface area to solid mass), L^2/m , m^2/g
 T = absolute temperature, θ , K
 δ = viscous skin depth, L, m
 ε = strain
 ε_0 = permittivity of vacuum, q^2t^2/mL^3 , F/m
 ε_r = relative dielectric permittivity
 η = absolute viscosity, m/Lt , $mPa \cdot s$
 κ^{-1} = Debye length, L, nm
 λ = mean free path, L, m
 ρ_{fl} = fluid density, m/L^3 , g/cm^3
 ρ_{gas} = gas density, m/L^3 , g/cm^3
 ρ_s = solid density, m/L^3 , g/cm^3
 σ = stress, m/Lt^2 , MPa
 σ'_1 = effective major principal stress, m/Lt^2 , MPa
 σ'_2 = effective intermediate principal stress, m/Lt^2 , MPa
 σ'_3 = effective minor principal stress, m/Lt^2 , MPa
 σ_c = strength at failure, unconfined compression test, m/Lt^2 , MPa
 σ_t = tensile strength, Brazilian test, m/Lt^2 , MPa
 σ_{yield} = stress at yield, m/Lt^2 , MPa
 φ = porosity

SI-metric conversion factors

cp \times 1.0*	E-00 = mPa·s
ft \times 3.048*	E-01 = m
$^{\circ}F$ $(^{\circ}F - 32)/1.8$	= $^{\circ}C$
lbf/gal \times 1.1998 264	E+02 = kg/m ³
psi \times 6.894757	E-03 = MPa

*Conversion factor is exact.

Acknowledgments

We are grateful to the associate editor and three anonymous reviewers for inspiring comments. We also thank Ole Hededal, DTU Byg, for good discussions and his invaluable contribution with the stress plots.

References

- Adam, L., Batzle, M., Lewallen, K.T. and van Wijk, K., 2009. Seismic Wave Attenuation in Carbonates. *Journal of Geophysical Research, American Geophysical Union*, **114** (B06208): 1–14. doi: 10.1029/2008JB005890.
- Andreassen, K.A., and Fabricius, I.L., 2010. Biot Critical Frequency Applied to Description of Failure and Yield of Highly Porous Chalk with Different Pore Fluids. *Geophysics, in press*.
- Biot, M.A., 1956a. Theory of Propagation of Elastic Waves in a Fluid-Saturated Porous Solid. I. Low-Frequency Range. *The Journal of the Acoustical Society of America*, **28** (2): 168–178. doi: 10.1121/1.1908239.
- Biot, M.A., 1956b. Theory of Propagation of Elastic Waves in a Fluid-Saturated Porous Solid. II. Higher Frequency Range. *The Journal of the Acoustical Society of America*, **28** (2): 179–191. doi: 10.1121/1.1908241.
- Boozer, G.D., Hiller, K.H. and Serdengecti, S., 1963. Effects of pore fluids on the deformation behavior of rocks subjected to triaxial compression. Proceedings to the 5th US Rock Mechanics Symposium, USA. 579–625.
- Bourbié, T., Coussy, O., and Zinzner, B., 1987. *Acoustics of Porous Media*. Editions Technip.
- Collin, F., Cui, Y.J., Schroeder, C., and Charlier, R., 2002. Mechanical Behaviour of Lixhe Chalk Partly Saturated by Oil and Water: Experiment and Modelling. *International Journal for Numerical and Analytical Methods in Geomechanics*, **26** (9): 897–924. doi: 10.1002/nag.229.
- De Gennaro, V. and Pereira, J.M., 2008. Viscoplastic Modelling of Unsaturated Geomaterials. *Proc.*, The 12th International Conference of International Association for Computer Methods and Advances in Geomechanics (IACMAG), Goa, India, 2232–2241.
- Delage, P., Schroeder, C., and Cui, Y.J., 1996. Subsidence and Capillary Effects in Chalks. *Proc.*, Eurock, Torino, Italy, 1291–1298.
- Fabre, D. and Gustkiewicz, J., 1997. Poroelastic Properties of Limestones and Sandstones Under Hydrostatic Conditions. *International Journal of Rock Mechanics and Mining Sciences*, **34** (1): 127–134. doi: 10.1016/S1365-1609(97) 80038-X.
- Fabricius, I.L., Baechle, G.T., and Eberli, G.P., 2010. Elastic moduli of dry and water-saturated carbonates – effect of depositional texture, porosity and permeability, *Geophysics*, **75** (3): N65–N78.
- Fabricius, I.L., 2010. A mechanism for water weakening of elastic moduli and mechanical strength of chalk, SEG 2010 International Exposition and 80th Annual Meeting, Denver, Colorado, 17–22 October.
- Fjær, E., Holt, R.M., Horsrud, P., Raaen, A.M., and Risnes, R., 2008. *Petroleum related rock mechanics*, volume 53 of *Developments in Petroleum Science*, second edition: Elsevier.
- Gutierrez, M., Øino, L.E., and Høeg, K., 2000. The Effect of Fluid Content on the Mechanical Behaviour of Fractures in Chalk. *Rock Mechanics and Rock Engineering*, **33** (2): 93–117.
- Hellmann, R., Renders, P.J.N., Gratier, J.P. and Guiguet, R., 2002. Experimental pressure solution compaction of chalk in aqueous solutions. Part 1. Deformation behavior and chemistry. *The Geochemical Society, Special publication No. 7*, 129–152.
- Hjuler, M.L. and Fabricius, I.L., 2009. Engineering Properties of Chalk Related to Diagenetic Variations of Upper Cretaceous Onshore and Offshore Chalk in the North Sea Area. *Journal of Petroleum Science and Engineering*, **68** (3-4): 151–170. doi: 10.1016/j.petrol.2009.06.005.
- Jaeger, J. C., Cook, N. G. W., and Zimmerman, R. W., 2007. *Fundamentals of rock mechanics*, fourth edition: Blackwell Publishing.
- Johnson, D.L., Koplík, J., and Dashen, R., 1987. Theory of Dynamic Permeability and Tortuosity in Fluid-Saturated Porous Media. *Journal of Fluid Mechanics Digital Archive*, **176**: 379–402. doi: 10.1017/S0022112087000727.
- Korsnes, R.I., Madland, M.V., and Austad, T., 2006. Impact of Brine Composition on the Mechanical Strength of Chalk at High Temperature. *Proc.*, Eurock, The International Symposium of the International Society for Rock Mechanics, Belgium, 9–12 May, 133–140. Taylor & Francis/Balkema.
- Korsnes, R.I., Madland, M.V., Austad, T., Haver, S., and Røslund, G., 2008a. The Effects of Temperature on the Water Weakening of Chalk by Seawater. *Journal of Petroleum Science and Engineering*, **60** (3–4): 183–193. doi: 10.1016/j.petrol.2007.06.001.
- Korsnes, R.I., Wersland, E., Austad, T., and Madland, M.V., 2008b. Anisotropy in Chalk Studied by Rock Mechanics. *Journal of Petroleum Science and Engineering*, **62** (1–2): 28–35. doi:10.1016/j.petrol.2008.06.004.
- Krenk, S., 2000. Characteristic state plasticity for granular materials: Part I: Basic theory. *International Journal of Solids and Structures*, **37** (43): 6343–6360. doi:10.1016/S0020-7683(99)00278-4.

- Lade, P.V., 1982. Three-Parameter Failure Criterion for Concrete. *Journal of the Engineering Mechanics Division, ASCE*, **108** (5): 850–863.
- Lyklema, J., 1991. *Fundamentals of Interface and Colloid Science*, Volume I. London: Academic Press.
- Madland, M.V., Finsnes, A., Alkafadgi, A., Risnes, R., and Austad, T., 2006. The Influence of CO₂ Gas and Carbonate Water on the Mechanical Stability of Chalk. *Journal of Petroleum Science and Engineering*, **51** (3–4): 149–168. doi: 10.1016/j.petrol.2006.01.002.
- Madland, M.V., Korsnes, R.I., and Risnes, R., 2002. Temperature Effects in Brazilian, Uniaxial and Triaxial Compressive Tests with High Porosity Chalk. Paper SPE 77761-MS presented at the 2002 SPE Annual Technical Conference and Exhibition, Texas, 29 September–2 October. doi: 10.2118/77761-MS.
- Mavko, G., Mukerji, T., and Dvorkin, J., 2009. *The Rock Physics Handbook: Tools for Seismic Analysis in Porous Media*. Second edition, New York: Cambridge University Press.
- Maxwell, J. C., 1866. The Bakerian Lecture: On the Viscosity or Internal Friction of Air and Other Gases. *Philosophical Transactions of the Royal Society of London*, **156**: 249–268. doi: 10.1098/rstl.1866.0013.
- Mellor, M. and Hawkes, I., 1971. Measurement of Tensile Strength by Diametral Compression of Discs and Annuli. *Engineering Geology*, **5** (3): 173–225. doi: 10.1016/0013-7952(71)90001-9.
- Mortensen, J., Engstrøm, F., and Lind, I., 1998. The Relation Among Porosity, Permeability, and Specific Surface of Chalk From the Gorm Field, Danish North Sea. Paper 31062-PA, *SPE Reservoir Evaluation & Engineering*, **1** (3): 245–251. doi: 10.2118/31062-PA.
- NIST, 2008, Thermophysical properties of fluid systems: webbook, accessed 23 September 2010; <http://webbook.nist.gov/chemistry/fluid/>.
- PASACHALK, 2000. Mechanical Behaviour of Partially and Multiphase Saturated Chalks Fluid–Skeleton Interaction : Main Factor of Chalk Oil Reservoirs Compaction and Related Subsidence, Part 1. Final report, European Joule III contract N° JOF3CT970033.
- PASACHALK2, 2003. Mechanical Behaviour of Partially and Multiphase Saturated Chalks Fluid–Skeleton Interaction : Main Factor of Chalk Oil Reservoirs Compaction and Related Subsidence, Part 2. Final report, European Joule III contract N° ENK6-2000-00089.
- Porterfield, W.W. and Kruse, W., 1995. Loschmidt and the Discovery of the Small (translation of Loschmidt, J., 1865. On the Size of the Air Molecules. *Sitzb. Akad. Wiss. Wien* 52, 395–413). *Journal of Chemical Education*, **72** (10), 870–875. doi: 10.1021/ed072p870.2.
- Priol, G., De Gennaro, V., Delage, P., and Servant, T., 2007. Experimental Investigation on the Time Dependent Behaviour of a Multiphase Chalk. In *Experimental Unsaturated Soil Mechanics*, volume 112 of *Springer Proceedings in Physics*, 161–167. Springer Berlin Heidelberg. doi: 10.1007/3-540-69873-6_15.
- Rhett, D. and Lord, C., 2001. Water Weakening in Sedimentary Rocks. DC Rocks 2001. *Proc., The 38th US Symposium on Rock Mechanics (USRMS)*, 121–128.
- Risnes, R., Garpestad, O.J., Gilje, M., Oland, L.T., Ovesen, M., and Vargervik, E., 1998. Strain Hardening and Extensional Failure in High Porosity Chalk. Paper SPE 47581-MS presented at the SPE/ISRM Eurock '98, Trondheim, Norway, 8–10 July, 475–484. doi: 10.2118/47581-MS.
- Risnes, R., Haghghi, H., Korsnes, R.I., and Natvik, O., 2003. Chalk–Fluid Interactions with Glycol and Brines. *Tectonophysics*, **370** (1–4): 213–226. doi: 10.1016/S0040-1951(03)00187-2.
- Risnes, R. and Kleppa, E., 1996. Plastic Behaviour of High Porosity Chalk in Constant K-Ratio Tests. Paper presented at the 5th North Sea Chalk Symposium, France.
- Risnes, R., Kristensen, C.N., and Andersen, M.A., 1996. Triaxial Tests on High Porosity Chalk with Different Saturating Fluids. Paper presented at the 5th North Sea Chalk Symposium, France.
- Risnes, R., Madland, M.V., Hole, M., and Kwabiah, N.K., 2005. Water Weakening of Chalk—Mechanical Effects of Water–Glycol Mixtures. *Journal of Petroleum Science and Engineering*, **48** (1–2): 21–36. doi: 10.1016/j.petrol.2005.04.004.
- Ruddy, I., Andersen, M.A., Pattillo, P.D., Bishlawi, M., and Foged, N., 1989. Rock Compressibility, Compaction, and Subsidence in a High-Porosity Chalk Reservoir: A Case-Study of Valhall Field. *Journal of Petroleum Technology*, **41** (7): 741–746. doi: 10.2118/18278-PA.
- Schroeder, Ch., 2002. Du coccolithe au réservoir pétrolier. Approche phénoménologique du comportement mécanique de la craie en vue de sa modélisation à différentes échelles. PhD dissertation, Université de Liège, Belgium.
- Schroeder, Ch., Bois, A.-P., Maury, V. and Halle, G., 1998. Water/chalk (or collapsible soil) interaction: Part II. Results of tests performed in laboratory on Lixhe chalk to calibrate water/chalk models. *Paper 47587 presented at Eurock, SPE/ISRM, Norway*, 833–840.

-
- Schroeder, Ch. and Shao, J., 1996. Plastic Deformation and Capillary Effects in Chalks. Paper presented at the 5th North Sea Chalk Symposium, France.
- Serway, R. A., Beichner, R. J. and Jewett, J. W., 2000. *Physics for Scientists and Engineers with Modern Physics*. Orlando: Saunders.
- Wood, D.M., 1990. *Soil Behaviour and Critical State Soil Mechanics*. New York: Cambridge University Press.
- Xiaoping, Y., Ottosen, N. S., Thelandersson, S. and Nielsen, M. P., 1989. *Review of Constructive Models for Concrete*. JRC Scientific and Technical Reports (EUR collection).

Table 1—Reference to studied data sets.

<u>Liège Chalk Li</u>	<u>ège Chalk</u>
Delage et al. (1996)	Collin et al. (2002)
Risnes and Kleppa (1996)	Madland et al. (2002)
Risnes et al. (1996)	Risnes et al. (2003)
Schroeder and Shao (1996)	Risnes et al. (2005)
Fabre and Gustkiewicz (1997)	Korsnes et al. (2006)
Risnes et al. (1998)	Korsnes et al. (2008b)
Rhett and Lord (2001)	
<u>Aalborg Chalk S</u>	<u>tevns Chalk</u>
Madland et al. (2002)	Korsnes et al (2006)
Risnes et al. (2003)	Korsnes et al. (2008a)
Madland et al. (2006)	Korsnes et al. (2008b)

Table 2—Supplementary experimental test series with unconfined compression tests (UCS) and Brazilian tests at 25°C. The specimen label states the specimen diameter and is either 50 mm or 54 mm.

UCS FI	<u>uid</u>	Porosity (%)	Bulk density (g/cm ³)	Dry density (g/cm ³)	f_c (s ⁻¹) [#]
SC54 A	Water	48.7	1.867	1.391	2.10×10 ⁷
SC50 C	Water	44.6	1.936	1.502	3.05×10 ⁷
SC50-2 C	Water	44.5	1.924	1.504	3.06×10 ⁷
ST50 I	sopar-L [‡] 4	4.1	1.841	1.514	6.72×10 ⁷
SC54 B	Dry	47.8	1.421	1.416	3.48×10 ⁸
SC50 B	Dry	45.4	1.481	1.481	4.29×10 ⁸
SC50-2 B	Dry	44.2	1.512	1.512	4.75×10 ⁸
SC50-2 A	Dry, Vacuum	44.6	1.501	1.501	1.50×10 ⁹
SC50 A	Dry, Vacuum	45.0	1.490	1.490	1.45×10 ⁹
Brazilian FI	<u>uid</u>	Porosity (%)	Bulk density (g/cm ³)	Dry density (g/cm ³)	f_c (s ⁻¹) [#]
SC54 D	Water	48.1	1.875	1.408	2.22×10 ⁷
SC54 C	Dry	48.4	1.399	1.399	3.30×10 ⁸
SC50-2 B	Dry	44.6	1.502	1.502	4.59×10 ⁸
ST50 I	sopar-L [‡] 4	5.1	1.819	1.488	6.19×10 ⁷

[#]Calculated according to Eq. 1 and Eq. 3; for water also Eq. 4 to 6 (giving $\kappa^{-1} = 5.52$ nm, Schroeder (2002) lists the chemical composition of the equilibrated water) and Eq. 7.

[‡]Mineral oil with $\rho_H = 0.763$ g/cm³ and $\eta = 1.674$ mPa×s.

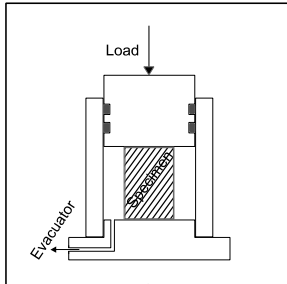


Fig. 1—Test set-up both for the UCS and the Brazilian tests.

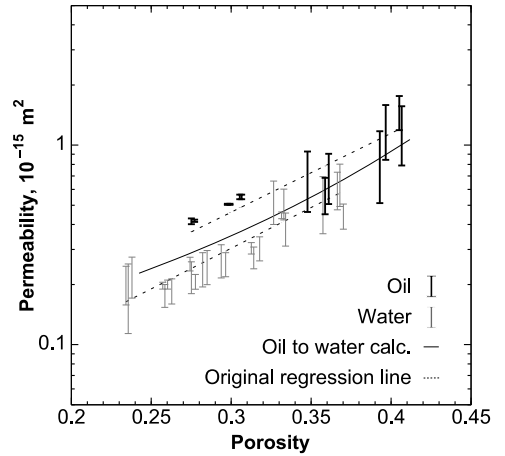


Fig. 2—Test of the skin depth hypothesis using a water film thickness of 5.52 nm obtained from the Debye length for equilibrated water at 20°C. Each bar represents a large number of test results for Liège chalk. The calculated water permeability from the oil regression line falls closely to the measured water permeability. Dataset from the PASACHALK project (PASACHALK 2000).

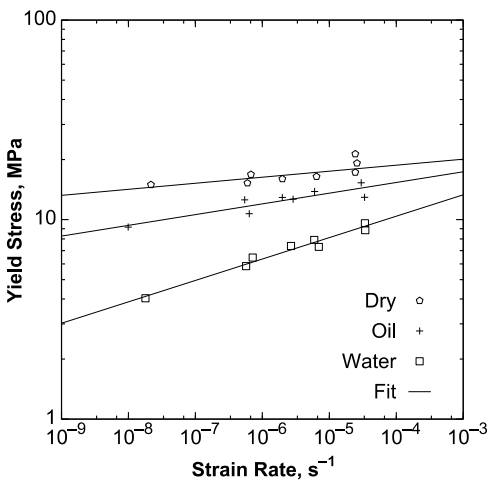


Fig. 3—Stress at yield from oedometer tests on Liège chalk with different pore fluids and at various strain rates, presented in log-log plot identically to the original plot by De Gennaro and Pereira (2008). There is a good correlation between stress at yield and the applied strain rate.

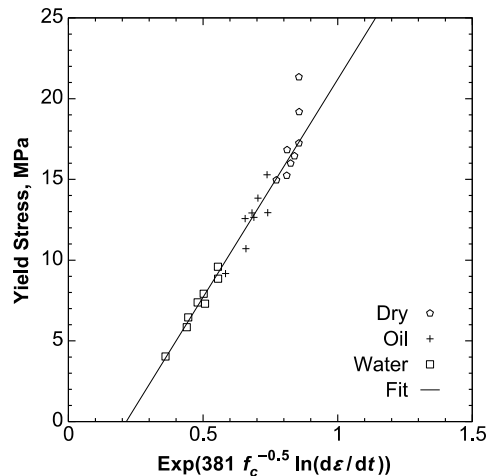


Fig. 4—Same dataset as Fig. 3. Correlation found from fitting the slopes in Fig. 3 to a function of the Biot critical frequency. The different pore fluids contribute with different density and viscosity to the critical frequency. This result in a good correlation across the whole range. Data from De Gennaro and Pereira (2008).

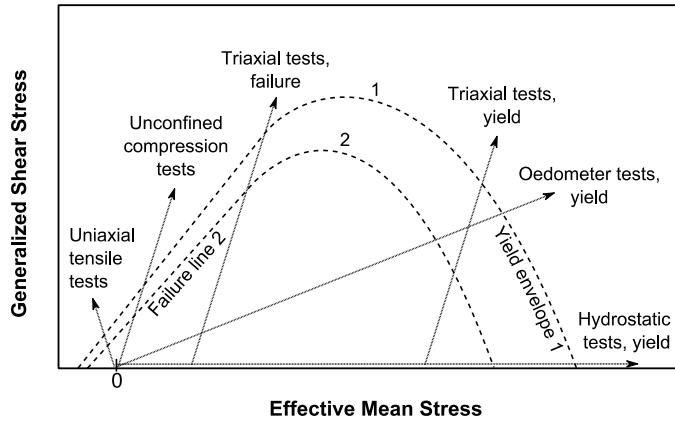


Fig. 5—Concept of p - q plot with the stress paths of the common rock mechanical tests. The sketch includes failure-yield envelopes for two different materials with rock 1 stronger than rock 2.

Table 3—Results for the supplementary experimental test series on Stevns chalk. Ambient temperature 25°C. Table 2 contains the classification data.

Specimen	Flu	id	σ_c (MPa)	Strain rate (%/hour) [#]
SC54 A	Water		2.1	3.4
SC50 C	Water		3.2	1.8
SC50-2 C	Water		3.2	1.9
ST50 I	sopar-L		5.9	2.8
SC54 B	Dry		5.9	3.0
SC50 B	Dry		7.9	2.4
SC50-2 B	Dry		8.5	3.0
SC50-2 A	Dry, Vacuum		9.9 2	.3
SC50 A*	Dry, Vacuum		4.4 1	.8
Specimen	Flu	id	σ_r (MPa)	
SC54 D	Water		0.35	
SC54 C	Dry		0.80	
SC50-2 B	Dry		0.91	
ST50 I	sopar-L		0.58	

*Premature failure by chipping at the bottom edge.

[#]Average value based on external strain measurement.

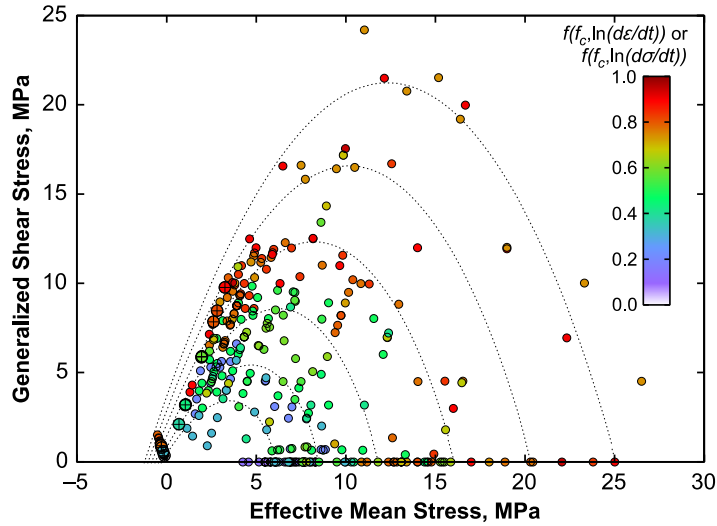


Fig. 6—Rock mechanical test results combined across chalk type, pore fluid, temperature and applied strain or stress rate. Isolines with assumed equal levels of $f(f_c, \ln(ds/dt))$ or $f(f_c, \ln(d\sigma/dt))$ are drawn at regular intervals to guide the interpretation. Each gray scaled circle represents a result from one test being either a Brazil, unconfined compression or triaxial test and either a failure or yield point. The larger circles with a cross represent results from the supplementary test series in Table 3.

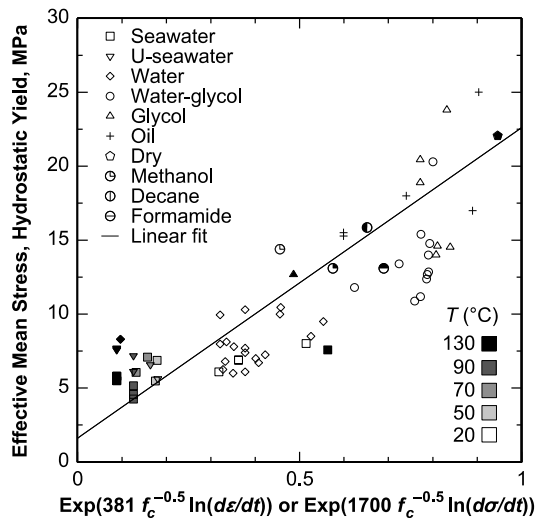


Fig. 7—Yield strength for both strain and stress rate controlled hydrostatic tests with specification of pore fluid and temperature. These data lie on the abscissa of Fig. 5. The water-glycol symbol represents a pore fluid mixture with different mol% water ranging from 80 mol% to 2 mol%. All data points for oil are at a temperature of 20°C with viscosity ranging from 3.0 mPa·s for Soltrol 170 to 120 mPa·s for liquid paraffin.

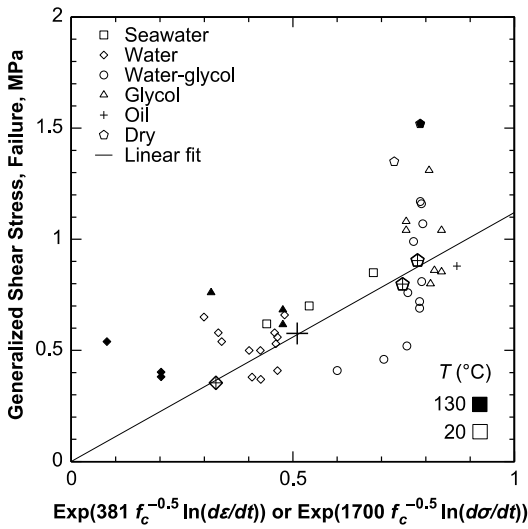


Fig. 8—Stress at failure for Brazilian tests (with the direct tensile interpretation $q = \sigma$). No rate dependence is included. As expected there is scattering of the results as the test method has inherent variability. A number of points correspond to test series as an average of 10 to 21 tests and some only correspond to one test. The seawater results are for high salinity seawater having a high density and viscosity compared to standard seawater and therefore a higher value for $f(f_c, \ln(d\varepsilon/dt))$. The larger symbols with a cross represent results from the supplementary test series in Table 3.

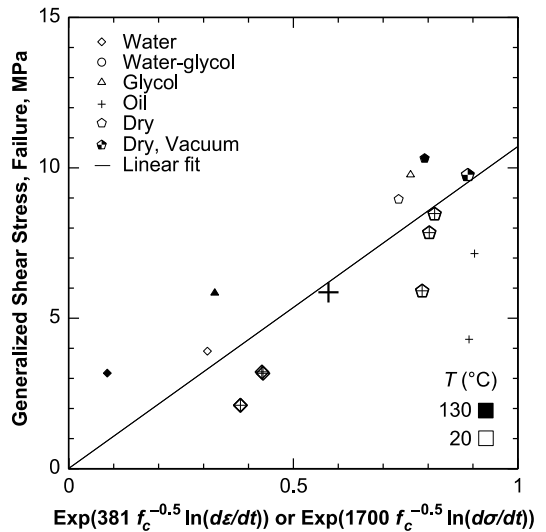


Fig. 9—Stress at failure for unconfined compression tests. Note the high strength for the dry specimen at high temperature corresponds to a high value of $f(f_c, \ln(d\varepsilon/dt))$. The failure points for the oil saturated chalk are outliers from their respective test series and may represent very weak chalk specimens. The larger symbols with a cross represent results from the supplementary test series in Table 3.

Table 4—Predicted failure and yield for field conditions. Strain rate of 0.0001%/hour for chalk with porosity of 45%, permeability of $1.44 \times 10^{-15} \text{ m}^2$, and at 90°C. The regression line equations are valid for the function $f(f_c, \ln(d\varepsilon/dt))$ as x input and σ as y given in MPa for output.

Test type	Brine	Light crude oil
Hydrostatic, yield, MPa	3.5	5.5
Brazilian, failure, MPa	0.08	0.20
Unconf. compr., failure, MPa	0.8	1.9
	<u>Regression line</u>	<u>R² (No. tests)</u>
Hydrostatic, yield, Fig. 7.	$y = 20 \times x + 2.0$	0.71 (71)
Brazilian, failure, Fig. 8.	$y = 1.12 \times x$	0.46 (362)
Unconf. compr., failure, Fig. 9.	$y = 10.7 \times x$	0.53 (15)

Appendix E

Paper III

Andreassen, K.A., and Fabricius, I.L. (2010).

Biot Critical Frequency Applied as Common Friction Factor for Chalk with Different Pore Fluids and Temperatures.

Paper ARMA 10-453 presented at the 44th Us Rock Mechanics Symposium and 5th U.S.-Canada Rock Mechanics Symposium, Salt Lake City, Utah, June 27–30.



ARMA 10-453

Biot Critical Frequency Applied as Common Friction Factor for Chalk with Different Pore Fluids and Temperatures

Andreassen, K.A. and Fabricius, I.L.

Technical University of Denmark, Kgs. Lyngby, Denmark

Copyright 2010 ARMA, American Rock Mechanics Association

This paper was prepared for presentation at the 44th US Rock Mechanics Symposium and 5th U.S.-Canada Rock Mechanics Symposium, held in Salt Lake City, UT June 27–30, 2010.

This paper was selected for presentation at the symposium by an ARMA Technical Program Committee based on a technical and critical review of the paper by a minimum of two technical reviewers. The material, as presented, does not necessarily reflect any position of ARMA, its officers, or members. Electronic reproduction, distribution, or storage of any part of this paper for commercial purposes without the written consent of ARMA is prohibited. Permission to reproduce in print is restricted to an abstract of not more than 300 words; illustrations may not be copied. The abstract must contain conspicuous acknowledgement of where and by whom the paper was presented.

ABSTRACT: Injection of water into chalk hydrocarbon reservoirs has led to mechanical yield and failure. Laboratory experiments on chalk samples correspondingly show that the mechanical properties of porous chalk depend on pore fluid and temperature. Water has a significant softening effect on elastic properties of chalk as calculated from wave data, and the softening increases with increasing critical frequency as defined by Biot. The critical frequency is the highest frequency where wave propagation is controlled by solid-fluid friction. The Biot critical frequency is thus a measure of this friction and we propose that the fluid effect on mechanical properties of highly porous chalk may be the result of liquid-solid friction. Applying a different strain or stress rate is influencing the rock strength and needs to be included. The resulting function is shown to relate to the material dependent and rate independent b -factor used when describing the time dependent mechanical properties of soft rock or soils. As a consequence it is then possible to further characterize the material constant from the porosity and permeability of the rock as well as from pore fluid density and viscosity which is highly influenced by temperature.

1. INTRODUCTION

Water weakening in chalk has been extensively studied. Many explanations have been proposed including capillary effects with local menisci at the grain contacts strengthening the chalk [1, 2], pressure solution weakening the chalk [3], attractive and repulsive forces at the grain contacts [4], and chemical dissolution followed by precipitation which is affected by the pore fluid composition [5]. These theories apply to a static system of solid and fluid leaving a subject which seems not to have been covered: the aspect of the moving fluid relative to the solid. The most important aspect when considering this subject is the friction arising at the solid-fluid interface. For weakly cemented porous media undergoing time dependent deformation, not only the strength of the rock frame but also the draining of pore fluid plays a role. This drainage is affected by the solid-fluid friction and we propose that an entity describing this friction could be used as an indicator for the mechanical properties.

In this paper we review the available literature on rock mechanical tests performed on highly porous chalk fully saturated with one fluid phase. The purpose is to look for underlying physical properties which might explain the water weakening.

1.1. Background

The Biot critical frequency, f_c , is defined as

$$f_c = \frac{\varphi\eta}{2\pi\rho_f k}, \quad (1)$$

where φ is porosity, η is absolute viscosity of the pore fluid, ρ_f is fluid density, and k is absolute permeability. Biot's critical frequency defines the transition from where the fluid is dominated by viscous forces at low frequencies to where the fluid is dominated by inertial forces at higher frequencies [6, 7]. The drag that the solid motion makes on the fluid and whether this is in the viscous or inertial regime are basically matters of friction between the liquid and the solid. The critical frequency may thus be regarded as a friction factor.

The critical frequency has the units Hertz and in order to non-dimensionalize the factor we chose to use the viscous skin depth, δ , with the definition [8]

$$\delta = \sqrt{\frac{\eta}{\pi\rho_f f}}, \quad (2)$$

where f is the applied frequency. On figure 1 the concept of the viscous skin depth is visualized for the case of a sound wave running through the specimen. For the present application it is the relative fluid-solid movement that is in focus as there both exist a strain of the

solid and a fluid expulsion during the rock mechanical test of the specimen. The situation can still be simplified to figure 1.

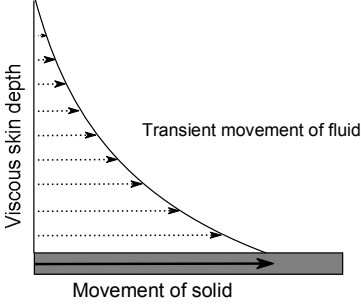


Fig. 1. The viscous skin depth explained from an applied sound wave causing a movement of the solid phase. The fluid-solid friction is determining the transient movement of the fluid, [9].

We choose to use the density and absolute viscosity of water at 20°C (see table 2) and Liège chalk as a reference and accordingly a dimensionless critical frequency becomes

$$\tilde{f}_c = \frac{f_c}{\eta_{\text{water}}/(\pi\rho_{\text{water}}\delta_L^2)}, \quad (3)$$

where the reference viscous skin depth, δ_L , is chosen to be 0.74 μm , which is the average pore diameter for Liège chalk [10]. Other choices are possible in order to make the critical frequency dimensionless but this is not considered further here.

A commonly known friction factor, which also relates to the transition from a flow regime dominated by viscous forces to a flow regime dominated by inertial forces, is the Reynolds number, Re . To estimate the friction for a fluid in laminar flow it is customary to use $64/Re$. As an analogy, the chalk-fluid system is in the flow regime dominated by viscous forces and a friction factor is the dimensionless Biot critical frequency.

On a large set of dry and water saturated carbonate rock samples, Fabricius et al. [11] found the amount of softening of elastic modulus to be correlated with the critical frequency. It is therefore relevant to investigate the influence of the critical frequency on the rock mechanical properties of chalk.

1.2. Time Dependence

In order to describe the time dependent properties of a material several concepts need explanation. The following section contains a brief overview:

The definition of creep index, ε_s , often termed C_a when addressed to the void ratio, is [12]

$$\varepsilon_s = \frac{d\varepsilon}{d(\log(t))}, \quad (4)$$

where ε is strain and t is time. ε_s is determined by plotting the strain vs. logarithmic time for a creep phase and approximate the last part of the curve with a linear regression. In soil mechanics it is the convention to use the void ratio, e , defined as pore volume to solid volume. The conversion from void ratio, e , to strain, ε , is

$$\varepsilon = \frac{\Delta e}{1+e_0}, \quad (5)$$

where e_0 is the initial void ratio.

The definition of compression index, Q , often termed C_c when addressed to the void ratio, is [12]

$$Q = \frac{d\varepsilon}{d(\log(\sigma))}, \quad (6)$$

where σ is stress. For soils Mesri and Godlewski [12] find the relation

$$\frac{\varepsilon_s}{Q} = \frac{d(\log(\sigma))}{d(\log(t))} = b, \quad (7)$$

where b is termed the b -factor or C_d/C_c . The factor b is a constant for any particular soil for all combinations of time, effective stress and strain level [12]. This relationship is also valid for sandstones [13].

For a sample run at interchanging strain rates as illustrated in figure 2, the relation is [13]

$$\frac{\sigma'_{\text{axial},1}}{\sigma'_{\text{axial},2}} = \left(\frac{d\varepsilon_{\text{axial},1}/dt}{d\varepsilon_{\text{axial},2}/dt} \right)^b, \quad (8)$$

where $\sigma'_{\text{axial},1}$ is the effective axial stress related to a point on the stress-strain curve with an applied strain rate of $d\varepsilon_{\text{axial},1}/dt$ and b is the material dependent b -factor.

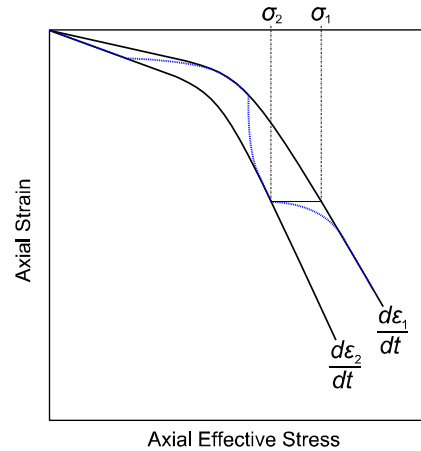


Fig. 2. Conceptual sketch of rate dependence of strain in soft rock. The blue line represents the stress-strain path following two interchanging strain rates. Strain rate 1 is higher than strain rate 2. The material responds as a stronger material when applying the higher strain rate 1. Based on [13].

Table 1. Overview of the included tests and their references. From [14].

Test Type	Fluid	Temp. (°C)	Applied Rate	Chalk Type	No.	Reference
Triax, Brazil, hydrostatic, UCS	Water, seawater, oil	Room	5.4%/hour or 3 MPa/hour	Liège	[15]	Risnes et al. 1996,
Triax	Water	Room	18.5%/hour	Liège	[16]	Risnes and Kleppa 1996
Triax, hydrostatic	Water, seawater, oil, liquid paraffin, dry	Room	0.4 MPa/hour	Liège	[17]	Schroeder and Shao 1996
UCS, hydrostatic	Water	Room	300 MPa/hour	Liège	[18]	Fabre and Gustkiewicz 1997
Hydrostatic	Methanol	Room	5.5 MPa/hour	Liège	[19]	Risnes et al. 1998
Hydrostatic, triax	Seawater, methanol, decane, formamide, dry	130	12.4 MPa/hour	Liège	[20]	Rhett and Lord 2001
Hydrostatic, triax	Water, oil	Room	3.6 MPa/hour	Liège	[21]	Collin et al. 2002
Triax, Brazil, UCS	Water, glycol	20, 130	0.5%/hour	Liège, Aalborg	[22]	Madland et al. 2002
Brazil, triax	Water, high salinity seawater, glycol	Room	2%/hour or 1%/hour	Liège	[23]	Risnes et al. 2003
Triax, Brazil, hydrostatic	Water, glycol, water-glycol mixture ^a	Room	1%/hour or 0.35%/hour	Liège	[4]	Risnes et al. 2005
Hydrostatic	Distilled water, seawater ^b	130	0.1%/hour	Stevns	[24]	Korsnes et al. 2006
Hydrostatic	Water	20	2.6 MPa/hour	Aalborg	[25]	Madland et al. 2006
Hydrostatic	Distilled water, seawater ^b	Room, 50, 70, 90	1%/hour or 0.1%/hour	Stevns	[26]	Korsnes et al. 2008a
Hydrostatic, Brazil	Water	Room	0.3%/hour	Liège, Stevns	[27]	Korsnes et al. 2008b

^aOf varying mol%. ^bOf different chemical composition.

1.3. Mean Stress-Generalized Shear Stress Plot

The conceptual plot on figure 3 illustrates the stress paths for the traditional rock mechanical tests: Brazil indirect tensile strength test, unconfined compression test, hydrostatic test, oedometer test, and triaxial test. The mean effective stress, p' , and generalized shear stress, q , are [28]

$$p' = \frac{1}{3}(\sigma'_1 + \sigma'_2 + \sigma'_3), \text{ and} \quad (9)$$

$$q = \frac{1}{\sqrt{2}}\sqrt{(\sigma'_1 - \sigma'_2)^2 + (\sigma'_2 - \sigma'_3)^2 + (\sigma'_1 - \sigma'_3)^2},$$

where $\sigma'_1, \sigma'_2,$ and σ'_3 are the effective principal stresses.

An expression which represents the failure-yield envelope is [29]

$$q = q_{\max} \left(1 - \left(\frac{p' - p_a}{p_{\max}} \right)^n \right) (p' - p_a), \quad (10)$$

with q_{\max} controlling the ordinate, p_{\max} controlling the abscissa, p_a controlling the attraction, and n is a shape parameter for the envelope.

The indirect tensile strength is here interpreted as being equivalent to the uniaxial tensile strength [30] and is therefore plotted on the negative p' axis [31].

We do this because the stress state for the Brazil test does not involve equal intermediate and minor stress, although this has been assumed in earlier publications. The intermediate stress, $\sigma'_2,$ is zero as stated by Jaeger et

al. in [32] and can therefore not be plotted directly in the same stress plane as the p' - q plane. The interpretation of the Brazil test result as the uniaxial tensile strength is needed in order to correct for this.

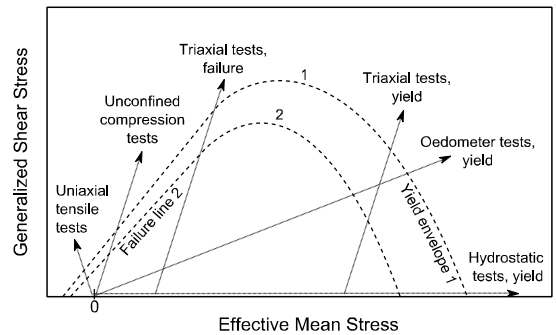


Fig. 3. Standard rock mechanical tests and their stress paths in a p' - q diagram. The rock with failure-yield envelope 1 is a stronger material than the rock with failure-yield envelope 2.

2. METHOD

This investigation is limited to high porosity chalk. The low cementation of this rock should cause the fluid effects to dominate with respect to the chalk frame. The tests are made on outcrop chalk from three different lo-

calities: Liège or Lixhe chalk from a quarry in Belgium, Aalborg chalk from a quarry in western Denmark, and Stevns Chalk from a quarry in eastern Denmark. The physical properties vary among the outcrop chalks, with Liège being characterized by a porosity of generally 0.40 and a permeability of $1.5 \times 10^{-15} \text{ m}^2$. Stevns chalk has a porosity of generally 0.45 and a permeability of $3.5 \times 10^{-15} \text{ m}^2$, whereas Aalborg chalk generally has a porosity of 0.45 and a slightly higher general permeability of $4 \times 10^{-15} \text{ m}^2$. Further characterization of these chalk lithologies is given in [33]. All the selected outcrop chalks have induration H2 and are weakly cemented. Table 1 gives a quick overview of the references included in this review.

For some test series permeability is only stated as a general value, while exact values are given for the porosity. The permeability, k , may be approximated from the porosity, ϕ , [34]

$$k = c \frac{\phi^3}{(1-\phi)^2 S_g^2} = c \frac{\phi^3}{(1-\phi)^2 (S_a \rho_s)^2}, \text{ and} \quad (11)$$

$$c = \left(4 \cos \left(\frac{1}{3} \arccos \left(\phi \frac{8^2}{\pi^3} - 1 \right) + \frac{4}{3} \phi \right) + 4 \right)^{-1},$$

where Kozenys factor c is stated for 3D circular interconnected tubes, and the solid density, ρ_s , of chalk is $2.7 \times 10^3 \text{ kg/m}^3$. The specific surface, S_g , is assumed to be a material property for each chalk locality and therefore does not change between different chalk blocks. Measured specific surface area, S_a , by BET (N_2 adsorption) is $1.7 \text{ m}^2/\text{g}$ to $2.0 \text{ m}^2/\text{g}$ for Liège chalk, $3.6 \text{ m}^2/\text{g}$ for Aalborg chalk, and $1.7 \text{ m}^2/\text{g}$ for Stevns chalk [33]. In order to confirm that these numbers represent the effective specific surface which is relevant to the flow, a back-calculation is applied to where porosity and permeability are known. The back-calculation gives an effective specific surface of $2.0 \text{ m}^2/\text{g}$ for Liège chalk, $1.6 \text{ m}^2/\text{g}$ for Aalborg chalk, and $2.0 \text{ m}^2/\text{g}$ for Stevns chalk. These values are then used for samples were only porosity is known (equation 9).

2.1. Rate Dependence

De Gennaro and Pereira, PASACHALK2 project [2, 41], describe a data set from CRS (constant rate of strain) oedometer tests with different applied strain rates on Liège chalk. The strain rate varies from approx. 10^{-8} s^{-1} to approx. $2.5 \times 10^{-5} \text{ s}^{-1}$ (0.004%/hour to 9%/hour). De Gennaro and Pereira [2] plot yield stress versus strain rate with logarithmic scale for both axes as seen on figure 4.

The slopes of the pore fluid specific regression lines are fitted to the critical frequency (eq. 1) calculated for each pore fluid and for the dry state. This gives a correlation between the yield strength and the applied strain rate (illustrated on figure 5) which is

$$\ln(\sigma_{\text{yield}}) = 0.79 \tilde{f}_c^{-0.466} \ln\left(\frac{d\varepsilon}{dt}\right) + 3.26, \quad (12)$$

Table 2. Physical properties of the various pore fluids.

Fluid	Temp. (°C)	Pres. (MPa)	Density (10^3 kg/m^3)	Viscosity (10^{-3} Paxs)	Ref.
Water	20	0	0.9982	1.0016	^a
	20	0.2	0.9983	1.0015	^a
	20	0.3	0.9983	1.0015	^a
	130	0.3	0.9349	0.2129	^a
	130	0.8	0.9352	0.2131	^a
Brine	20	0	1.0211	1.0706	^a
	50	0.7	1.0114	0.6019	^b
	70	0.7	1.0013	0.4446	^b
	90	0.7	0.9892	0.3462	^b
	130	0.7	0.9595	0.2344	^b
	130	0.8	0.9595	0.2344	^b
Me- thanol	130	0	0.6747	0.1790	^c
Forma- ma- mide	130	0	1.0360	0.6095	^e
De- cane	130	0	0.6445	0.2866	^e
Soltrol	20	0	0.7826	3.0085	^f
Glycol	20	0	1.1134	21.813	^c
	130	0	1.0310	1.1884	^c
Liq. pa- raffin	20	0	0.8835	120	^e
Air	20	0	0.001193	0.01829	^d
	130	0	0.0008632	0.02324	^d

^a[35] and [36]. ^b[35] and [37]. ^c[38]. ^d[39]. ^e[35]. ^f[40].

where $d\varepsilon/dt$ in principle should be divided by a reference rate and σ_{yield} by a reference yield. This is an empirical equation and we choose to keep the above format without forcing the strain rate and yield strength to be non-dimensionalized and keep the units as s^{-1} and MPa. The constant 3.26 is the average constant of the three linear regressions on figure 4.

In order to include stress rate controlled test results it is necessary to find a correlation from a similar data set. The PASACHALK2 project [41] presents a series of tests and while the results for water saturated chalk show nearly no stress rate dependence, the oil saturated results are close to the expression in eq. 12 and assuming the same formulation as for the strain rate results:

$$\ln(\sigma_{\text{yield}}) = 0.79 \tilde{f}_c^{-0.466} \ln\left(\frac{d\sigma}{dt}\right) + 3.26, \quad (13)$$

where the stress rate, $d\sigma/dt$, is given in MPa/s.

From two interchanging strain rates we may express the b -factor (eq. 12 and eq. 8):

$$\ln\left(\frac{\sigma_1/\text{exp}(3.26)}{\sigma_2/\text{exp}(3.26)}\right) = 0.79 \tilde{f}_c^{-0.5} \ln\left(\frac{d\varepsilon_1/dt}{d\varepsilon_2/dt}\right), \text{ so}$$

$$b = 0.79 \tilde{f}_c^{-0.5}, \quad (14)$$

This correlation is given further consideration in the results section.

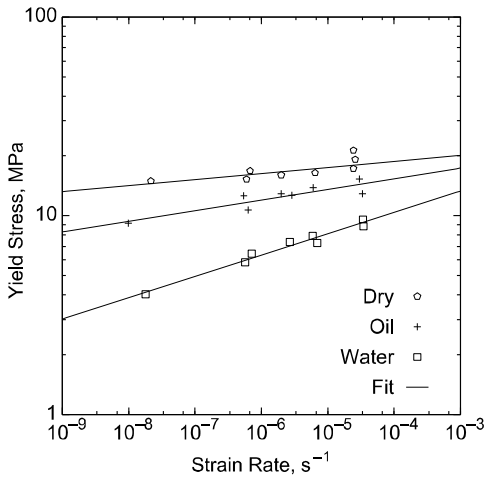


Fig. 4. CRS oedometer data set from [2, 41] on Liège chalk. The oil is soltrol. There is a correlation between applied strain rate and yield strength depending on the content of the pores. Regression lines: Dry $y = \exp(0.03013 \times \ln(x) + 3.208)$, oil $y = \exp(0.0537 \times \ln(x) + 3.226)$, and water $y = \exp(0.1073 \times \ln(x) + 3.330)$.

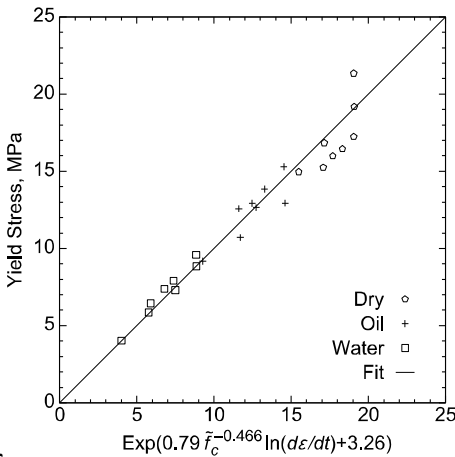


Fig. 5. Calculated from the same data set as figure 4. Through the use of the Biot critical frequency we find a clear correlation between the yield strength and strain rate irrespective of pore fluid.

2.2. Creep

The creep of a material is a time dependent phenomenon and because we find that the critical frequency is correlated with the other time dependent phenomenon: the

strain rate, we find it relevant to investigate if a correlation exists also with creep.

Priol et al. [42] made a large test series on Liège chalk in conventional high pressure oedometer equipment. Figure 6 illustrates data after conversion from void ratio based creep index to the strain based creep index by using eq. 5. There is one outlier for the oil test series which is excluded from the fit.

The Biot critical frequency for the dry, water and oil saturated chalk correlates with the slope of the regression lines in figure 5 and we obtain:

$$\varepsilon_s = 0.08 \tilde{f}_c^{-1} \sigma_{axial} + c, \quad (15)$$

with the units for σ_{axial} in MPa. The assigned unit for the factor 0.08 is MPa^{-1} . The constant c has a small magnitude and not exactly equal for each fluid this is due to the correlation is for creep results after yield where the yield point is different for each fluid.

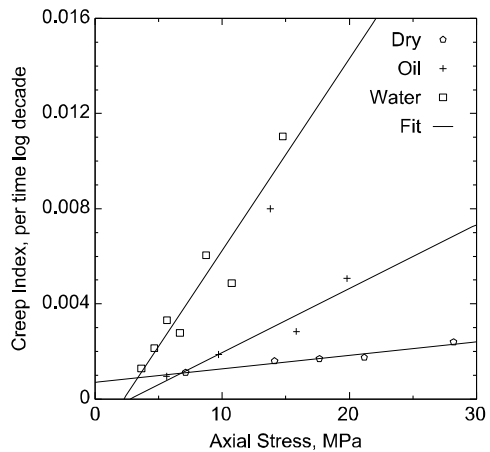


Fig. 6. High pressure oedometer data set for Liège chalk with creep results for higher stress than the yield stress. The oil is soltrol. Each data point corresponds to one creep phase at the indicated axial stress which is held constant throughout the creep phase. Regression lines: Dry $y = 5.67 \times 10^{-4} \times \ln(x) + 7.03 \times 10^{-4}$, oil $y = 2.69 \times 10^{-4} \times \ln(x) - 7.48 \times 10^{-4}$, and water $y = 8.07 \times 10^{-4} \times \ln(x) - 1.84 \times 10^{-3}$. After [42].

The next step in order to compare creep data and the b -factor found from the rate dependence is using eq. 6 to calculate the compression index. The data from Priol et al. [38] converted by using eq. 5 are shown in figure 7 and this gives the compression index at the highest stress levels.

The compression index and corresponding creep index combine at the stress level for a chosen creep phase. We choose the largest stress level for the further calculations as presented in the results section.

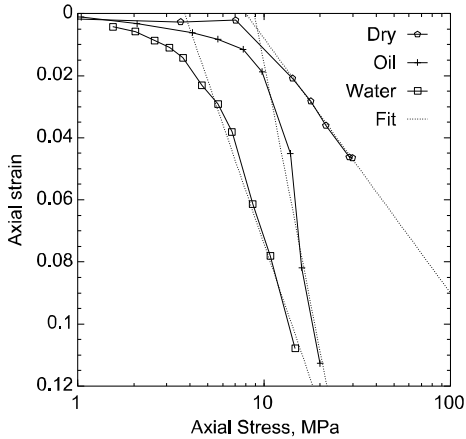


Fig. 7. Stress-strain evolution for the high pressure oedometer tests presented on figure 5. The oil is soltrol. The dashed lines indicate determination of the Q values used when calculating the data points in figure 8. Q values obtained: Dry $Q = 0.0845$ per stress log decade, oil $Q = 0.308$ per stress log decade, and water $Q = 0.1923$ per stress log decade. After [42].

3. RESULTS

The strain and stress rate correlations together with the Biot critical frequency (eq. 12 and eq. 13) are applied on the failure and pore collapse results listed in table 1. The critical frequency for each pore fluid is given in table 3 for comparison. The resulting figure is figure 8. We find that the larger the failure-yield surface the higher the value of the functions $f(\tilde{f}_c \ln(ds/dt))$ or $f(\tilde{f}_c \ln(d\sigma/dt))$ (eq. 12 and eq. 13).

The failure-yield envelope expression of eq. 10 is shown in figure 8 in order to illustrate presumed equal levels of the functions, and how they increase with strength. The hydrostatic yield results are singled out and presented in figure 9. This plot also states the temperature for each hydrostatic test result and increasing temperature weakens the chalk.

A test of the time dependent correlations is given in figure 10. The material parameter b determined from the creep index of figure 6 and the corresponding compression index of figure 7 are one data set. Another is calculated from the compression index (figure 7) and by using eq. 15. The final data set is from de Waal [13], where we assume a porosity of 0.4 for the data from outcrop chalk and 0.3 for the North Sea reservoir chalk as these are not characterized in the reference. The b -factors increase with increasing value of $0.79 \tilde{f}_c^{-0.5}$ independent of origin of the data whether the chalk is saturated with water, oil or dry.

Table 3. Biot critical frequency for the various fluids.

Fluid	Temp. (°C)	f_c (Hz)*
Methanol	130	1.17×10^7
Decane	130	1.97×10^7
Formamide	130	2.60×10^7
Water	20	5.22×10^7
	130	1.22×10^8
Soltrol	20	1.70×10^8
	130	6.78×10^8
Dry	20	1.19×10^9
	130	1.19×10^9
Glycol	20	8.66×10^8
	130	5.10×10^7
Liquid paraffin	20	6.00×10^9

*Assuming a chalk with porosity of 0.40 and permeability of $1.44 \times 10^{-15} \text{ m}^2$.

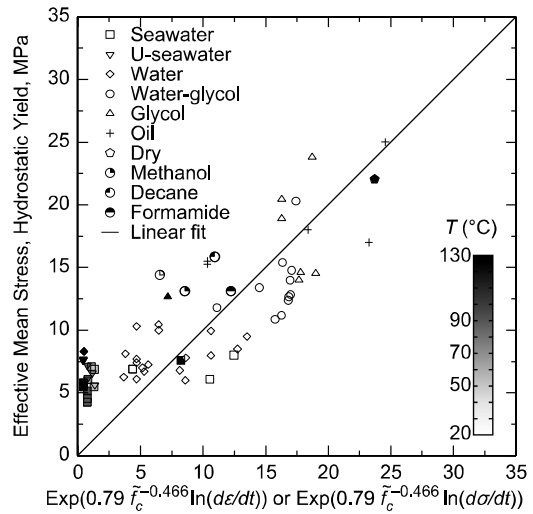


Fig. 9. Yield strength for both strain and stress rate controlled hydrostatic tests with specification of pore fluid and temperature. These data lie on the abscissa of figure 7. The water-glycol symbol represents a pore fluid mixture with different mol% water ranging from 80 mol% to 2 mol%. U-seawater is synthetic seawater without magnesium or sulfate. All data points for oil are at a temperature of 20°C with viscosity ranging from 3.0 mPaxs for soltrol to 120 mPaxs for liquid paraffin.

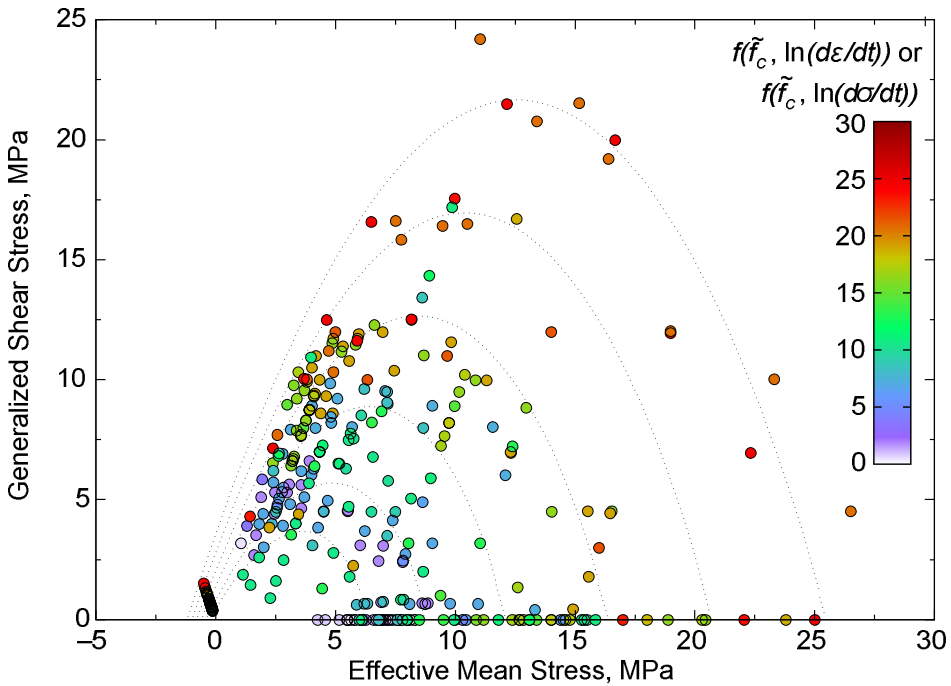


Fig. 8. Applying the correlations for either strain rate controlled or stress rate controlled test results. Each circle is one result from either a Brazil, unconfined compression, triaxial or hydrostatic test and either a failure or yield strength. Note that the failure-yield envelopes drawn at regular intervals are guide to the interpretation and not data points.

4. DISCUSSION

The derived strain rate dependence model is based on CRS and conventional high pressure oedometer tests. Despite this, we apply the rate model to all data regardless of rock mechanical testing method. We base this on the work of Wood [43]. Wood [43] finds that when changing the type of rate control, the yield surface retains its shape, although the size of the yield surface depends on the rate. So we find it justified to apply the correlation for all stress paths. This needs to be further examined and it remains to be verified.

A large scattering is apparent. Most of this is due to the normal variability of geologic material but an additional shortcoming of this review is the missing details for some of the referenced tests and their incomplete chalk characterization. The procedure would benefit from knowledge of the exact porosity, permeability or specific surface for each specimen examined. This shortcoming contributes to the scattering although the correlation with the Biot critical frequency clearly dominates.

Very low functions of the critical frequency is seen for the seawater test series at higher temperature. The reason is low strain rates combined with the low viscosity because of the higher temperature. This might be due to the fact that the strain rate relation is experimentally obtained at room temperature and consequently the temperature influence needs to be tested more in this regard.

The stress rate relation is not tested against known results besides the oil correlation from which it was taken and it remains open for further investigation.

When the b -factor appears from the time dependent relation it is a good illustration of the scope of the model. Although a scatter is apparent in the comparison of previously published b -factors and specifically calculated b -factors, we find a correlation. We interpret the interval of the different calculated b -factors for each pore fluid as the uncertainty related to experimentally obtaining such a b -factor. Additionally, the results for oil would be expected higher than what are observed in figure 9. Further testing of the hypothesis is warranted.

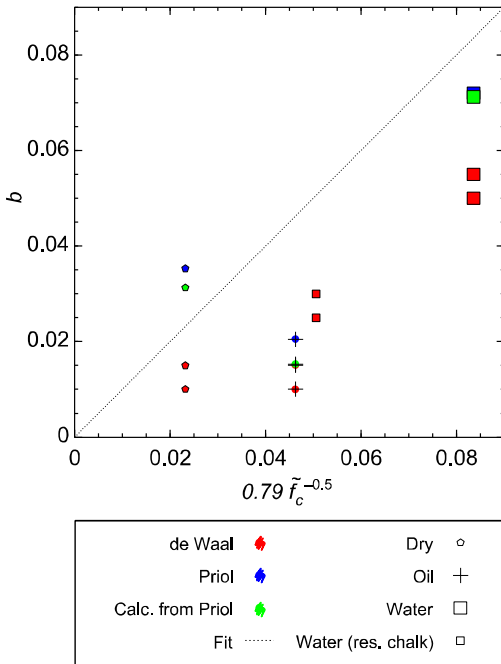


Fig. 10. Comparing b -factors with the correlations. Those stated by de Waal [13] for dry, oil, and water saturated outcrop chalk (porosity 0.4) and water saturated North Sea reservoir chalk (porosity 0.3) are marked with red. The creep data presented in figures 6 and 7 from Priol et al. [42] combines in eq. 7 to give the b -factors with blue color. Using both eq. 7 and eq. 15 with the known Q values gives the b -factors with green color.

5. CONCLUSION

The Biot critical frequency is applied as a friction factor for highly porous and low cemented chalk. A procedure is set up incorporating both the Biot critical frequency and the strain and stress rate dependence of failure and pore collapse properties. A large set of previously published test results on chalk used as input provide a good correlation. The correlation is valid for all low cemented chalk types, all pore fluids, and all temperatures although scattering is observed.

The time dependent relation found from the strain rate and Biot critical frequency correlation is further analyzed and is proposed to be similar to the b -factor. This opens for using the critical frequency broadly as a characterizing friction factor for chalk and for scaling from laboratory to field scale.

REFERENCES

- Papamichos, E., M. Brignoli, and F.J. Santarelli. 1997. An experimental and theoretical study of a partially saturated collapsible rock. *Mechanics of Cohesive-Frictional Materials*, 2 (3):251–278.
- De Gennaro, V. and J.M. Pereira. 2008. Viscoplastic Modelling of Unsaturated Geomaterials. In *Proc. The 12th International Conference of International Association for Computer Methods and Advances in Geomechanics (IACMAG)*, Goa, India, 2232–2241.
- Hellmann, R., P.J.N. Renders, J.P. Gratier, and R. Guiguet. 2002. Experimental pressure solution compaction of chalk in aqueous solutions Part 1. Deformation behavior and chemistry. In *Water-Rock Interactions, Ore Deposits, and Environmental Geochemistry, A Tribute to David A. Crerar*, eds. R. Hellmann and S.A. Wood, The Geochemical Society, Special publication No. 7, 129–152.
- Risnes, R., M.V. Madland, M. Hole, and N.K. Kwabiah. 2005. Water weakening of chalk — Mechanical effects of water–glycol mixtures. *Journal of Petroleum Science and Engineering*, 48 (1–2):21–36.
- Heggheim, T., M.V. Madland, R. Risnes, and T. Austad. 2005. A chemical induced enhanced weakening of chalk by seawater. *Journal of Petroleum Science and Engineering*, 46 (3):171–184.
- Biot, M.A. 1956. Theory of propagation of elastic waves in a fluid–saturated porous solid. I. Low–frequency range. *The Journal of the Acoustical Society of America*, 28 (2):168–178.
- Biot, M.A. 1956. Theory of propagation of elastic waves in a fluid–saturated porous solid. II. Higher frequency range. *The Journal of the Acoustical Society of America*, 28 (2):179–191.
- Johnson, D.L., J. Koplik, and R. Dashen. 1987. Theory of dynamic permeability and tortuosity in fluid-saturated porous media. *Journal of Fluid Mechanics Digital Archive*, 176: 379–402.
- Bourbié, T., O. Coussy, and B. Zinzner. 1987. *Acoustics of Porous Media*. Editions Technip.
- De Gennaro, V., P. Delage, G. Priol, F. Collin, and Y.-J. Cui. 2004. On the collapse behaviour of oil reservoir chalk. *Geotechnique*, 54 (6): 415–420.
- Fabricius, I.L., G.T. Bäechle, and G.P. Eberli. 2010. Elastic moduli of dry and watersaturated carbonates – effect of depositional texture, porosity and permeability. *Geophysics (in press)*.
- Mesri, G. and P.M. Godlewski. 1977. Time- and Stress-Compressibility Interrelationship. *Journal of the Geotechnical Engineering Division, Proceedings of the American Society of Civil Engineers*, 103, No. GT5:417–430.

13. de Waal, J.A. 1986. On the rate type compaction behaviour of sandstone reservoir rock. Ph.D. thesis, Technische Hogeschool, Delft, The Netherlands.
14. Andreassen, K.A. and I.L. Fabricius. 2010. Water weakening of chalk explained from a fluid-solid friction factor, *Rock Mechanics in the Nordic Countries, Kongsberg, Norway, 9–12 June*.
15. Risnes, R. and E. Kleppa. 1996. Plastic behaviour of high porosity chalk in constant K-ratio tests. *Paper presented at the 5th North Sea Chalk Symposium, France*.
16. Risnes, R., C.N. Kristensen, and M.A. Andersen. 1996. Triaxial tests on high porosity chalk with different saturating fluids. *Paper presented at the 5th North Sea Chalk Symposium, France*.
17. Schroeder, Ch. and J. Shao. 1996. Plastic deformation and capillary effects in chalks. *Paper presented at the 5th North Sea Chalk Symposium, France*.
18. Fabre, D. and J. Gustkiewicz. 1997. Poroelastic properties of limestones and sandstones under hydrostatic conditions. *International Journal of Rock Mechanics and Mining Sciences*, 34 (1):127–134.
19. Risnes, R., O.J. Garpestad, M. Gilje, L.T. Oland, M. Ovesen, and E. Vargervik. 1998. Strain hardening and extensional failure in high porosity chalk. *Paper SPE 47581-MS presented at the SPE/ISRM Eurock '98, Trondheim, Norway, 8–10 July, 475–484*.
20. Rhett, D. and C. Lord. 2001. Water weakening in sedimentary rocks. In *DC Rocks 2001, The 38th US Symposium on Rock Mechanics (USRMS)*, 121–128.
21. Collin, F., Y.J. Cui, C. Schroeder, and R. Charlier. 2002. Mechanical behavior of Lixhe chalk partly saturated by oil and water: experiment and modelling. *International Journal for Numerical and Analytical Methods in Geomechanics*, 26 (9):897–924.
22. Madland, M.V., R.I. Korsnes, and R. Risnes. 2002. Temperature effects in Brazilian, uniaxial and triaxial compressive tests with high porosity chalk. *Paper SPE 77761-MS presented at the 2002 SPE Annual Technical Conference and Exhibition, Texas, 29 September–2 October*.
23. Risnes, R., H. Haghghi, R.I. Korsnes, and O. Natvik. 2003. Chalk-fluid interactions with glycol and brines. *Tectonophysics*, 370 (1–4):213–226.
24. Korsnes, R.I., M.V. Madland, and T. Austad. 2006. Impact of brine composition on the mechanical strength of chalk at high temperature. In *Eurock, Proceedings of the International Symposium of the International Society for Rock Mechanics, 9–12 May 2006, Belgium*, 133–140. Taylor & Francis/Balkema.
25. Madland, M.V., A. Finsnes, A. Alkafadgi, R. Risnes, and T. Austad. 2006. The influence of CO₂ gas and carbonate water on the mechanical stability of chalk. *Journal of Petroleum Science and Engineering*, 51 (3–4):149–168.
26. Korsnes, R.I., M.V. Madland, T. Austad, S. Haver, and G. Rslund. 2008a. The effects of temperature on the water weakening of chalk by seawater. *Journal of Petroleum Science and Engineering*, 60 (3–4):183–193.
27. Korsnes, R.I., E. Wersland, T. Austad, and M.V. Madland. 2008b. Anisotropy in chalk studied by rock mechanics. *Journal of Petroleum Science and Engineering*, 62 (1–2):28–35. Mortensen, J., F. Engstrøm, and I. Lind. 1998. The relation among porosity, permeability, and specific surface of chalk from the Gorm field, Danish North Sea. *SPE Reservoir Evaluation & Engineering*, 1 (3):245–251.
28. Fjær, E., R.M. Holt, P. Horsrud, A.M. Raaen, and R. Risnes. 2008. *Petroleum related rock mechanics*, volume 53 of *Developments in Petroleum Science*. 2nd ed. Elsevier.
29. Krenk, S. 2000. Characteristic state plasticity for granular materials: Part I: Basic theory. *International Journal of Solids and Structures*, 37 (43):6343–6360.
30. Mellor, M. and I. Hawkes. 1971. Measurement of tensile strength by diametral compression of discs and annuli. *Engineering Geology*, 5 (3):173–225.
31. Andreassen, K.A., I.L. Fabricius, and N.N. Foged. 2010. Biot Critical Frequency Applied as Common Friction Factor for Pore Collapse and Failure of Chalk with Different Pore Fluids and Temperatures. *Paper SPE 130447-MS presented at SPE EUROPEC, Annual Conference and Exhibition, 14–17 June, Barcelona, Spain*.
32. Jaeger, J.C., N.G.W. Cook, and R.W. Zimmerman. 2007. *Fundamentals of rock mechanics*. 4th ed. Blackwell Publishing.
33. Hjuler, M. L. and I. L. Fabricius. 2009. Engineering properties of chalk related to diagenetic variations of Upper Cretaceous onshore and offshore chalk in the North Sea area. *Journal of Petroleum Science and Engineering*, 68 (3-4):151–170.
34. Mortensen, J., F. Engstrøm, and I. Lind. 1998. The relation among porosity, permeability, and specific surface of chalk from the Gorm field, Danish North Sea. *SPE Reservoir Evaluation & Engineering*, 1 (3):245–251.
35. NIST. 2008. *Thermophysical properties of fluid systems*. Webbook, accessed 23 October 2009; <http://webbook.nist.gov/chemistry/fluid/>.
36. Mavko, G., T. Mukerji, and J. Dvorkin. 1998. *The rock physics handbook: Tools for seismic analysis in porous media*. Cambridge University Press.
37. Palliser, C., and R. McKibbin. 1998. A model for deep geothermal brines, III: Thermodynamic properties – enthalpy and viscosity. *Transport in Porous Media*, 33: 155–171.
38. Yaws, C., ed. 1999. *Chemical properties handbook*. McGraw-Hill. E-book, accessed 11 June 2009; http://www.knovel.com/web/portal/browse/display?_EXT_KNOVEL_DISPLAY_bookid=49.

39. Lide, D.R., ed. 2008. *CRC handbook of chemistry and physics*. 89th ed. Taylor and Francis Group. E-book, accessed 11 June 2009; <http://www.hbcponline.com/>.
40. Schroeder, Ch. 2002. *Du coccolithe au réservoir pétrolier. Approche phénoménologique du comportement mécanique de la craie en vue de sa modélisation à différentes échelles*. PhD thesis. Université de Liège.
41. PASACHALK2, 2003. Mechanical Behaviour of Partially and Multiphase SATurated CHALKs Fluid Skeleton Interaction : Main Factor of Chalk Oil Reservoirs Compaction and Related Subsidence. Part 2. Final report, European Joule III contract No. ENK6-2000-00089.
42. Priol, G., V.D. Gennaro, P. Delage, and T. Servant. 2007. Experimental Investigation on the Time Dependent Behaviour of a Multiphase Chalk. In *Experimental Unsaturated Soil Mechanics*, volume 112, Part III of *Springer Proceedings in Physics*, Springer Berlin Heidelberg, 161–167.
43. Wood, D.M. 1990. *Soil Behaviour and Critical State Soil Mechanics*. Cambridge University Press.

Appendix F

Paper IV

Andreassen, K.A., and Fabricius, I.L. (2010).

Water Weakening of Chalk Explained from a Fluid-Solid Friction Factor.

Paper presented at Rock Mechanics in the Nordic Countries Conference, 9–12 June, Kongsberg, Norway.

WATER WEAKENING OF CHALK EXPLAINED FROM A FLUID-SOLID FRICTION FACTOR

Katrine A. Andreassen

Department of Civil Engineering, Technical University of Denmark

Ida L. Fabricius

Department of Environmental Engineering, Technical University of Denmark

ABSTRACT

The hypothesis behind this paper proposal is that the Biot critical frequency can be used to characterize the water weakening phenomenon physically. The Biot critical frequency determines the transition from where an applied sound velocity on a saturated porous chalk is dominated by viscous forces to where it is dominated by inertial forces, i.e. when the pore fluid motion lags behind the applied frequency. It is therefore a measure of the internal surface friction between solid and fluid which can be interpreted as a friction factor on the pore scale and we propose it can be extrapolated to the macroscale failure and pore collapse properties.

The Biot critical frequency incorporates the porosity, permeability, fluid density and fluid viscosity, where the latter is highly temperature dependent – it does not include the applied sound velocity frequency. The listed parameters are usually determined during laboratory tests and the fluid viscosity and density may be found in tabulated references.

There exist a number of previously published laboratory test results on chalk which was collected from Brazilian, unconfined compression and triaxial tests. The data spans four different chalk types which were tested at temperatures from 20°C to 130°C with the following pore fluids: fresh water, synthetic seawater of different chemical compositions, methanol, glycol, and oil of varying viscosity. The data was evaluated according to failure lines and yield envelopes for all fluids and temperatures while using the Biot critical frequency as a single reference. Other viscoplastic parameters were investigated in the same manner to verify the range of the functioning of the friction factor. The findings show that the Biot critical frequency can be used as a common friction factor and is useful in combining laboratory results. It is also inferred that the observed water weakening phenomenon may be attributed to the friction between solid and fluid.

INTRODUCTION

The well known phenomenon of water weakening in chalk has been extensively studied. Many explanations have been proposed including capillary effects with local menisci at the grain contacts strengthening the chalk [1, 2], pressure solution weakening the chalk [3], attractive and repulsive forces at the grain contacts [4], and chemical dissolution followed by precipitation which is affected by the pore fluid composition [5]. These theories apply to a static system of solid and fluid leaving a subject which seems not to have been covered: the aspect of the moving fluid relative to the solid. The most important aspect when considering this subject is the friction arising at the solid-fluid interface. For weakly cemented porous media undergoing time dependent deformation, not only the strength of the rock frame but also the draining of pore fluid plays a role. This drainage is affected by the solid-fluid friction and we propose that an entity describing this friction could be used as an indicator for the mechanical properties. In this paper we review the available literature on rock mechanical tests per-

formed on highly porous chalk fully saturated with one fluid phase. The purpose is to look for underlying physical properties which might explain the water weakening.

The Biot critical frequency, f_c , is defined as

$$f_c = \frac{\varphi\eta}{2\pi\rho_{fl}k}, \quad (1)$$

where φ is porosity, η is absolute viscosity of the pore fluid, ρ_{fl} is fluid density, and k is absolute permeability. Biot's critical frequency defines the transition from where the fluid is dominated by viscous forces at low frequencies to where the fluid is dominated by inertial forces at higher frequencies [6, 7]. The drag that the solid motion makes on the fluid and whether this is in the viscous or inertial regime are basically matters of friction between the liquid and the solid. The critical frequency may thus be regarded as a friction factor. It combines the fluid properties of absolute fluid viscosity and fluid density with the material properties porosity and permeability. Additionally, it is related to the viscous skin depth. The skin depth is the fluid affected by the movement of the solid or – in the case of draining in rock mechanical tests – as the fluid not being able to drain freely. As such, the critical frequency should not be looked at as a sound wave parameter but rather as a critical factor describing the combined rock-fluid system. A commonly known friction factor, which also relates to the transition from a flow regime dominated by viscous forces to a flow regime dominated by inertial forces, is the Reynolds number, Re. To estimate the friction for a fluid in laminar flow it is customary to use $64/Re$. As an analogy, the chalk-fluid system is in the flow regime dominated by viscous forces and a friction factor is the Biot critical frequency. On a large set of dry and water saturated carbonate rock samples, Fabricius et al. [8] found the amount of softening of elastic modulus to be correlated with the critical frequency. It is therefore relevant to investigate the influence of the critical frequency on the rock mechanical properties of chalk.

In order to describe the time dependent properties of a material several concepts need explanation. The following section contains a brief overview:

The definition of creep index, ε_s , often termed C_α when addressed to the void ratio, is [9]

$$\varepsilon_s = \frac{d\varepsilon}{d(\log(t))}, \quad (2)$$

where ε is strain and t is time. ε_s is determined by plotting the strain vs. logarithmic time for a creep phase and approximate the last part of the curve with a linear regression. In soil mechanics it is the convention to use the void ratio, e , defined as pore volume to solid volume. The conversion from void ratio, e , to strain, ε , is

$$\varepsilon = \frac{\Delta e}{1+e_0}, \quad (3)$$

where e_0 is the initial void ratio. The definition of compression index, Q , often termed C_c when addressed to the void ratio, is [9]

$$Q = \frac{d\varepsilon}{d(\log(\sigma))}, \quad (4)$$

where σ is stress. For soils Mesri and Godlewski [9] find the relation

$$\frac{\varepsilon_s}{Q} = \frac{d(\log(\sigma))}{d(\log(t))} = b, \quad (5)$$

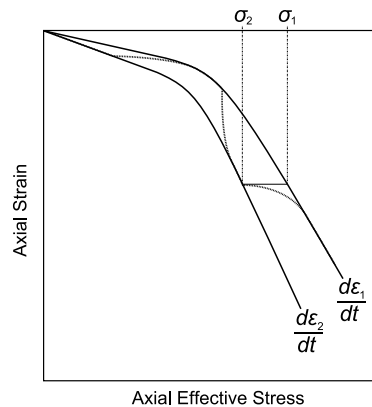


Figure 1. Conceptual sketch of rate dependence of strain in soft rock. The blue line represents the stress-strain path following two interchanging strain rates. Strain rate 1 is higher than strain rate 2. The material responds as a stronger material when applying the higher strain rate 1. Based on [10].

where b is termed the b -factor or C_d/C_c . The factor b is a constant for any particular soil for all combinations of time, effective stress and strain level [9]. This relationship is also valid for sandstones [10]. For a sample run at interchanging strain rates as illustrated in figure 1, the relation is [10]

$$\frac{\sigma'_{\text{axial},1}}{\sigma'_{\text{axial},2}} = \left(\frac{d\varepsilon_{\text{axial},1}/dt}{d\varepsilon_{\text{axial},2}/dt} \right)^b \quad (6)$$

where $\sigma'_{\text{axial},1}$ is the effective axial stress related to a point on the stress-strain curve with an applied strain rate of $d\varepsilon_{\text{axial},1}/dt$ and b is the material dependent b -factor.

The conceptual plot on figure 2 illustrates the stress paths for the traditional rock mechanical tests: Brazil indirect tensile strength test, unconfined compression test, hydrostatic test, oedometer test, and triaxial test. The mean effective stress, p' , and generalized shear stress, q , are [11]

$$p' = \frac{1}{3}(\sigma'_1 + \sigma'_2 + \sigma'_3), \text{ and} \quad (7)$$

$$q = \frac{1}{\sqrt{2}}\sqrt{(\sigma'_1 - \sigma'_2)^2 + (\sigma'_2 - \sigma'_3)^2 + (\sigma'_1 - \sigma'_3)^2},$$

where σ'_1 , σ'_2 , and σ'_3 are the effective principal stresses.

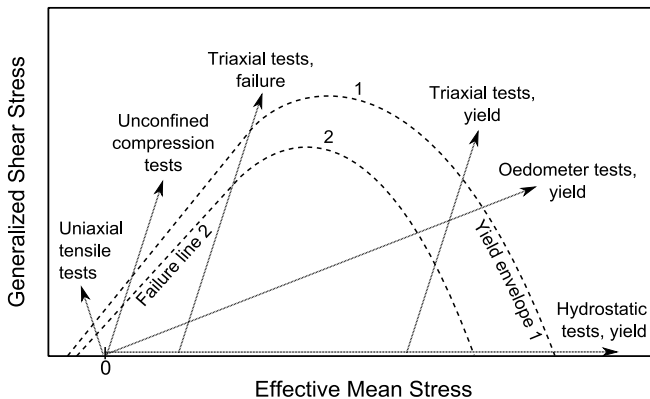


Figure 2. Standard rock mechanical tests and their stress paths in a p' - q diagram. The rock with failure-yield envelope 1 is a stronger material than the rock with failure-yield envelope 2. From [12].

An expression which represents the failure-yield envelope is [13]

$$q = q_{\max} \left(1 - \left(\frac{p' - p_a}{p_{\max}} \right)^n \right) (p' - p_a), \quad (8)$$

with q_{\max} controlling the ordinate, p_{\max} controlling the abscissa, p_a controlling the attraction, and n is a shape parameter for the envelope.

The indirect tensile strength is here interpreted as being equivalent to the uniaxial tensile strength [14] and is therefore plotted on the negative p' axis. We do this because the stress state for the Brazil test does not involve equal intermediate and minor stress, although this has been assumed in earlier publications. The intermediate stress, σ'_2 , is zero as stated by Jaeger et al. in [15] and can therefore not be plotted directly in the same stress plane as the p' - q plane. The interpretation of the Brazil test result as the uniaxial tensile strength is needed in order to correct for this.

Table 1. Overview of the included tests and their references.

Test Type	Fluid	Temp. (°C)	Applied Rate	Chalk Type	No.	Reference
Triax, Brazil, hydrostatic, UCS	Water, seawater, oil	Room	5.4%/hour or 3 MPa/hour	Liège	[16]	Risnes et al. 1996,
Triax	Water	Room	18.5%/hour	Liège	[17]	Risnes and Kleppa 1996
Triax, hydrostatic	Water, seawater, oil, liquid paraffin, dry	Room	0.4 MPa/hour	Liège	[18]	Schroeder and Shao 1996
UCS, hydrostatic	Water	Room	300 MPa/hour	Liège	[19]	Fabre and Gustkiewicz 1997
Hydrostatic	Methanol	Room	5.5 MPa/hour	Liège	[20]	Risnes et al. 1998
Hydrostatic, triax	Seawater, methanol, decane, formamide, dry	130	12.4 MPa/hour	Liège	[21]	Rhett and Lord 2001
Hydrostatic, triax	Water, oil	Room	3.6 MPa/hour	Liège	[22]	Collin et al. 2002
Triax, Brazil, UCS	Water, glycol	20, 130	0.5%/hour	Liège, Aalborg	[23]	Madland et al. 2002
Brazil, triax	Water, high salinity seawater, glycol	Room	2%/hour or 1%/hour	Liège	[24]	Risnes et al. 2003
Triax, Brazil, hydrostatic	Water, glycol, water-glycol mixture ^a	Room	1%/hour or 0.35%/hour	Liège	[4]	Risnes et al. 2005
Hydrostatic	Distilled water, seawater ^b	130	0.1%/hour	Stevns	[25]	Korsnes et al. 2006
Hydrostatic	Water	20	2.6 MPa/hour	Aalborg	[26]	Madland et al. 2006
Hydrostatic	Distilled water, seawater ^b	Room, 50, 70, 90	1%/hour or 0.1%/hour	Stevns	[27]	Korsnes et al. 2008a
Hydrostatic, Brazil	Water	Room	0.3%/hour	Liège, Stevns	[28]	Korsnes et al. 2008b

^aOf varying mol%. ^bOf different chemical composition.

METHOD

This investigation is limited to high porosity chalk. The low cementation should cause the fluid effects to dominate with respect to the chalk frame. The tests are made on outcrop chalk from three different localities: Liège or Lixhe chalk from a quarry in Belgium, Aalborg chalk from a quarry in western Denmark, and Stevns Chalk from a quarry in eastern Denmark. The physical properties vary among the outcrop chinks, with Liège being characterized by a porosity of generally 0.40 and a permeability of $1.5 \times 10^{-15} \text{ m}^2$. Stevns chalk has a porosity of generally 0.45 and a permeability of $3.5 \times 10^{-15} \text{ m}^2$, whereas Aalborg chalk generally has a porosity of 0.45 and a slightly higher general permeability of $4 \times 10^{-15} \text{ m}^2$. Further characterization of these chalk lithologies is given in [29]. All the selected outcrop chinks have induration H2 and are weakly cemented. Table 1 gives a quick overview of the references included in this review. The pore fluid density and absolute viscosity are found in tabulated references.

For some test series permeability is only stated as a general value, while exact values are given for the porosity. The permeability, k , may be approximated from the porosity, φ , [30]

$$k = c \frac{\varphi^3}{(1-\varphi)^2 S_s^2} = c \frac{\varphi^3}{(1-\varphi)^2 (S_a \rho_s)^2}, \text{ and} \quad (9)$$

$$c = \left(4 \cos \left(\frac{1}{3} \arccos \left(\varphi \frac{8^2}{\pi^3} - 1 \right) + \frac{4}{3} \varphi \right) + 4 \right)^{-1},$$

where Kozenys factor c is stated for 3D circular interconnected tubes, and the solid density, ρ_s , of chalk is $2.7 \times 10^3 \text{ kg/m}^3$. The specific surface, S_s , is assumed to be a material property for each chalk locality and therefore does not change between different chalk blocks. Measured specific surface area, S_a , by BET (N_2 adsorption) is $1.7 \text{ m}^2/\text{g}$ for Liège chalk, $3.6 \text{ m}^2/\text{g}$ for Aalborg chalk, and $1.7 \text{ m}^2/\text{g}$ for Stevns chalk [29]. In order to confirm that these numbers represent the effective specific surface which is relevant to the flow, a back-calculation is applied to where porosity and permeability are known. The back-calculation gives an effective specific surface of $2.0 \text{ m}^2/\text{g}$ for Liège chalk, $1.6 \text{ m}^2/\text{g}$ for Aalborg chalk, and $2.0 \text{ m}^2/\text{g}$ for Stevns chalk, which also correspond with [26]. These values are then used for samples where only porosity is known (equation 9).

Rate Dependence

De Gennaro and Pereira, PASACHALK2 project [2, 31], describe a data set from CRS (constant rate of strain) oedometer tests with different applied strain rates on Liège chalk. The strain rate varies from approx. 10^{-8} s^{-1} to approx. $2.5 \times 10^{-5} \text{ s}^{-1}$ (0.004%/hour to 9%/hour). De Gennaro and Pereira [2] plot yield stress versus strain rate with logarithmic scale for both axes as seen on figure 3.

The slopes of the pore fluid specific regression lines are fitted to the critical frequency (equation 1) calculated for each pore fluid and for the dry state. This gives a correlation between the yield strength and the applied strain rate (illustrated on figure 4) which is

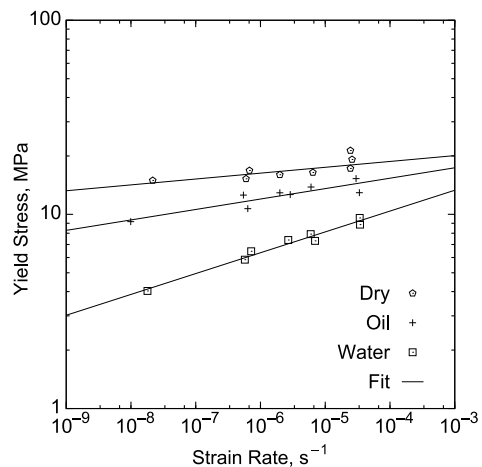


Figure 3. CRS oedometer data set from [2, 31] on Liège chalk. There is a correlation between applied strain rate and yield strength depending on the content of the pores.

$$\ln(\sigma_{\text{yield}}^{\text{hypothetical}}) = 381 f_c^{-0.5} \ln\left(\frac{d\varepsilon}{dt}\right), \quad (10)$$

where $d\varepsilon/dt$ in principle should be divided by a reference rate and the multiplied constant should have the unit $s^{0.5} \cdot \text{MPa}$ in order to arrive at a correct unit for the yield. For simplicity we choose to keep the above format with the strain rate required as s^{-1} and the Biot critical frequency as s^{-1} , which gives values in the 0–1 range for the hypothetical σ_{yield} parameter as seen on figure 4 (a scaling factor).

In order to include stress rate controlled test results it is necessary to find a correlation from a similar data set. The PASACHALK2 project [31] presents a series of tests and while the results for water saturated chalk show nearly no stress rate dependence, the oil saturated results gives the following correlation when assuming the same formulation as for the strain rate results:

$$\ln(\sigma_{\text{yield}}^{\text{hypothetical}}) = 1700 f_c^{-0.5} \ln\left(\frac{d\sigma}{dt}\right), \quad (11)$$

where the stress rate, $d\sigma/dt$, is given in 10^{-1} GPa/s and the critical frequency is in s^{-1} . From two interchanging strain rates we may express the b -factor (eq. 10 and eq. 6):

$$\ln\left(\frac{\sigma_1}{\sigma_2}\right) = 381 f_c^{-0.5} \ln\left(\frac{d\varepsilon_1/dt}{d\varepsilon_2/dt}\right), \quad \text{so} \\ b = 381 f_c^{-0.5}. \quad (12)$$

This correlation is given further considerations in the results section.

Creep

The creep of a material is a time dependent phenomenon and because we find that the critical frequency is correlated with the time dependent phenomenon: the strain rate, we find it relevant to investigate if a correlation also with creep exists. Priol et al. [32] made a large test series on Liège chalk in conventional high pressure oedometer equipment. Figure 5 illustrates data after conversion from void ratio based creep index to the strain based creep index by using equation 3. There is one outlier for the oil test series with is excluded from the fit.

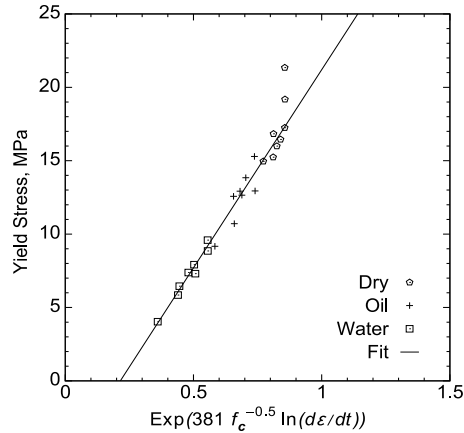


Figure 4. Calculated from the same data set as figure 3. Through the use of the Biot critical frequency we find a clear correlation between the yield strength and strain rate irrespective of pore fluid. From [12].

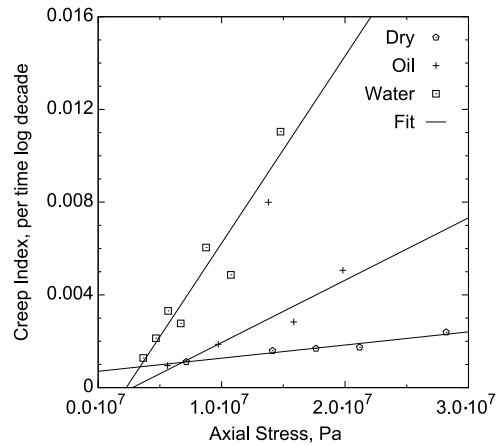


Figure 5. High pressure oedometer data set for Liège chalk with creep results for higher stress than the yield stress. Each data point corresponds to one creep phase at the indicated axial stress which is held constant throughout the creep phase. After [32].

The Biot critical frequency for the dry, water and oil saturated chalk correlates with the slope of the regression lines in figure 5 and we obtain:

$$\epsilon_s = 0.04 f_c^{-1} \sigma_{axial}, \quad (13)$$

with the units for σ_{axial} in Pa and for f_c in s^{-1} . The assigned unit for the constant 0.04 is $(s \cdot Pa)^{-1}$.

The next step in order to compare creep data and the b -factor found from the rate dependence is by using equation 4 to calculate the compression index. The data from Priol et al. [32] converted by using equation 3 are shown in figure 6 and this gives the compression index at the highest stress levels. The compression index and corresponding creep index combine at the stress level for a chosen creep phase. We choose the largest stress level for the further calculations and results of these are presented in the results section.

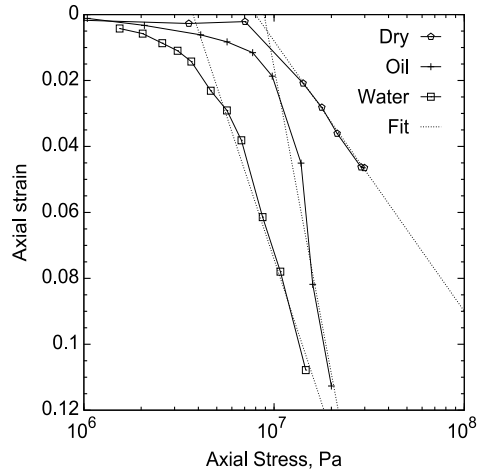


Figure 6. Stress-strain evolution for the high pressure oedometer tests presented on figure 5. The dashed lines indicate determination of the Q values used when calculating the data points in figure 7. After [32].

RESULTS

The strain and stress rate correlations together with the Biot critical frequency (equation 10 and equation 11) are applied on the failure and pore collapse results listed in table 1. These results are presented in figure 7. We find that the larger the failure-yield surface the higher the value of the functions $f(f_c, \ln(d\epsilon/dt))$ or $f(f_c, \ln(d\sigma/dt))$ (equation 10 and equation 11). The failure-yield envelope expression of eq. 8 is shown in figure 7 in order to illustrate presumed equal levels of the functions, and how they increase with strength.

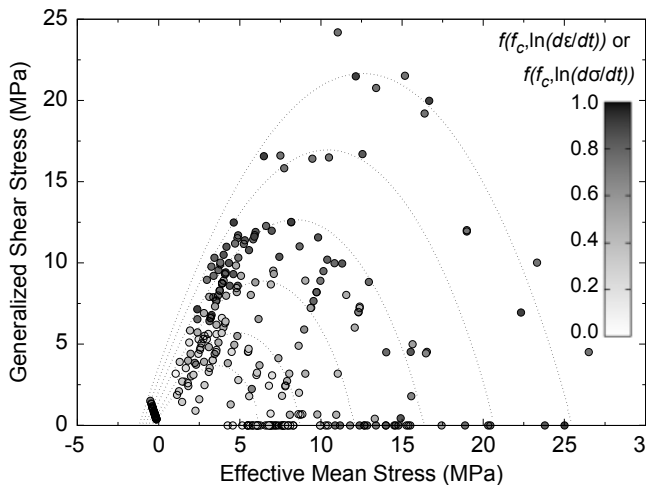


Figure 7. Applying the correlations for either strain rate controlled or stress rate controlled test results. Each circle is one result from either a Brazil, unconfined compression, triaxial or hydrostatic test and either a failure or yield strength. Note that the failure-yield envelopes drawn at regular intervals are guide to the interpretation and not datapoints.

A test of the time dependent correlations is given in figure 8. The material parameter b determined from the creep index of figure 5 and the corresponding compression index of figure 6 are one data set. Another is calculated from the compression index (figure 6) and by using equation 13. The final data set is from de Waal [10] who states an interval for the b -factor. For this data set we assume a porosity of 0.4 for the data from outcrop chalk and a porosity of 0.3 for the North Sea reservoir chalk as these are not further characterized in the reference. The resulting figure 8 shows an interval of b -factors for each specific rock/fluid system based on three different calculations compared with the $381 f_c^{-0.5}$ term. This term is calculated from the known fluid viscosity, fluid density and chalk porosity while using eq. 9 for the permeability. Interpolated between the results from different pore fluids we find that the b -factors grow with increasing value of $381 f_c^{-0.5}$ independent of origin of the data.

DISCUSSION

The derived strain rate dependence correlations are based on CRS and conventional high pressure oedometer tests. Despite this, we apply the rate model to all data regardless of rock mechanical testing method. We base this on the work of Wood [33]. Wood [33] finds that when changing the type of rate control, the yield surface retains its shape, although the size of the yield surface depends on the rate. So we find it justified applying the correlation for all stress paths but this can only be verified by conducting more test series at different rates and with different stress paths.

The results show an apparent scattering. Most of this is due to the normal variability of geologic material but an additional shortcoming of this review is the missing details for some of the referenced tests and their incomplete chalk characterization. The model would benefit from knowledge of the exact porosity, permeability or specific surface for each specimen examined. This shortcoming contributes to the scattering although the correlation with the Biot critical frequency clearly dominates. The stress rate relation is not tested against known results besides the oil correlation from which it was taken and it remains open for further investigation.

When the b -factor appears from the time dependent relation it is a good illustration of the possible scope of the model. Although a scatter is apparent in the comparison of previously

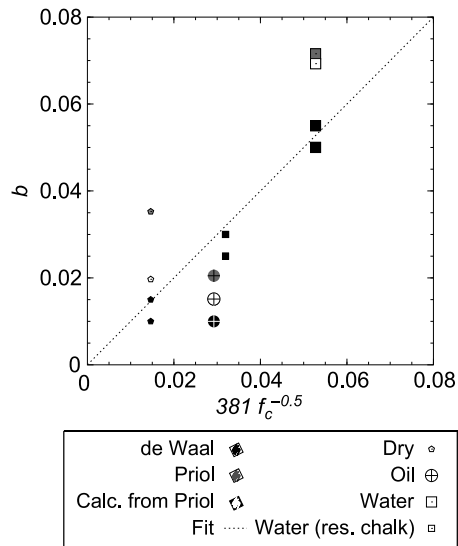


Figure 8. Comparing b -factors with the correlations. Those stated by de Waal [10] for dry, oil, and water saturated outcrop chalk and water saturated North Sea reservoir chalk are marked with black. The creep data presented in figures 5 and 6 from Priol et al. [32] combines in eq. 5 to give the b -factors with gray. Using both eq. 5 and eq. 13 with the obtained Q values from figure 6 gives the b -factors with white points framed by black border.

published b -factors and specifically calculated b -factors, we find a correlation. Further testing of the hypothesis is warranted.

CONCLUSION

The Biot critical frequency is applied as a friction factor for highly porous and low cemented chalk. A model is set up incorporating both the Biot critical frequency and the strain and stress rate dependence of failure and pore collapse properties. A large set of previously published test results on chalk used as input in the model shows a good correlation.

The time dependent relation found from the strain rate and Biot critical frequency correlation is further analyzed and is proposed to correlate to the b -factor. This opens for using the critical frequency broadly as a characterizing friction factor for chalk and for scaling from laboratory to field scale.

REFERENCES

1. Papamichos, E., M. Brignoli, and F.J. Santarelli. "An experimental and theoretical study of a partially saturated collapsible rock". *Mechanics of Cohesive-Frictional Materials*, 2 (3):251–278. 1997.
2. De Gennaro, V. and J.M. Pereira. "Viscoplastic Modelling of Unsaturated Geomaterials". In *Proc. The 12th International Conference of International Association for Computer Methods and Advances in Geomechanics (IACMAG)*, Goa, India, 2232–2241. 2008.
3. Hellmann, R., P.J.N. Renders, J.P. Gratier, and R. Guiguet. "Experimental pressure solution compaction of chalk in aqueous solutions Part I. Deformation behavior and chemistry". In *Water-Rock Interactions, Ore Deposits, and Environmental Geochemistry, A Tribute to David A. Crerar*, eds. R. Hellmann and S.A. Wood, The Geochemical Society, Special publication No. 7, 129–152. 2002.
4. Risnes, R., M.V. Madland, M. Hole, and N.K. Kwabiah. "Water weakening of chalk — Mechanical effects of water–glycol mixtures". *Journal of Petroleum Science and Engineering*, 48 (1–2):21–36. 2005.
5. Heggheim, T., M.V. Madland, R. Risnes, and T. Austad. "A chemical induced enhanced weakening of chalk by seawater". *Journal of Petroleum Science and Engineering*, 46 (3):171–184. 2005.
6. Biot, M.A. "Theory of propagation of elastic waves in a fluid–saturated porous solid. I. Low-frequency range". *The Journal of the Acoustical Society of America*, 28 (2):168–178. 1956.
7. Biot, M.A. "Theory of propagation of elastic waves in a fluid–saturated porous solid. II. Higher frequency range". *The Journal of the Acoustical Society of America*, 28 (2):179–191. 1956.
8. Fabricius, I.L., G.T. Bäechele, and G.P. Eberli. "Elastic moduli of dry and watersaturated carbonates – effect of depositional texture, porosity and permeability". *Geophysics* (in press).
9. Mesri, G. and P.M. Godlewski. "Time- and Stress-Compressibility Interrelationship". *Journal of the Geotechnical Engineering Division, Proceedings of the American Society of Civil Engineers*, 103, No. GT5:417–430. 1977.
10. de Waal, J.A. "On the rate type compaction behaviour of sandstone reservoir rock". Ph.D. thesis, Technische Hogeschool, Delft, The Netherlands. 1986.
11. Fjær, E., R.M. Holt, P. Horsrud, A.M. Raaen, and R. Risnes. "Petroleum related rock mechanics". Volume 53 of *Developments in Petroleum Science*. 2nd ed. Elsevier, 2008.
12. Andreassen, K.A., I.L. Fabricius, and N.N. Foged. "Biot Critical Frequency Applied as Common Friction Factor for Pore Collapse and Failure of Chalk with Different Pore Fluids and Temperatures". Paper SPE 130447-MS presented at SPE EUROPEC, Annual Conference and Exhibition, 14–17 June, Barcelona, Spain. 2010.

13. Krenk, S. "Characteristic state plasticity for granular materials: Part I: Basic theory". *International Journal of Solids and Structures*, 37 (43):6343–6360. 2000.
14. Mellor, M. and I. Hawkes. "Measurement of tensile strength by diametral compression of discs and annuli". *Engineering Geology*, 5 (3):173–225. 1971.
15. Jaeger, J.C., N.G.W. Cook, and R.W. Zimmerman. "Fundamentals of rock mechanics". 4th ed. Blackwell Publishing, 2007.
16. Risnes, R. and E. Kleppa. "Plastic behaviour of high porosity chalk in constant K-ratio tests". Paper presented at the 5th North Sea Chalk Symposium, France. 1996.
17. Risnes, R., C.N. Kristensen, and M.A. Andersen. "Triaxial tests on high porosity chalk with different saturating fluids". Paper presented at the 5th North Sea Chalk Symposium, France. 1996.
18. Schroeder, Ch. and J. Shao. "Plastic deformation and capillary effects in chalks". Paper presented at the 5th North Sea Chalk Symposium, France. 1996.
19. Fabre, D. and J. Gustkiewicz. "Poroelastic properties of limestones and sandstones under hydrostatic conditions". *International Journal of Rock Mechanics and Mining Sciences*, 34 (1):127–134. 1997.
20. Risnes, R., O.J. Garpestad, M. Gilje, L.T. Oland, M. Ovesen, and E. Vargervik. "Strain hardening and extensional failure in high porosity chalk". Paper SPE 47581-MS presented at the SPE/ISRM Eurock '98, Trondheim, Norway, 8–10 July, 475–484. 1998.
21. Rhett, D. and C. Lord. "Water weakening in sedimentary rocks". In *DC Rocks 2001, The 38th US Symposium on Rock Mechanics (USRMS)*, 121–128. 2001.
22. Collin, F., Y.J. Cui, Ch. Schroeder, and R. Charlier. "Mechanical behavior of Lixhe chalk partly saturated by oil and water: experiment and modeling". *International Journal for Numerical and Analytical Methods in Geomechanics*, 26 (9):897–924. 2002.
23. Madland, M.V., R.I. Korsnes, and R. Risnes. "Temperature effects in Brazilian, uniaxial and triaxial compressive tests with high porosity chalk". Paper SPE 77761-MS presented at the 2002 SPE Annual Technical Conference and Exhibition, Texas, 29 September–2 October. 2002.
24. Risnes, R., H. Haghghi, R.I. Korsnes, and O. Natvik. "Chalk-fluid interactions with glycol and brines". *Tectonophysics*, 370 (1–4):213–226. 2003.
25. Korsnes, R.I., M.V. Madland, and T. Austad. "Impact of brine composition on the mechanical strength of chalk at high temperature". In *Eurock, Proceedings of the International Symposium of the International Society for Rock Mechanics*, 9–12 May 2006, Belgium, 133–140. Taylor & Francis/Balkema, 2006.
26. Madland, M.V., A. Finsnes, A. Alkafadgi, R. Risnes, and T. Austad. "The influence of CO₂ gas and carbonate water on the mechanical stability of chalk". *Journal of Petroleum Science and Engineering*, 51 (3–4):149–168. 2006.
27. Korsnes, R.I., M.V. Madland, T. Austad, S. Haver, and G. Rslund. "The effects of temperature on the water weakening of chalk by seawater". *Journal of Petroleum Science and Engineering*, 60 (3–4):183–193. 2008.
28. Korsnes, R.I., E. Wersland, T. Austad, and M.V. Madland. "Anisotropy in chalk studied by rock mechanics". *Journal of Petroleum Science and Engineering*, 62 (1–2):28–35. 2008.
29. Hjuler, M. L. and I. L. Fabricius. "Engineering properties of chalk related to diagenetic variations of Upper Cretaceous onshore and offshore chalk in the North Sea area". *Journal of Petroleum Science and Engineering*, 68 (3–4):151–170. 2009.
30. Mortensen, J., F. Engstrøm, and I. Lind. "The relation among porosity, permeability, and specific surface of chalk from the Gorm field, Danish North Sea". *SPE Reservoir Evaluation & Engineering*, 1 (3):245–251. 1998.
31. PASACHALK2. "Mechanical Behaviour of Partially and Multiphase Saturated CHALKs Fluid Skeleton Interaction : Main Factor of Chalk Oil Reservoirs Compaction and Related Subsidence". Part 2. Final report, European Joule III contract No. ENK6-2000-00089. 2003
32. Priol, G., V.D. Gennaro, P. Delage, and T. Servant. "Experimental Investigation on the Time Dependent Behaviour of a Multiphase Chalk". In *Experimental Unsaturated Soil Mechanics*, volume 112, Part III of Springer Proceedings in Physics, Springer Berlin Heidelberg, 161–167. 2007.
33. Wood, D.M. "Soil Behaviour and Critical State Soil Mechanics". Cambridge University Press, 1990.

Appendix G

Paper V

Andreassen, K.A., Fabricius, I.L., and Foged, N.N. (2010).

Biot Critical Frequency Applied as Common Friction Factor for Pore Collapse and Failure of Chalk with Different Pore Fluids and Temperatures.

SPE Paper MS-130447 presented at the SPE EUROPEC/EAGE Annual Conference and Exhibition, Barcelona, Spain, 14–17 June.



SPE 130447

Biot Critical Frequency Applied as Common Friction Factor for Pore Collapse and Failure of Chalk with Different Pore Fluids and Temperatures

Katrine Alling Andreassen, SPE, Ida Lykke Fabricius, SPE, and Niels Nielsen Foged, SPE, Technical University of Denmark

Copyright 2010, Society of Petroleum Engineers

This paper was prepared for presentation at the SPE EUROPEC/EAGE Annual Conference and Exhibition held in Barcelona, Spain, 14–17 June 2010.

This paper was selected for presentation by an SPE program committee following review of information contained in an abstract submitted by the author(s). Contents of the paper have not been reviewed by the Society of Petroleum Engineers and are subject to correction by the author(s). The material does not necessarily reflect any position of the Society of Petroleum Engineers, its officers, or members. Electronic reproduction, distribution, or storage of any part of this paper without the written consent of the Society of Petroleum Engineers is prohibited. Permission to reproduce in print is restricted to an abstract of not more than 300 words; illustrations may not be copied. The abstract must contain conspicuous acknowledgment of SPE copyright.

Abstract

A fluid effect towards higher strengths for oil saturated chalk compared to water saturated chalk has previously been identified and labeled the water weakening phenomenon, but has not been further characterized physically until now. The hypothesis of this paper is that the Biot critical frequency can be used to explain this behavior on the pore scale and be extrapolated to the macroscale failure and pore collapse properties. A large set of previously published laboratory test results on chalk was collected. The data spans three different chalk types which were tested at temperatures from 20°C to 130°C with the following pore fluids besides dry chalk: fresh water, synthetic seawater of different chemical compositions, methanol, glycol, formamide, decane and crude oil of varying viscosity.

The Biot critical frequency determines the transition from where an applied sound velocity is dominated by viscous forces to where it is dominated by inertial forces, i.e. when the pore fluid motion lags behind the applied frequency. It is therefore a measure of the internal surface friction between solid and fluid and is interpreted as a friction factor. The Biot critical frequency incorporates the porosity, permeability, fluid density and fluid viscosity, where the latter is highly temperature dependent. All these parameters are usually determined during laboratory tests and the fluid viscosity and density may be found in tabulated references. Besides the fluid effect there is an effect from the applied strain or stress rate on both the strength and yield properties. This phenomenon couples with the critical frequency through the use of a previously published study on the rate dependence.

The data show that the Biot critical frequency can be used as a common friction factor and is useful in combining laboratory results. It is also inferred that the observed water weakening phenomenon may be attributed to the friction between solid and fluid. The scope for the applicability of the Biot critical frequency as a friction factor is in analysis of the compaction of chalk fields where the effect of different fluids and temperatures is relevant.

Introduction

The weakening effect of water in chalk is significant for North Sea reservoir subsidence and several experimental studies have focused on the subject. This paper reviews the results from these test series in order to match the theoretical considerations and find the governing physical properties.

Gutierrez et al. (2000) found higher friction for oil saturated chalk (42°) than water saturated (38°) in simple tilt tests on a large test series on chalk samples submerged in either oil or water. The chalk studied is Lägerdorf chalk from a quarry in northwest Germany. While the solid-solid friction is one location for the friction forces in the submerged simple tilt test, the fluid-solid friction should thus be considered as well. This causes our focus on fluid-solid friction as a possible mechanism for weakening when assuming no alteration of the chalk surface and consequently no change in solid-solid friction for oil and water saturated chalk. So we turn to the theory of wave propagation in porous media with the critical frequency as a central measure. Bourbié et al. (1987) and Mavko et al. (2009) list critical frequencies for various materials and fluids where an increasing critical frequency from water to oil is observed depending on the type of rock studied. On a large set of dry and water saturated carbonate rock samples, Fabricius et al. (2010) found the amount of softening of elastic modulus to be correlated with the critical frequency.

The Biot critical frequency, f_c , is defined as

$$f_c = \frac{\varphi\eta}{2\pi\rho\eta k}, \dots\dots\dots (1)$$

where ϕ is porosity, η is absolute viscosity of the pore fluid, ρ_f is fluid density, and k is absolute permeability. Biot's critical frequency marks the limit between a low frequency regime with the pore fluid following viscous forces and a high frequency regime with inertial forces dominating the fluid motion (Biot 1956a, 1956b). The drag that the solid motion makes on the fluid and whether this is in the viscous or inertial regime are basically matters of friction between the liquid and the solid. The critical frequency is thus here interpreted as a friction factor. A commonly know friction factor, which also relates to the transition from a flow regime dominated by viscous forces to a flow regime dominated by inertial forces, is the Reynolds number, Re , with a friction proportional to $64/Re$ valid for laminar flow of fluids. As an analogy, the chalk-fluid system is in the flow regime dominated by viscous forces and a friction factor is the Biot critical frequency.

When applying stress to a rock with high porosity and low cementation, a significant part of the resulting deformation is displacement of pore fluid. The displacement of fluid involves flow in the open pore space. Therefore any change in the open pore volume caused by changing the pore fluid is important. The viscous skin depth, δ , as defined by Johnson et al. (1987) determines the fluid depth affected by an oscillatory transverse movement of solid with frequency, f :

$$\delta = \sqrt{\frac{2\eta}{\rho_f 2\pi f}} \dots\dots\dots (2)$$

During rock mechanical testing f approaches zero so δ should make no distinction among fluids. As described below, electrical forces may nevertheless create a skin in some pore fluids.

Another phenomenon is the rate dependence of strength in porous media. The higher applied strain or stress rate the stronger the rock. The knowledge of this effect links laboratory testing of chalk to reservoir behavior at field scale, as illustrated initially in 1989 by Ruddy et al. The subject is well covered experimentally by Schroeder (2002) and PASACHALK2 (2003).

Methods

This investigation is limited to high porosity chalk. The low cementation should cause the fluid effects to dominate with respect to the chalk frame. The tests are made on outcrop chalk from three different localities: Liège or Lixhe chalk from a quarry in Belgium, Aalborg chalk from a quarry in western Denmark, and Stevns Chalk from a quarry in eastern Denmark. The physical properties vary among the outcrop chalks, with Liège being characterized by a porosity of generally 0.40 and a permeability of $1.5 \times 10^{-15} \text{ m}^2$. Stevns chalk has a porosity of generally 0.45 and a permeability of $3.5 \times 10^{-15} \text{ m}^2$, whereas Aalborg chalk generally has a porosity of 0.45 and a slightly higher general permeability of $4 \times 10^{-15} \text{ m}^2$. Further characterization of these chalk lithologies is given in Hjuler and Fabricius (2009). All the selected outcrop chalks have induration H2 and are weakly cemented. **Table 1** lists the references included in this review. For some of the references the permeability is stated as a general value while the porosity is given exactly. In order to take this problem into account, the permeability, k , in these cases is calculated from the porosity, ϕ , with the Kozeny equation, (Mortensen et al. 1998):

$$k = c \frac{\phi^3}{(1-\phi)^2 S_g^2} = c \frac{\phi^3}{(1-\phi)^2 (S_d \rho_s)^2}, \text{ and}$$

$$c = \left(4 \cos \left(\frac{1}{3} \arccos \left(\phi \frac{8^2}{\pi^3} - 1 \right) + \frac{4}{3} \phi \right) + 4 \right)^{-1} \dots\dots\dots (3)$$

Liège Chalk	Liège Chalk
Delage et al. (1996)	Collin et al. (2002)
Risnes and Kleppa (1996)	Madland et al. (2002)
Risnes et al. (1996)	Risnes et al. (2003)
Schroeder and Shao (1996)	Risnes et al. (2005)
Fabre and Gustkiewicz (1997)	Korsnes et al. (2006)
Risnes et al. (1998)	Korsnes et al. (2008b)
Rhett and Lord (2001)	
Aalborg Chalk	Stevns Chalk
Madland et al. (2002)	Korsnes et al (2006)
Risnes et al. (2003)	Korsnes et al. (2008a)
Madland et al. (2006)	Korsnes et al. (2008b)

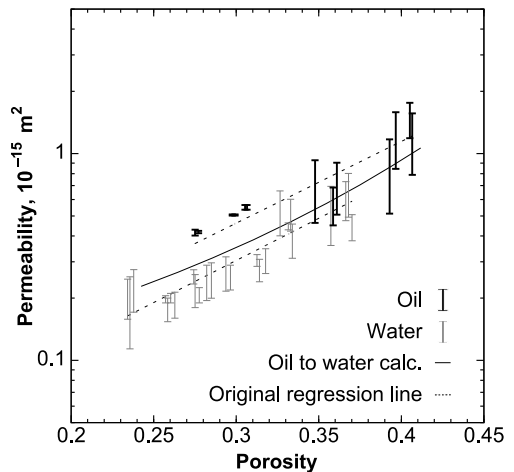


Fig. 1—Test of the skin depth hypothesis using a water film thickness of 5.52 nm obtained from the Debye length for equilibrated water at 20°C. Each bar represents a large number of test results for Liège chalk. The calculated water permeability from the oil regression line falls closely to the measured water permeability. Dataset from the PASACHALK project (PASACHALK 2000).

where Kozenys factor c is stated for 3D circular interconnected tubes, and the solid density, ρ_s , of chalk is $2.7 \times 10^3 \text{ kg/m}^3$. The specific surface, S_s , is assumed to be a material property for each chalk locality and therefore does not change between different chalk blocks. Measured specific surface area, S_a , by BET (N_2 adsorption) is $1.7 \text{ m}^2/\text{g}$ for Liège chalk, $3.6 \text{ m}^2/\text{g}$ for Aalborg chalk, and $1.7 \text{ m}^2/\text{g}$ for Stevns chalk (Hjuler and Fabricius 2009). In order to confirm that these numbers represent the effective specific surface which is relevant to the flow, a back-calculation is applied to where porosity and permeability are known. The back-calculation gives an effective specific surface of $2.0 \text{ m}^2/\text{g}$ for Liège chalk, $1.6 \text{ m}^2/\text{g}$ for Aalborg chalk, and $2.0 \text{ m}^2/\text{g}$ for Stevns chalk. These values are then used for samples where only porosity is known (Eq. 3).

Viscous skin depth. As the purpose of this review is to combine the results regardless of pore fluid we need to take the electrical charge of the chalk surface into account and whether this affects the fluid close to the solid surface. Water with dissolved ions is an electrolyte and the solid surface influence the charge balance to the distance where the ions totally screen the surface charge. Ions positioned further than this distance from the surface, will not be influenced. For oil there is no effect. If the water influenced by the charge is held back compared to the flow in the pores it is a viscous effect and we term it the viscous skin depth in accordance with the use by Johnson et al. (1987). The Debye-Hückel theory gives the screening length, κ , for an electrolyte (Lyklema 1991) as

$$\kappa = \left(\frac{2N_A e^2 I}{\epsilon_0 \epsilon_r k_B T} \right)^{1/2}, \dots \dots \dots (4)$$

where N_A is Avogadro's number, e is the elementary charge, ϵ_0 is the permittivity of vacuum, ϵ_r is relative dielectric permittivity, k_B is Boltzmann's constant, and T is absolute temperature. The number of ions and ionic strength, I , are determined from the chemical composition of the water. We test if this may approximate the skin depth by κ by comparing a series of permeability data on Liège chalk (Fig. 1). Schroeder (2002) lists the composition for Liège tap water and equilibrated water and this in turn gives a Debye screening length of $\kappa = 2.42 \text{ nm}$ for tap water and $\kappa = 5.52 \text{ nm}$ for equilibrated water. We then approximate the viscous skin depth with κ . It acts as a reduction of the porosity and it also affects the permeability. This is quantified with respect to the specific surface by

$$\phi_{\text{reduced}} = \phi - (1 - \phi)\kappa S_a \rho_s, \dots \dots \dots (5)$$

and with the use of Kozenys equation this can in principle transfer a permeability measured on an oil saturated specimen to a permeability valid for the specimen being water saturated. The specific surface is not known and is found for regular intervals of porosity from the actual permeability read from the oil regression line. We assume that the specific surface is practically unaffected by the skin and use the Debye length of equilibrated water inserted in Eq. 4-5 for calculating reduced porosity, ϕ_{reduced} caused by replacing oil with water. Through Eq. 3 we then model permeability in water saturated state and obtain the calculated "Oil to water calc." line in Fig. 1. It shows the permeability measured on Liège chalk for specimens saturated with oil or water. The result is a permeability line in good proximity to the measured permeability for water saturated specimens and supports the hypothesis that skin depth may be approximated by κ .

Rate dependence. From De Gennaro and Pereira (2008) and Priol et al. (2007) a dataset on oedometer tests on Liège chalk

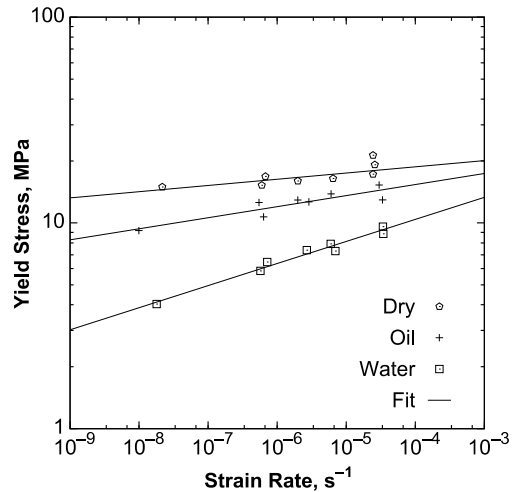


Fig. 2—Stress at yield from oedometer tests on Liège chalk with different pore fluids and at various strain rates, presented in log-log plot identically to the original plot by De Gennaro and Pereira (2008). There is a good correlation between stress at yield and the applied strain rate.

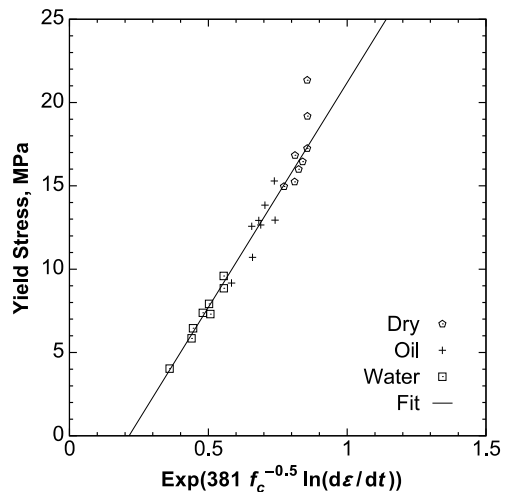


Fig. 3—Same dataset as Fig. 2. Correlation found from fitting the slopes in Fig. 2 to a function of the Biot critical frequency. The different pore fluids contribute with different density and viscosity to the critical frequency. This result in a good correlation across the whole range. Data from De Gennaro and Pereira (2008).

gives the strain rate ($d\epsilon/dt$) dependence of the stress at yield, σ_{yield} , illustrated in Fig. 2. Fitting the slope of the regression lines to the Biot critical frequency for the dry, water and oil saturated states gives the correlation

$$\ln(\sigma_{yield}) = 381 f_c^{-0.5} \ln\left(\frac{d\epsilon}{dt}\right), \dots\dots\dots (6)$$

where $d\epsilon/dt$ in principle should be divided by a reference rate and the multiplied constant should have the unit $s^{0.5} \cdot \text{MPa}$ in order to arrive at a correct unit for the yield. For simplicity we choose to keep the above format with the strain rate required as s^{-1} and the Biot critical frequency as s^{-1} , which gives values in the 0–1 range for the hypothetical σ_{yield} as seen on Fig. 3.

PASACHALK2 (2003) presents data from a series of hydrostatic tests with stress rate dependence. This is a different stress path than for the data set giving Eq. 6 but Wood (1990) finds that the yield surface retains its shape, although the size of the yield surface depends on the rate. Fitting with the Biot critical frequency in the same manner as above gives

$$\ln(\sigma_{yield}) = 1700 f_c^{-0.5} \ln\left(\frac{d\sigma}{dt}\right), \dots\dots\dots (7)$$

where the stress rate, $d\sigma/dt$, is given in 10^{-1} GPa/s and the critical frequency is in s^{-1} .

Stress plots. The mean effective stress p' , and the generalized shear stress, q , definitions are (Fjær et al. 2008):

$$p' = \frac{1}{3}(\sigma'_1 + \sigma'_2 + \sigma'_3), \text{ and}$$

$$q = \frac{1}{\sqrt{2}}\sqrt{(\sigma'_1 - \sigma'_2)^2 + (\sigma'_2 - \sigma'_3)^2 + (\sigma'_1 - \sigma'_3)^2} \dots\dots\dots (8)$$

This defines the axes in a traditional way of representing failure and yield results for different rock mechanical tests. Krenk (2000) defines an expression to draw a combined failure and yield envelope for each material:

$$q = q_{max} \left(1 - \left(\frac{p' - p_a}{p_{max}}\right)^n\right) (p' - p_a) \dots (9)$$

The conceptual plot on Fig. 4 illustrates the stress paths for the traditional rock mechanical tests: Brazil indirect tensile strength test, unconfined compression test, hydrostatic test, and triaxial test. The indirect tensile strength is here interpreted as being equivalent to the uniaxial tensile strength (Mellor and Hawkes 1971) and is therefore plotted on the negative p' axis. We do this because the stress state for the Brazil test does not involve equal intermediate and minor stress, although this has been assumed in earlier publications.

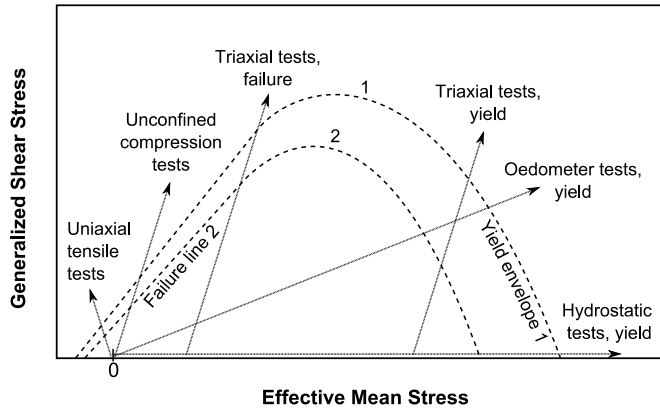


Fig. 4—Concept of p - q plot with the stress paths of the common rock mechanical tests. The sketch includes failure-yield envelopes for two different materials with rock 1 stronger than rock 2.

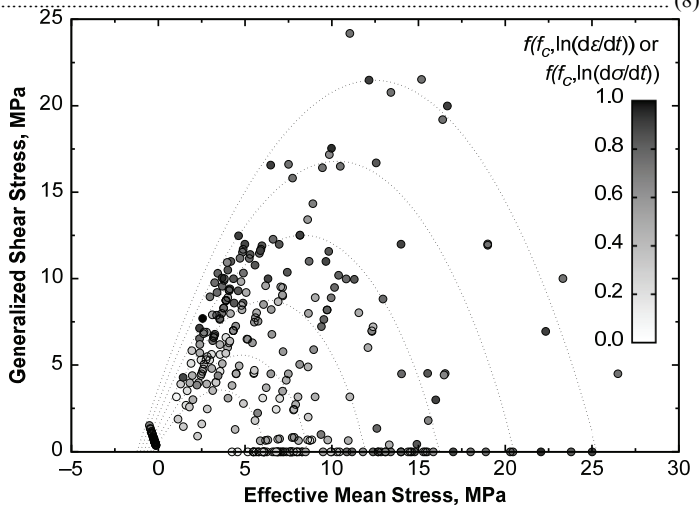


Fig. 5—Rock mechanical test results combined across chalk type, pore fluid, temperature and applied strain or stress rate. Isolines with assumed equal levels of $f(f_c, \ln(d\epsilon/dt))$ or $f(f_c, \ln(d\sigma/dt))$ are drawn at regular intervals to guide the interpretation. Each gray scaled circle represents a result from one test being either a Brazil, unconfined compression or triaxial test and either a failure or yield point.

The intermediate stress, σ_2 , is zero as stated in Jaeger et al. (2007) and can therefore not be plotted directly in the same stress plane as the p' - q plane. The interpretation of the Brazil test result as the uniaxial tensile strength is needed in order to correct for this.

Results

By using the procedures described above, all the test results for high porosity and low cemented chalk from the references listed in Table 1 show a consistent pattern regardless of material properties, test type, pore fluid, and temperature. Combining for each test the strain or stress rate dependencies with the Biot critical frequency result in the gray-scaled generalized shear stress versus effective mean stress plot shown in Fig. 5.

We find that data points with dark shading represent higher yield stress or stress at failure than points with light shading. The function $f(f_c, \ln(d\varepsilon/dt))$ represents from Eq. 6 and the function $f(f_c, \ln(d\sigma/dt))$ represents Eq. 7.

Results from hydrostatic, Brazil, and unconfined compression tests are singled out and presented in Fig. 6, Fig. 7, and Fig. 8. These also illustrate the effect of pore fluid type and temperature.

Discussion

Note that increased temperature weakens the chalk. Although some 20°C to 130°C data are from within the same test series, e.g. glycol on Fig. 6, and can be seen to follow the correlation, others are from different series and have different rates and porosities, e.g. methanol and seawater on Fig. 6. These latter sets should not be compared with each other but only with the general correlation, which they fit. The U-seawater is artificial seawater without either sulphate or magnesium, for further details see Korsnes et al. (2006).

To illustrate the implications of our work, we apply the regression lines from Fig. 6 and Fig. 8 to experimental data on Valhall chalk (Ruddy et al. 1989). When we use the estimated

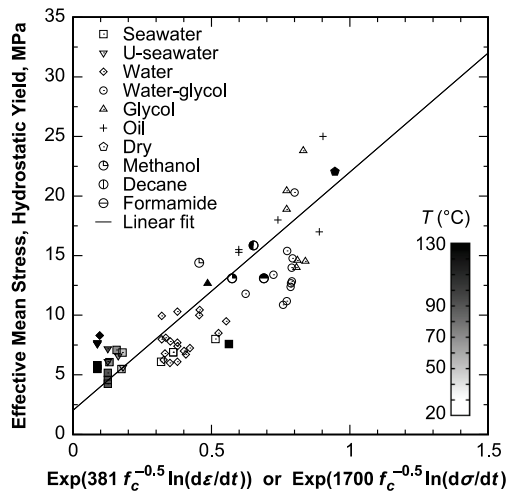


Fig. 6—Yield strength for both strain and stress rate controlled hydrostatic tests with specification of pore fluid and temperature. These data lie on the abscissa of Fig. 5. The water-glycol symbol represents a pore fluid mixture with different mol% water ranging from 80 mol% to 2 mol%. All data points for oil are at a temperature of 20°C with viscosity ranging from 3.0 mPa-s for Soltrol 170 to 120 mPa-s for liquid paraffin.

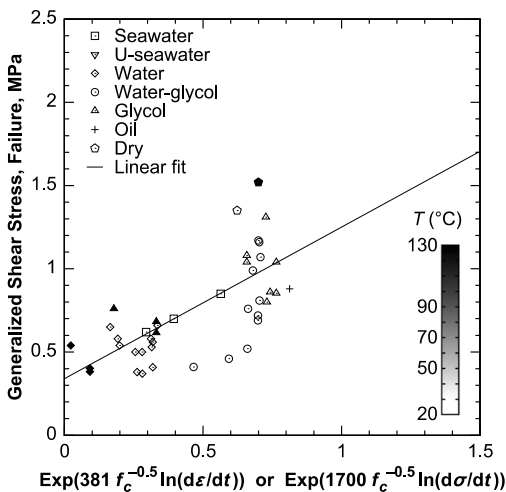


Fig. 7—Stress at failure for Brazil tests. No rate dependence is included. As expected there is scattering of the results as the test method has inherent variability. A number of points correspond to test series as an average of 10 to 21 tests and some only correspond to one test. The seawater results are for high salinity seawater having a high density and viscosity compared to standard seawater and therefore a higher value for $f(f_c, \ln(d\varepsilon/dt))$.

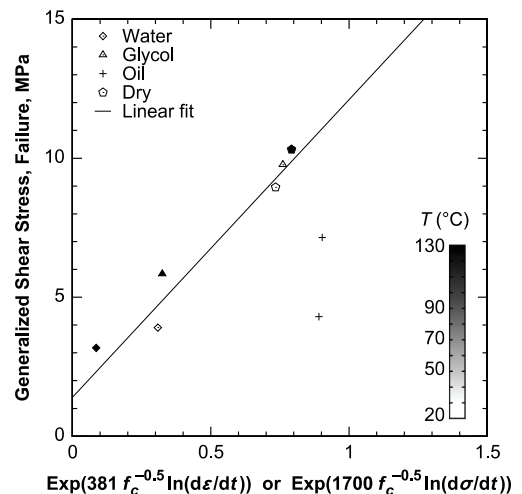


Fig. 8—Stress at failure for unconfined compression tests. Note the high strength for the dry specimen at high temperature corresponds to a high value of $f(f_c, \ln(d\varepsilon/dt))$. The two failure points for the oil saturated chalk are outliers from their respective test series and may represent very weak chalk specimens.

parameters in **Table 2** then the laboratory determined yield strength of 5.5 to 6.9 MPa from Ruddy et al. (1989) reduces to a yield strength of 5.5 MPa at field conditions for chalk saturated with light oil. This result was obtained by taking into account the change in deformation rate from $2.8 \times 10^{-7} \text{ s}^{-1}$ (0.1%/hour) in the laboratory to a field rate of $2.8 \times 10^{-10} \text{ s}^{-1}$ (0.0001%/hour) and a change in temperature from 23°C to approximately 90°C. The calculation uses the following approximate values: The density for brine at 90°C is $1.01 \times 10^3 \text{ kg/m}^3$ and the viscosity is 0.37 mPa·s. For a light crude oil at the same temperature the density is $8.2 \times 10^2 \text{ kg/m}^3$ and the viscosity is 0.67 mPa·s. The porosity of 0.45 used in Table 2 is similar to Valhall and chosen for comparison.

The plots of the failure-yield envelopes and the specific rock mechanical test results illustrate the Biot critical frequency coupled with the rate dependence. There is a clear correlation among the data, and we propose that the scatter in the results may be due to the normal variability of geologic materials.

The correlation is less distinct for the Brazil plot on Fig. 7 but focusing on trends of temperature effect gives a correlation for glycol and water which are similar. The seawater results fitting the correlation exactly represent high salinity seawater where the high content of salts, 100–250 g/l NaCl to 50–700 g/l CaCl₂·2H₂O (Risnes et al. 2003) has a large effect on the density and viscosity. The Biot critical frequency increases with temperature for dry media and the dry Brazil and unconfined compression test results show an increase in failure strength with temperature (Fig. 7 and Fig. 8).

Upscaling from laboratory results to reservoir application at reservoir conditions (stress level, field deformation rate and field temperatures for a light crude oil with low viscosity and density) is exemplified in Table 2 when stating initial input parameters and using the correlations. This is just one example and show the possible improvement which the present model could contribute with.

Conclusion

The Biot critical frequency can be used as a friction factor in fully saturated chalk with a ratedependent term included. This allows us to predict the effect of changing the pore fluid properties. We find that the critical frequency is correlated to both the failure and the yield results obtained from standard rock mechanical tests: Brazil, unconfined compression, hydrostatic, and triaxial tests. These correlations are used to extrapolate from laboratory conditions to reservoir conditions, which are exemplified for brine and a light crude oil for reservoir chalk at 130°C. A perspective for the use of this friction factor is in relation to water flooding of chalk reservoirs, where we may predict the consequence of replacing the natural pore fluids with injected water.

A systematic observed difference in absolute permeability measured with oil and with water has by earlier workers been explained as a consequence of wettability. We find that the high permeability measured by oil is the “true” absolute permeability, whereas the lower permeability measured with water can be explained by a narrowing of the effective pores caused by the space taken up by the viscous skin. The skin depth is here approximated by the Debye length for an electrolyte.

Nomenclature

- e = elementary charge, q, C
- f_c = Biot critical frequency, 1/t, s⁻¹
- f = frequency of elastic wave, 1/t, s⁻¹
- I = ionic strength of electrolyte, n/L³, mol/L
- k = absolute permeability (fluid flow), L², m²
- k_B = Boltzmann's constant, mL²/t² θ, JK⁻¹
- N_A = Avogadro number, n⁻¹, mol⁻¹
- p' = effective mean stress, m/Lt², MPa
- q = generalized shear stress, m/Lt², MPa
- S_s = specific surface area (grain surface area to grain volume), L²/L³, m²/m³
- S_a = specific surface area (grain surface area to solid mass), L²/m, m²/g
- T = absolute temperature, θ, K
- δ = viscous skin depth, L, m
- ε = strain
- ε_0 = permittivity of vacuum, q²t²/mL³, F/m

Table 2—Predicted failure and yield for field conditions. Strain rate of 0.0001%/hour for chalk with porosity of 0.45, permeability of $1.44 \times 10^{-15} \text{ m}^2$, and at 90°C. The regression line equations are valid for the function $f(f_c, \ln(d\varepsilon/dt))$ as x input and σ as y given in MPa for output.

Test type	Brine	Light crude oil
Hydrostatic, yield, MPa	3.5	5.5
Brazil, failure, MPa	0.41	0.50
Unconf. compr., failure, MPa	2.2	3.3
	<u>Regression line</u>	
Hydrostatic, yield, Fig. 6.	$y = 20 \times x + 2.0$	
Brazil, failure, Fig. 7.	$y = 0.91 \times x + 0.34$	
Unconf. compr., failure, Fig. 8.	$y = 10.7 \times x + 1.4$	

- ε_r = relative dielectric permittivity
 η = absolute viscosity, m/Lt, mPa·s
 κ = Debye length, L, nm
 ρ_{fl} = fluid density, m/L³, kg/m³
 ρ_s = solid density, m/L³, kg/m³
 σ = stress, m/Lt², MPa
 σ_1' = effective major principal stress, m/Lt², MPa
 σ_2' = effective intermediate principal stress, m/Lt², MPa
 σ_3' = effective minor principal stress, m/Lt², MPa
 σ_{yield} = stress at yield, m/Lt², MPa
 ϕ = porosity

SI-metric conversion factors

cp × 1.0*	E-00 = mPa·s
ft × 3.048*	E-01 = m
°F (°F - 32)/1.8	= °C
lbf/gal × 1.1998 264	E+02 = kg/m ³
psi × 6.894757	E-03 = MPa

*Conversion factor is exact.

References

- Biot, M.A., 1956a. Theory of Propagation of Elastic Waves in a Fluid-Saturated Porous Solid. I. Low-Frequency Range. *The Journal of the Acoustical Society of America*, **28** (2): 168–178. doi: 10.1121/1.1908239.
- Biot, M.A., 1956b. Theory of Propagation of Elastic Waves in a Fluid-Saturated Porous Solid. II. Higher Frequency Range. *The Journal of the Acoustical Society of America*, **28** (2): 179–191. doi: 10.1121/1.1908241.
- Bourbié, T., Coussy, O., and Zinzner, B., 1987. *Acoustics of Porous Media*. Editions Technip.
- Collin, F., Cui, Y.J., Schroeder, C., and Charlier, R., 2002. Mechanical Behaviour of Lixhe Chalk Partly Saturated by Oil and Water: Experiment and Modelling. *International Journal for Numerical and Analytical Methods in Geomechanics*, **26** (9): 897–924. doi: 10.1002/nag.229.
- De Gennaro, V. and Pereira, J.M., 2008. Viscoplastic Modelling of Unsaturated Geomaterials. *Proc.*, The 12th International Conference of International Association for Computer Methods and Advances in Geomechanics (IACMAG), Goa, India, 2232–2241.
- Delage, P., Schroeder, C., and Cui, Y.J., 1996. Subsidence and Capillary Effects in Chalks. *Proc.*, Eurock, Torino, Italy, 1291–1298.
- Fabre, D. and Gustkiewicz, J., 1997. Poroelastic Properties of Limestones and Sandstones Under Hydrostatic Conditions. *International Journal of Rock Mechanics and Mining Sciences*, **34** (1): 127–134. doi: 10.1016/S1365-1609(97)80038-X.
- Fabricius, I.L., Baechle, G.T., and Eberli, G.P., 2010. Elastic moduli of dry and water-saturated carbonates – effect of depositional texture, porosity and permeability. *Geophysics (in press)*.
- Fjær, E., Holt, R.M., Horsrud, P., Raaen, A.M., and Risnes, R., 2008. *Petroleum related rock mechanics*, volume 53 of *Developments in Petroleum Science*, second edition: Elsevier.
- Gutierrez, M., Øino, L.E., and Høeg, K., 2000. The Effect of Fluid Content on the Mechanical Behaviour of Fractures in Chalk. *Rock Mechanics and Rock Engineering*, **33** (2): 93–117.
- Hjuler, M.L. and Fabricius, I.L., 2009. Engineering Properties of Chalk Related to Diagenetic Variations of Upper Cretaceous Onshore and Offshore Chalk in the North Sea Area. *Journal of Petroleum Science and Engineering*, **68** (3-4): 151–170. doi: 10.1016/j.petrol.2009.06.005.
- Jaeger, J. C., Cook, N. G. W., and Zimmerman, R. W., 2007. *Fundamentals of rock mechanics*, fourth edition: Blackwell Publishing.
- Johnson, D.L., Koplik, J., and Dashen, R., 1987. Theory of Dynamic Permeability and Tortuosity in Fluid-Saturated Porous Media. *Journal of Fluid Mechanics Digital Archive*, **176**: 379–402. doi: 10.1017/S0022112087000727.
- Korsnes, R.I., Madland, M.V., and Austad, T., 2006. Impact of Brine Composition on the Mechanical Strength of Chalk at High Temperature. *Proc.*, Eurock, The International Symposium of the International Society for Rock Mechanics, Belgium, 9–12 May, 133–140. Taylor & Francis/Balkema.
- Korsnes, R.I., Madland, M.V., Austad, T., Haver, S., and Rosland, G., 2008a. The Effects of Temperature on the Water Weakening of Chalk by Seawater. *Journal of Petroleum Science and Engineering*, **60** (3–4): 183–193. doi: 10.1016/j.petrol.2007.06.001.
- Korsnes, R. I., Wersland, E., Austad, T., and Madland, M.V., 2008b. Anisotropy in Chalk Studied by Rock Mechanics. *Journal of Petroleum Science and Engineering*, **62** (1–2): 28–35. doi:10.1016/j.petrol.2008.06.004.
- Krenk, S., 2000. Characteristic state plasticity for granular materials: Part I: Basic theory. *International Journal of Solids and Structures*, **37** (43): 6343–6360. doi:10.1016/S0020-7683(99)00278-4.
- Lyklema, J., 1991. *Fundamentals of Interface and Colloid Science*, Volume I. London: Academic Press.
- Madland, M.V., Finsnes, A., Alkafadgi, A., Risnes, R., and Austad, T., 2006. The Influence of CO₂ Gas and Carbonate Water on the Mechanical Stability of Chalk. *Journal of Petroleum Science and Engineering*, **51** (3–4): 149–168. doi: 10.1016/j.petrol.2006.01.002.
- Madland, M.V., Korsnes, R.I., and Risnes, R., 2002. Temperature Effects in Brazilian, Uniaxial and Triaxial Compressive Tests with High Porosity Chalk. Paper SPE 77761-MS presented at the 2002 SPE Annual Technical Conference and Exhibition, Texas, 29 September–2 October. doi: 10.2118/77761-MS.
- Mavko, G., Mukerji, T., and Dvorkin, J., 2009. *The Rock Physics Handbook: Tools for Seismic Analysis in Porous Media*. Second edition, New York: Cambridge University Press.

- Mellor, M. and Hawkes, I., 1971. Measurement of Tensile Strength by Diametral Compression of Discs and Annuli. *Engineering Geology*, **5** (3): 173–225. doi: 10.1016/0013-7952(71)90001-9.
- Mortensen, J., Engstrøm, F., and Lind, I., 1998. The Relation Among Porosity, Permeability, and Specific Surface of Chalk From the Gorm Field, Danish North Sea. Paper 31062-PA, *SPE Reservoir Evaluation & Engineering*, **1** (3): 245–251. doi: 10.2118/31062-PA.
- PASACHALK, 2000. Mechanical Behaviour of Partially and Multiphase Saturated CHALKs Fluid–Skeleton Interaction : Main Factor of Chalk Oil Reservoirs Compaction and Related Subsidence, Part 1. Final report, European Joule III contract N° JOF3CT970033.
- PASACHALK2, 2003. Mechanical Behaviour of Partially and Multiphase Saturated CHALKs Fluid–Skeleton Interaction : Main Factor of Chalk Oil Reservoirs Compaction and Related Subsidence, Part 2. Final report, European Joule III contract N° ENK6-2000-00089.
- Priol, G., De Gennaro, V., Delage, P., and Servant, T., 2007. Experimental Investigation on the Time Dependent Behaviour of a Multiphase Chalk. In *Experimental Unsaturated Soil Mechanics*, volume 112 of *Springer Proceedings in Physics*, 161–167. Springer Berlin Heidelberg. doi: 10.1007/3-540-69873-6_15.
- Rhett, D. and Lord, C., 2001. Water Weakening in Sedimentary Rocks. DC Rocks 2001. *Proc.*, The 38th US Symposium on Rock Mechanics (USRMS), 121–128.
- Risnes, R., Garpestad, O.J., Gilje, M., Oland, L.T., Ovesen, M., and Vargervik, E., 1998. Strain Hardening and Extensional Failure in High Porosity Chalk. Paper SPE 47581-MS presented at the SPE/ISRM Eurock '98, Trondheim, Norway, 8–10 July, 475–484. doi: 10.2118/47581-MS.
- Risnes, R., Haghghi, H., Korsnes, R.I., and Natvik, O., 2003. Chalk–Fluid Interactions with Glycol and Brines. *Tectonophysics*, **370** (1–4): 213–226. doi: 10.1016/S0040-1951(03)00187-2.
- Risnes, R. and Kleppa, E., 1996. Plastic Behaviour of High Porosity Chalk in Constant K-Ratio Tests. Paper presented at the 5th North Sea Chalk Symposium, France.
- Risnes, R., Kristensen, C.N., and Andersen, M.A., 1996. Triaxial Tests on High Porosity Chalk with Different Saturating Fluids. Paper presented at the 5th North Sea Chalk Symposium, France.
- Risnes, R., Madland, M.V., Hole, M., and Kwabiah, N.K., 2005. Water Weakening of Chalk—Mechanical Effects of Water–Glycol Mixtures. *Journal of Petroleum Science and Engineering*, **48** (1–2): 21–36. doi: 10.1016/j.petrol.2005.04.004.
- Ruddy, I., Andersen, M.A., Pattillo, P.D., Bishlawi, M., and Foged, N., 1989. Rock Compressibility, Compaction, and Subsidence in a High-Porosity Chalk Reservoir: A Case-Study of Valhall Field. *Journal of Petroleum Technology*, **41** (7): 741–746. doi: 10.2118/18278-PA.
- Schroeder, C., 2002. Du coccolithe au réservoir pétrolier. Approche phénoménologique du comportement mécanique de la craie en vue de sa modélisation à différentes échelles. PhD dissertation, Université de Liège, Belgium.
- Schroeder, C. and Shao, J., 1996. Plastic Deformation and Capillary Effects in Chalks. Paper presented at the 5th North Sea Chalk Symposium, France.
- Wood, D.M., 1990. *Soil Behaviour and Critical State Soil Mechanics*. New York: Cambridge University Press.

Appendix H

Abstract I

Andreassen, K.A., Fabricius, I.L., and Foged, N.N. (2010).

Creep of Highly Porous Chalk and Biot Critical Frequency.

Student abstract SP-44 presented at the 72nd EAGE Conference & Exhibition, Barcelona, Spain, 14–17 June.

Introduction

Creep in chalk is a time and stress dependent phenomenon and reach significant levels depending on pore fluid. Water injection is used in chalk by the petroleum industry to enhance the oil recovery and this change of pore fluids increases the creep. This is labelled the water weakening and is just one mechanism where it is observed. For highly porous chalk (with porosity above 0.3) the weakening effect of the fluid dominates and the degree of cementation is not considered. The definition of creep index is, see Ruddy et al. (1989),

$$\epsilon_s = \frac{d\epsilon}{d(\log(t))},$$

where ϵ is strain, and t is time. It is the additional creep per one time decade.

As observed by Fabricius and Eberli (2009) on a large set of carbonate rocks the Biot critical frequency is a measure to combine laboratory results with different rock properties and pore fluids. The definition of the Biot critical frequency (often also termed characteristic, cross-over, or reference frequency) is

$$f_c = \frac{\phi\eta}{2\pi\rho_f k},$$

where ϕ is porosity, η is the fluid absolute viscosity, ρ_f is fluid density, and k is absolute permeability. The Biot critical frequency is the limit between a low frequency regime with the pore fluid following viscous forces and a high frequency regime with inertial forces dominating the fluid motion, Biot (1956a,b). These regimes have been verified experimentally by Johnson et al. (1987) and examples can be found in Mavko et al. (1998). The drag that the solid motion makes on the fluid and whether this is in the viscous or inertial regime is basically a matter of friction between the liquid and the solid. The critical frequency can be seen as a friction factor similarly to Reynolds number, Re , which is usually interpreted with a friction proportional to $64/Re$ valid for laminar flow. The Reynolds number also marks the transition from a flow regime dominated by viscous forces to a flow regime dominated by inertial forces.

Method

The data reviewed here are from high pressure oedometer tests made by Priol et al. (2007) on Liège Lixhe chalk. It is an outcrop chalk from a quarry in Belgium and has a general porosity of 0.43 and general permeability of $2.0 \cdot 10^{-15} \text{ m}^2$. The recalculation from void ratio units, e , to strain units is

$$\epsilon = \frac{\Delta e}{1 + e_0},$$

with e_0 the initial void ratio, and $\Delta e = e_0 - e$. The result is in Figure 1. The dry specimens are oven dried at 105°C for 24 hours before testing, the oil is Soltrol 170, and the water is equilibrated with chalk before use.

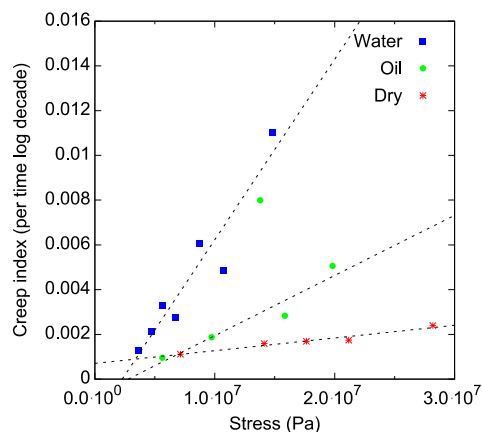


Figure 1: Finding the stress dependent creep index relation beyond yield. Recalculated from Priol et al. 2007. One outlier is excluded from the regression for oil.



Table 1 states the slope of the stress dependent creep index for each fluid and in the region beyond yield (pore collapse) found from Figure 1. The main focus here is the inclination of the regression line and not the intercept with the axis because the creep index is only influenced by the stress level relatively to the stress at onset of yield.

Table 1: Fluid properties and results.

Fluid	Density (10^3 kg/m^3)	Viscosity ($10^{-3} \text{ Pa}\cdot\text{s}$)	Biot critical frequency (s^{-1})	Slope in Figure 1
Water	0.9982 ^b	1.0016 ^b	3.40e7	8.07e-9
Oil ^a	0.7826	3.0085	1.30e8	2.69e-10
Dry	0.001193 ^c	0.01829 ^c	5.19e8	5.67e-11

^aSoltrol 170, ^bNIST (2008), ^cLide (2008). All data at 20°C and atmospheric pressure.

The resulting correlation between Biot critical frequency, stress, σ , and the creep index is

$$\epsilon_s = 0.04 \cdot f_c^{-1} \cdot \sigma,$$

where $[\sigma] = \text{Pa}$, and $[f_c] = \text{s}^{-1}$. So the constant 0.04 should have the units $(\text{Pa}\cdot\text{s})^{-1}$.

Conclusions

The implications of this finding are that the friction between fluid and solid correlates with the creep process in highly porous chalk. In other words, the flow of the fluid in the chalk is significant for the time dependent deformation. The found correlation can be applied in interpretation of laboratory tests with different pore fluids and different basic rock properties.

References

- Biot, M. A. [1956a] Theory of propagation of elastic waves in a fluid-saturated porous solid. I. Low-frequency range. *The Journal of the Acoustical Society of America*, **28**, 168–178.
- Biot, M. A. [1956b] Theory of propagation of elastic waves in a fluid-saturated porous solid. II. Higher frequency range. *The Journal of the Acoustical Society of America*, **28**, 179–191.
- Fabricius, I. L. and Eberli, G. P. [2009] Dispersion of elastic waves in carbonate rocks. *79th Annual International Meeting, SEG*, Expanded Abstracts.
- Johnson, D. L., Koplik, J. and Dashen, R. [1987] Theory of dynamic permeability and tortuosity in fluid-saturated porous media. *Journal of Fluid Mechanics Digital Archive*, **176**, 379–402.
- Lide, D. R., ed. [2008] *CRC handbook of chemistry and physics*, 89th ed., Taylor and Francis Group, e-book, <http://www.hbcponline.com/>, accessed 11 June 2009.
- Mavko, G., Mukerji, T. and Dvorkin, J. [1998] *The rock physics handbook: Tools for seismic analysis in porous media*. Cambridge University Press.
- NIST [2008] *Thermophysical properties of fluid systems*. Webbook, <http://webbook.nist.gov/chemistry/fluid/>, accessed 23 October 2009.
- Priol, G., Gennaro, V. D., Delage, P. and Servant, T. [2007] Experimental Investigation on the time dependent behaviour of a multiphase chalk experimental unsaturated soil mechanics. *Experimental Unsaturated Soil Mechanics, Springer Berlin*, **112**, 161–167.
- Ruddy, I., Andersen, M. A., Pattillo, P. D., Bishlawi, M. and Foged, N. [1989] Rock compressibility, compaction, and subsidence in a high-porosity chalk reservoir: A case-study of Valhall field. *Journal of Petroleum Technology*, **41**, 741–746.

In petroleum engineering, the concepts of water-weakening and temperature weakening are important mechanisms. This thesis reviews previously published rock mechanical test results on chalk. It covers an analysis on which physical properties correlates with the failure and pore collapse strengths. It is proposed that the strength of chalk is correlated with the Biot critical frequency comprising the fluid properties viscosity and density, and the material properties porosity and permeability. The critical frequency is interpreted as a measure of the solid-fluid friction and includes both the water-weakening and temperature weakening.

DTU Civil Engineering
Department of Civil Engineering
Technical University of Denmark

Brovej, Building 118
2800 Kgs. Lyngby
Telephone 45 25 17 00

www.byg.dtu.dk

ISBN: 9788778773166
ISSN: 1601-2917